LAPPEENRANTA UNIVERSITY OF TECHNOLOGY
LUT School of Engineering Science
Degree Program of Chemical Engineering

Lassi Huusari

ANALYSIS OF PHASE SEPARATOR DESIGN CRITERIA USING COMPUTATIONAL FLUID DYNAMICS

Examiners: Professor, DSc (Tech) Tuomas Koiranen
Lic.Sc. (Tech) Veli Matti Purola

Instructors: Lic.Sc. (Tech) Veli Matti Purola
DSc (Tech) Johanna Vaittinen
MSc (Tech) Mika Kettunen

FOREWORDS

This Master's thesis was completed in the Technology & Product Development department of Neste Jacobs between April and October 2015.

I would like to express my gratitude for all of my instructors, Veli Matti Purola, Johanna Vaittinen and Mika Kettunen, for their belief in me and for taking the time from their schedules to always provide guidance when needed. Many thanks to the great Neste Jacobs CFD team of Johanna, Niina, Tuomo and Denis as well as the people at Engys for their invaluable advice along the way. Thanks also to all of the people at NJ Porvoo office for support, both professional and personal. Thanks to my supervising professor Tuomas Koiranen for his participation and for introducing me to CFD, without which I may have never started this work in the first place.

To my fellow chemical engineering students at LUT, thanks for the last five years and good luck in your future endeavors. Last but not least, my deepest thanks to my family for letting me pursue my own interests right from an early age. I am honored to constantly enjoy your support even though I know for the past few years you have probably had no idea of what I have spent my time and efforts on.

Porvoo, 21st of September, 2015

Lassi Huusari

ABSTRACT

Lappeenranta University of Technology
School of Engineering Science
Degree Program of Chemical Engineering

Lassi Huusari

Evaluation of Phase Separator Design Criteria Using Computational Fluid Dynamics

Master's Thesis

2015

118 pages, 68 figures, 12 tables, 7 appendices

Examiners: Professor, DSc (Tech) Tuomas Koiranen
Lic.Sc. (Tech) Veli Matti Purola

Keywords: separation, gravitational, gas-liquid, CFD, OpenFOAM

Gravitational phase separation is a common unit operation found in most large-scale chemical processes. The need for phase separation can arise e.g. from product purification or protection of downstream equipment. In gravitational phase separation, the phases separate without the application of an external force. This is achieved in vessels where the flow velocity is lowered substantially compared to pipe flow. If the velocity is low enough, the denser phase settles towards the bottom of the vessel while the lighter phase rises.

To find optimal configurations for gravitational phase separator vessels, several different geometrical and internal design features were evaluated based on simulations using OpenFOAM computational fluid dynamics (CFD) software. The studied features included inlet distributors, vessel dimensions, demister configurations and gas phase outlet configurations. Simulations were conducted as single phase steady state calculations. For comparison, additional simulations were performed as dynamic single and two-phase calculations.

The steady state single phase calculations provided indications on preferred configurations for most above mentioned features. The results of the dynamic simulations supported the utilization of the computationally faster steady state model as a practical engineering tool. However, the two-phase model provides more truthful results especially with flows where a single phase does not determine the flow characteristics.

TIIVISTELMÄ

Lappeenrannan Teknillinen Yliopisto
School of Engineering Science
Kemiantekniikan koulutusohjelma

Lassi Huusari
Faasierottimien suunnittelukriteerien arviointi virtauslaskennan avulla

Diplomityö
2015

118 sivua, 68 kuvaa, 12 taulukkoa, 7 liitettä

Tarkastajat: Professori, TkT Tuomas Koiranen
TkL Veli Matti Purola

Avainsanat: erotus, painovoimainen, kaasu-neste, CFD, OpenFOAM

Painovoimainen faasierotus on yleinen yksikköoperaatio joka löytyy useimmista laajan mittakaavan kemiallisista prosesseista. Erotusta voidaan tarvita esimerkiksi tuotteen puhdistamiseksi tai alavirtaan sijoitettujen laitteiden suojaamiseksi. Painovoimaisessa erotuksessa faasit erottuvat ilman ulkoisen voiman hyödyntämistä. Erotus tapahtuu säiliöissä, joissa virtausnopeudet laskevat huomattavasti putkivirtausta pienemmiksi. Jos virtausnopeus on tarpeeksi pieni, tiheämpi faasi laskeutuu säiliön pohjalle, kevyemmän faasin noustessa.

Optimaalisen painovoimaisen erotussäiliörakenteen löytämiseksi useita mitoitukseen ja sisäisiin rakenteisiin liittyä ratkaisuja vertailtiin perustuen virtausmallinnuksiin OpenFOAM-ohjelmistolla. Vertaillut ratkaisut liittyivät syötönjakajiin, säiliön mittasuhteisiin, demisterin kiinnitykseen ja kaasun ulostuloyhteen rakenteeseen. Simulaatiot suoritettiin tasapainotilaan perustuvina yksifaasilaskentoina. Lisäksi suoritettiin täydentäviä vertailusimulaatiota aikariippuvaisia yksi- ja kaksifaasimalleja käyttäen.

Tasapainotilaan perustuvat yksifaasilaskennat antoivat viitteitä tiettyjen geometrioiden paremmuudesta aiemmin mainituissa kategorioissa. Aikariippuvaisten laskentojen tulokset tukivat päätöstä hyödyntää laskennallisesti nopeampaa tasapainotilaan perustuvaa mallia insinöörityökaluna. Kaksifaasilaskenta antaa kuitenkin totuudenmukaisempia tuloksia etenkin tilanteissa, joissa yksittäinen faasi ei määritä kokonaisvirtauksen luonnetta.

SYMBOLS

A	Area, m^2
C_D	Drag coefficient, -
Co	Courant number, -
d,D	Diameter (d for droplets, D for vessels and pipes), m
F	Force, N OR process control factors, -
Fr	Froude number, -
g	Gravitational constant, 9.81 m/s^2
H	Height, m
K	Maximum allowable velocity coefficient, m/s
k	Fluctuation of kinetic energy, m^2/s^2
L	Length, m
n	Number of observations, -
P	Pressure, Pa
Re	Reynolds number, -
SG	Specific gravity, -
s_n	Standard deviation, -
t	Time, s
U, u	Velocity, m/s
V	Volume, m^3
Q	Volumetric flow, m^3/s
ε	Rate of dissipation of k, m^2/s^3
ω	Large eddy frequency, 1/s
ψ	Entrainment value, -
ρ	Density, kg/m^3
τ	Shear stress, Pa
μ	Viscosity, Pas

SUBSCRIPTS

B	Buoyancy
D	Drag
G	Gravitational
g	Gas
H	Horizontal
h	Hydraulic
in	Inlet
l	Liquid
max	Maximum value
min	Minimum value
mix	Mixture
out	Outlet
p	Particle OR packing
t	Terminal
w	Wire

ABBREVIATIONS

CFD	Computational Fluid Dynamics
DNS	Direct Numerical Simulation
SST	Shear Stress Transport
HLL	High Liquid Level
LES	Large Eddy Simulation
LLL	Low Liquid Level
NLL	Normal Liquid Level
VIEC	Vessel Internal Electrostatic Coalescer
VOF	Volume Of Fluid

TABLE OF CONTENTS

1. INTRODUCTION

1.1 Background

Phase separation is an integral part in most chemical engineering processes. Products and by-products need to be separated, sensitive equipment need protection from moisture and hazardous gases need to be vented. These are just a few examples of possible uses for phase separation techniques in the field of chemical engineering. Phase separator vessels are utilized because stream velocities in the process are typically too high for phase separation. Vessels provide more cross-sectional area than pipes, thus lowering the stream velocity and facilitating phase separation. Further advances in separation efficiency can be sought by using designs that employ inertial or centrifugal forces and enhance droplet coalescence.

Design and sizing of the separator vessels has up to now been primarily based on simple velocity based formulas and empirical correlations. With the increase in computational power and developments in mathematical algorithms, computational fluid dynamics (CFD) has become a viable tool in the design and troubleshooting of all types of vessels in the field of process industry. Implementation of reliable CFD models early on in the design process can lead to considerable savings in e.g. decreasing the need to construct pilot scale devices and even avoiding design flaws in full scale devices.

1.2 Objective

Objective of the work was to study the effects of different design parameters and structural solutions on the separation efficiency of phase separators using CFD techniques. Flow phenomena, mainly velocity and profile, were studied to gain information on the efficiency of separation. Simulations were employed to gain verification for experience based knowledge of fluid separation inside separator vessels.

Results of this study can be used in unifying the design process of phase separators by providing computational data to support the selection of certain structural components and vessel dimensions. Drawbacks of designs can also be identified so they can be taken into account in equipment selection and design. While outside of the scope of this thesis, the

results can be used in creating a design tool for phase separators that would calculate basic dimensions for the separator vessel and provide recommendations for internal components.

1.3 Scope of work

The literature part of this thesis reviews the traditional sizing criteria of phase separators. Different types of phase separators are introduced with the emphasis placed on gravitational separators which are studied in the experimental part. Effect of different flow variables are also listed, as well as some common indicators on which the performance of different separators can be assessed.

Experimental part focuses on using CFD to model the effects of different structural designs on key performance indicators in gas-liquid separation. CFD calculations were conducted using OpenFOAM open source software with some additions from commercial HELYX® software package. The main monitored indicator is the velocity in the vertical direction, which is sampled over several cross-sectional planes. Most of the simulations in the experimental part were simplified to include only a single phase in a steady state calculation. Additional simulations were conducted as time-dependent calculations and using two-phase methods. Flow profiles and numerical data were interpreted to find reasons behind the differences in performance between different designs. Based on the interpretations, recommendations on preferred designs from a CFD standpoint are given.

LITERATURE PART

2. GENERAL OVERVIEW OF PHASE SEPARATORS

2.1 Phase systems

Two main phase separation systems are considered in the literature part of this work: gas-liquid and liquid-liquid. Many of the same principles apply to both phase systems and emphasis is placed on the differences between gas-liquid and liquid-liquid separation. The main difference is the significantly lower velocity allowed in liquid-liquid separation due to smaller phase density difference.

Solids, which are outside the scope of this review, can be generally equated to liquids but with smaller capability of coalescence. A three-phase gas-liquid-liquid system is a combination of the two main phase systems. The basic phenomena in a three-phase system are the same as for gas-liquid and liquid-liquid systems. A three-phase system differs in the complexity of equipment required for separation.

2.1.1 Gas-liquid systems

Primarily, gas-liquid systems can be divided into two categories based on the continuous phase. In a gas-phase continuous system the liquid is dispersed as small droplets within the gas phase. In a liquid-phase continuous system the gas bubbles are dispersed within the liquid flow. The nomenclature used to describe the system depends on the particle or droplet size. A chart indicating the generally classified particle sizes and equipment used in their removal is presented in Fig. 1. (Perry, 1984)

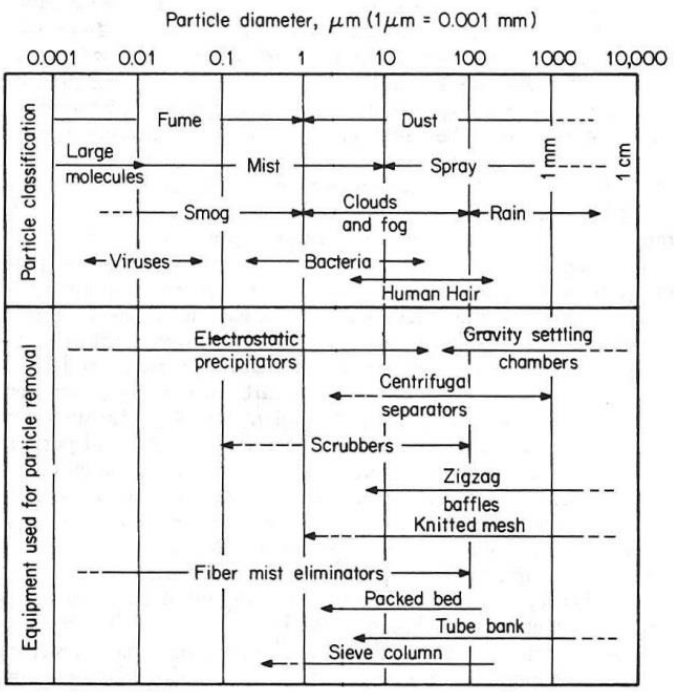

FIGURE 1. Classifications of different sized particles and equipment used to remove them (Perry, 1984)

Mist refers to suspended particles which in gas-phase continuous systems are often the result of condensation. Spray refers to larger droplets which are often generated inadvertently in the process through entrainment from the liquid phase. Fumes and dust are the solid equivalents for the aforementioned liquid classes. The key difference concerning separation of liquid and solids from gas is the coalescence of liquids which greatly enhances separation. (Perry, 1984)

A gas-liquid system can also be one where liquid is the continuous phase. Gas can be dispersed in the liquid in two forms, stable and unstable. In an unstable dispersion, the phases separate naturally by buoyancy once the dispersing force is removed. Then only a sufficient amount of time and volume is required for separation. Stable dispersions are harder to separate. As the name suggests, the gas remains dispersed even without an external mixing force. Foam is a practical example of such a system, formed through concentration of additional stabilizing substance on the interface of the gas and liquid phases. (Perry, 1984)

2.1.2 Liquid-liquid systems

A typical system containing two liquid components is a water and oil mixture. As with gas-liquid systems, two variations exist. In liquid-liquid systems, a stable dispersion is referred to as an emulsion and is usually purposefully created not to be separated. Separation is mainly conducted for unstable dispersions that can be separated by gravity in the absence of mixing forces. In batch settlers, the separation of the two liquid phases for most systems happens in two steps. First step is fast and leaves a cloud of very small droplets of parts per million concentration dispersed in the continuous phase. The second step is the separation of these droplets, which is slow and can often be neglected in normal plant operations, especially when using a multistage separation process. (Perry, 1984)

The separation times in liquid-liquid separator are measured in minutes, a typical value being 5-10 min if no disturbing emulsification effects are observed. This is a major difference to gas-liquid separation, where residence times in vessels are usually measured in seconds. Coalescence aids separation as in gas-liquid separation by creation of larger droplets that settle faster. Coalescence is usually fast in systems with high interfacial tension at the phase surface. Impurities tend to build up on the interface and hinder coalescence. Settling velocity is also influenced by the continuous phase viscosity. In many cases, by increasing the temperature, the viscosity can be lowered and separation rate increased. (Perry, 1984)

Compared to gas-liquid systems, separation in liquid-liquid systems is almost always slower due to smaller density difference between the phases. Turbulence at the phase interface further decreases the rate of separation. To prevent disturbances at the interface, the inlet flow velocity should be kept low. (Perry, 1984) The difficulties caused by small density differences or high viscosities can be countered by utilizing e.g. centrifugal forces in the form of cyclone separators. It is, however, important to note that the separation of stable dispersions cannot be enhanced by the addition of an external force alone. (Trambouze, 2000)

2.2 Separator types

A selection of different phase separators has been developed over the years for various applications. This chapter focuses on specific separation needs and introduces some commonly used equipment fulfilling the separation requirement.

2.2.1 Gravitational separation

Removal of dispersed phase droplets is commonly needed e.g. in steam networks. Gravitational separation is achieved in different types of vessels. In flash tanks, the gas is flashed from the liquid stream by lowering the pressure. In scrubbers and knock-out drums the inlet flow already contains both phases. A line drip is a special vessel designed only for the simplest phase separation. The purpose of a line drip is the separation of free liquid from an inlet stream with high gas to liquid ratio, leaving entrained droplets to travel with the gas stream. The above mentioned equipment are examples of gas-liquid separators. Geometrically similar vessels are utilized in liquid-liquid separation.

Due to the whole cross-sectional area being available for droplet separation, a vertical vessel is best employed when gas to liquid ratio is high (Svrcek *et al.* 1993; Soares, 2002). A layout of a typical vertical phase separator is presented in Fig. 2.

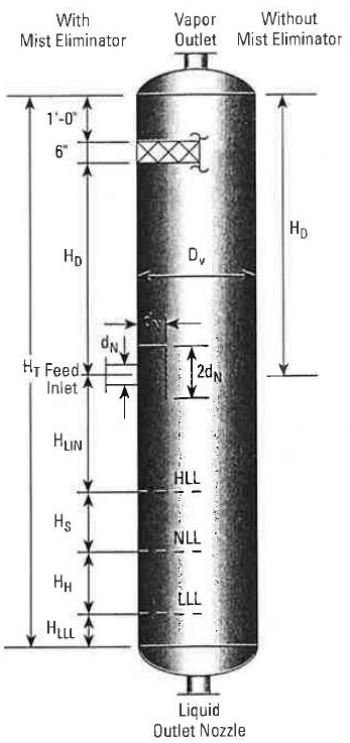

FIGURE 2. Vertical phase separator with characteristic dimensions indicated (Svrcek *et al.* 1993)

Gas inlet in a vertical separator can be oriented in many ways, but it is typical to configure the inlet normal to the vessel axis. Usually the vessel is equipped with an inlet distributor that helps to spread the flow evenly across the vessel. If no distributor is used, the first separating force to be exerted on the liquid particles is impingement to the vessel wall on the opposite side of the inlet. Placing the inlet opposite to the vessel axis also forces the gas flow to change direction on its way to the outlet. This exerts centrifugal force on the liquid particles, leading to impingement to the walls or contact with the liquid surface at the bottom of the vessel. (Soares, 2002)

Removal of liquid droplets from the gas stream happens as it travels from the inlet to the outlet. Larger drops experience more gravitational pull compared to smaller ones and are therefore drawn to the bottom of the vessel. (Soares, 2002) Phase separators usually contain a mist eliminator which is used to further induce drop coalescence.

Horizontal vessels are preferred when the ratio of gas to liquid is low (Svrcek *et al.* 1993). The simplest form of a horizontal separator is the single barrel design which is shown in Fig. 3.

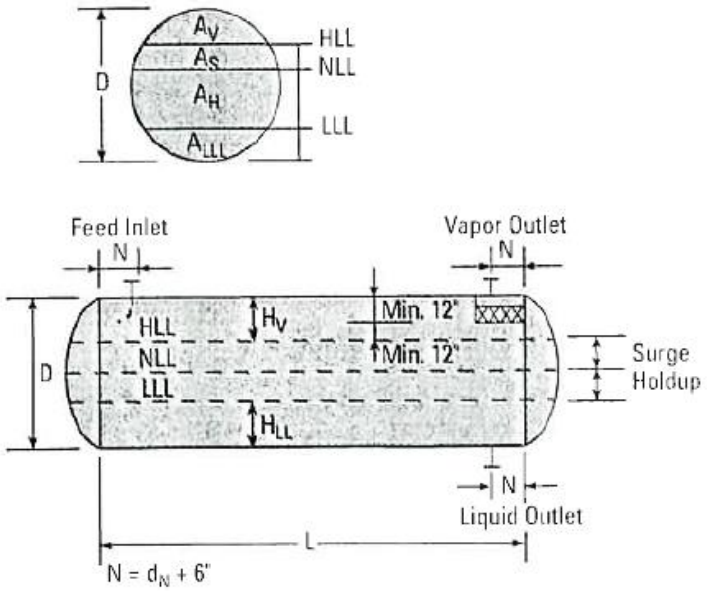

FIGURE 3. Side and cross-sectional views of a horizontal phase separator with characteristic dimensions indicated (Svrcek *et al.* 1993)

In the simple design illustrated in Fig. 3, a single multiphase flow enters the separator vessel at the top of one side of the vessel and the two separated flows exit the vessel at the other end through top and bottom outlets. With horizontal separators it is important to note that vapor disengagement can only happen in a small part of the cross-sectional area of the vessel as indicated by the upper part of Fig. 3. Therefore a sufficient vessel diameter is required to provide adequate gas flow capacity. (Svrcek *et al.* 1993) One major advantage of a horizontal design is the possibility of liquid droplet removal by collision with the liquid surface all along the length of the vessel.

A slightly more complex design is the dual barrel unit illustrated in Fig. 4.

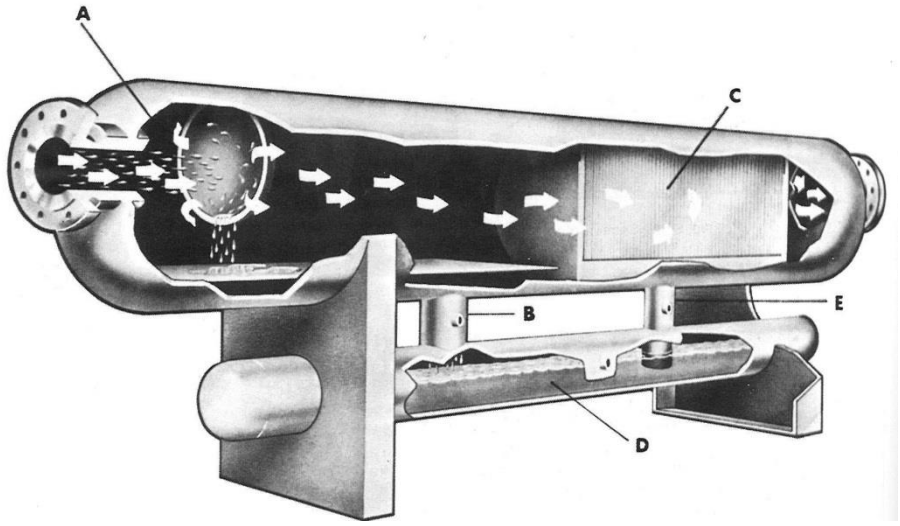

FIGURE 4. Horizontal phase separator with dual barrel configuration (Soares, 2002)

In the dual barrel configuration the feed stream enters the vessel similarly to the single barrel design in Fig 3. An impact plate (A) can be used to initially separate larger drops. The initially separated liquid phase flows down through the first downcomer (B) as the gas flow continues to the mist separator (C). Here the smaller liquid droplets coalesce and flow down through the second downcomer (E), where they join the liquid phase exiting through the bottom barrel. The tip of the second downcomer (E) is submerged to prevent gas exiting though the lower tube. This more complex design offers a few advantages over the single barrel design. Liquid re-entrainment is minimized due to physical separation of phases in two different vessels. Lower liquid level in the upper tube also facilitates the installation of larger auxiliary separators such as mist extractors. (Soares, 2002)

Multiple-phase separators and often also liquid-liquid separators utilize a set of baffles to direct the liquid flow into overflows. An example of both a vertical and a horizontal three-phase separator configuration is shown in Fig. 5.

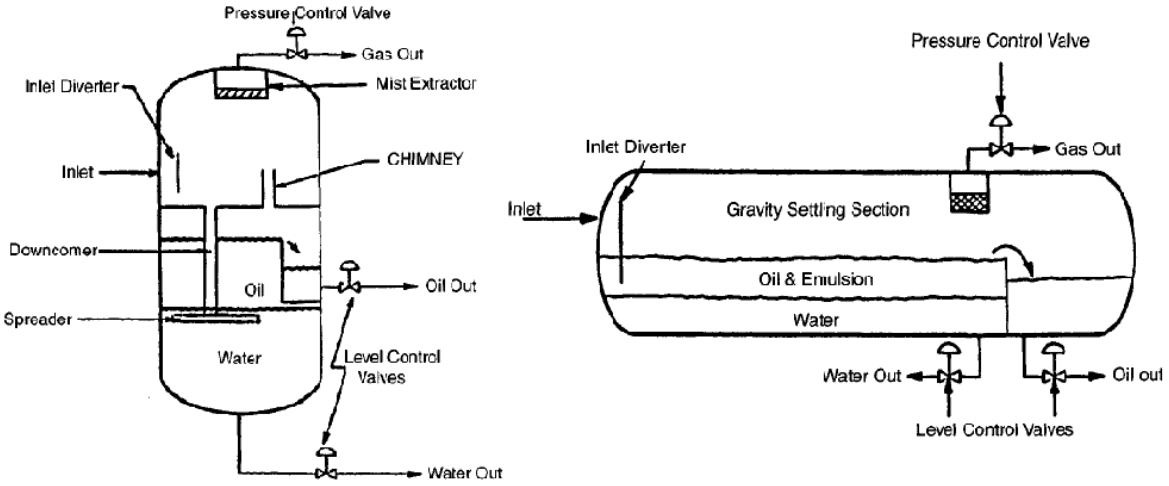

FIGURE 5. Typical configurations of three-phase separators: vertical (left) and horizontal (right) (Lyons & Plisga, 2005)

The implementation of a good level control strategy becomes increasingly important in separators containing multiple liquid phases. Too high liquid surface level leads to heavier liquid escaping through the wrong outlet.

2.2.2 Centrifugal and inertial separation

When simple gravitational forces are insufficient in achieving the desired separation rate or efficiency, centrifugal and inertial forces can be utilized through vessel and inlet designs. A vessel designed to primarily separate components by centrifugal force is commonly referred to as a cyclone. Cyclones operate by forcing the inlet flow into a vortex where the heavier phase is pushed outwards and lighter phase exits upwards from the center of the cyclone. Cyclone separation can be utilized in any combination of solid, liquid and gas separation. The benefit in fluid separation is that liquids coalesce on capture which promotes their removal from the device. (Perry, 1984) An illustration of the cyclone operating principle is presented in Fig. 6

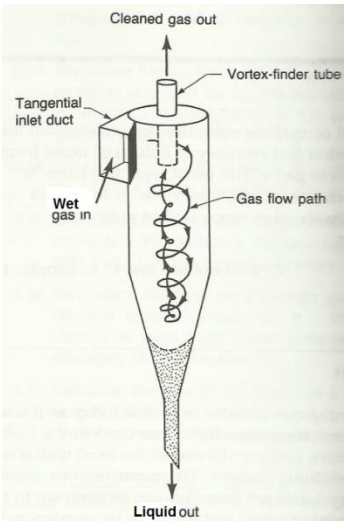

FIGURE 6. Cyclone separator operating principle (Cooper et al. 1986)

As the inlet flow enters the cyclone, it follows a circular path towards the bottom of the cyclone. The phase with a higher density is more strongly affected by the centrifugal force and is pushed towards the cyclone wall. The lighter phase forms an inner spiral in the center of the cyclone, exiting through the top outlet. (Perry, 1984) Cyclones used in liquid-liquid separation are commonly known as hydrocyclones. They employ the same principle as all other cyclones and have slightly modified geometries to accommodate optimal flow profile formation inside the cyclone.

Cyclones can be used inside vessel type phase separators as the first stage of separation. Foam, having a very low density, can be separated and broken up by a cyclone at the inlet of the phase separator vessel. Foam can easily plug a demister pad or vanes if present in the gas stream. (Kalis, 2004) Centrifugal forces can also be utilized in phase separator vessels through the use of tangential inlets (Bahadori, 2014).

Inertial separators function by sharply altering the path of the fluid flow. Due to inertia, denser components in the flow are slower to react to changes in the flow path and thus collide and impinge on the inertial separator. In its simplest form, inertial separator is an impact plate placed on the path of a high velocity fluid flow as in Fig 4. (Perry, 1984) Coalescers and demisters discussed in the next section employ the same inertial principle.

2.2.3 Coalescing devices

A mist eliminator used to increase droplet size of the dispersed phase is referred to as a demister in the case of gas-liquid separation and a coalescer in liquid-liquid separation. Rather than standalone devices, coalescers and demisters can be mounted inside separation vessels to serve as additional stages of separation. The working principle of these devices is to slow down or stop the motion of droplets in the denser phase through forces of impingement, centrifugal motion and surface tension. In the simplest form this is achieved through a baffle placed perpendicular to the direction of the flow as in Fig 4. This is enough to break up larger slugs of liquid. (Soares, 2002) The usual configuration is a wire mesh or a set of vanes with a distinct geometry. (Fabian *et al.* 1993) The cut sizes of some demister designs are presented in Table I along with typical particle sizes generated by different phenomena.

TABLE I. Cut sizes of some demister elements with typical particle sizes for reference (Kalis, 2004)

Particle type	Size range, µm	Demister element	Size range, µm
Large organic molecules	< 0.004		
Smoke	0.0045 to 1.0		
Condensation fog	0.1 to 30	**Fiber candles or panels**	> 0.1
Atmospheric clouds and fog	4 to 50	**Mesh with coknit yarn**	> 2.0
Generated by gas atomization nozzle	1 to 500	**0.15 mm knitted mesh**	> 5.0
Atmospheric "mist"	50 to 100	**0.28 mm knitted mesh**	> 10
Atmospheric "drizzle"	10 to 400	**Double pocket vanes**	> 10
Generated by boiling liquid	20 to 1 000	**Conventional vane arrays**	> 15
Generated by 2-phase flow in pipes	10 to 2 000		
Atmospheric raindrops	400 to 4 000		

By constantly altering the path of the fluid flow, demisters and coalescers cause the droplets of the denser phase to collide with the wire mesh or vane walls. Surface tension forces keep the droplets attached to the metal surface and thus droplets start to coalesce on the surface. (Soares, 2002) The enlarged droplets are then pulled by gravity to the bottom of the vessel. By helping to remove small droplets from the continuous phase, the demister or coalescer makes it possible to shorten the dimensions of the separator vessel. Two examples of mist eliminators combining both mesh and vane units are shown in Fig. 7.

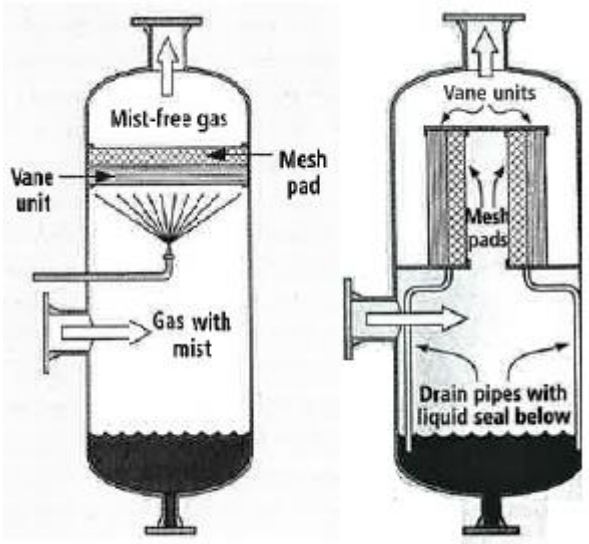

FIGURE 7. Demister configurations in a vertical phase separator (Kalis, 2004)

Left side of Fig. 7 shows a normal demister configuration with added spray system. The spray system can be useful in preventing fouling and plugging of the mist eliminator by more effective removal of deposits. In a case where fouling substances are present in the process, it is also beneficial to place the mesh unit downstream of the vane unit when using a two stage demister, as indicated by the left side of Fig. 7. Since the vane pack with more free volume is less likely to become plugged by deposits or flooded by sudden surges of liquid, it is able to reliably perform initial cleaning of the gas stream before the tighter mesh pad. Right side of Fig. 7 shows a typical retrofit design where effective surface area of an earlier demister has been increased by vertical placement in a vertical vessel. (Kalis, 2004) As with vertical vessels, demisters and coalescers can just as easily be utilized in horizontal vessels. To achieve even wetting of the demister in horizontal gas-liquid separators, the preferred orientation for the demister is also horizontal. This is illustrated in Fig. 8.

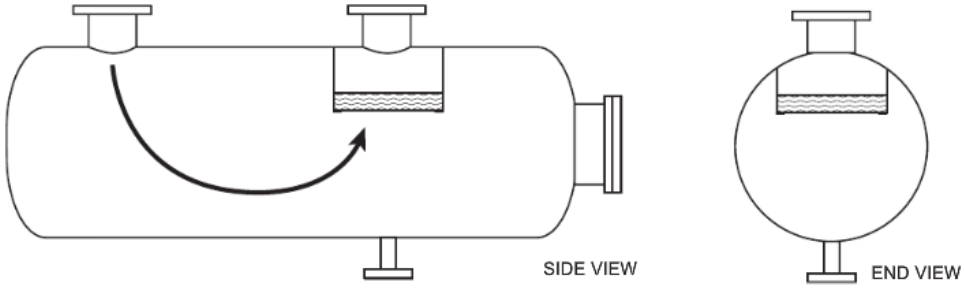

FIGURE 8. Placement of a demister inside a horizontal separator vessel (Moss & Basic, 2013)

The most important factor in utilizing the full separation potential of a demister or a coalescer is a unified flow profile. Velocity differences across the mesh or vanes can result in re-entrainment of the dispersed phase in some regions, while in other parts of the unit the flow of droplets is significantly lower than the unit could potentially handle. (Kalis, 2004; Fabian *et al*. 1993) Good performance is usually expected with velocities between 30% and 110% of the optimal velocity. Lower velocities do not allow the droplets to impinge on the demister surface, while higher velocities promote re-entrainment of already separated droplets (Couper *et al.* 2012). The inlet distributors introduced in the next section are crucial in the formation of the flow profile. Mesh pads are constructed from thin (0.08 - 0.40 mm) wires of either plastic or metal. Some indication of performance of different pad designs can be obtained by comparing the nominal surface areas, typical values range from 160 to 2000 m^2/m^3. (Moss & Basic, 2013)

Other means of affecting droplet size include employing an electric field. Electrostatic precipitators can be used for enhanced phase separation between two liquid phases in liquid-liquid or gas-liquid-liquid –separation. The electric field of these devices helps water droplets move closer to each other in a liquid phase thus promoting coalescence. Modern electrostatic precipitators are now able to handle even all-gas and all-water flows, which have previously often led to short circuiting of the electrodes. (Mhatre *et al*. 2015) Placement of a commercial Vessel Internal Electrostatic Coalescer (VIEC) unit for processing of crude oil is demonstrated in Fig. 9.

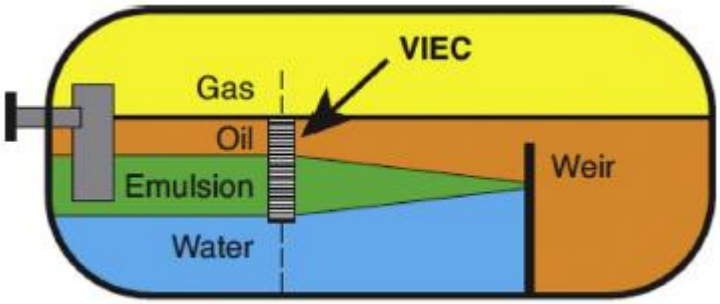

FIGURE 9. Placement of a commercial VIEC electrostatic precipitator unit inside a horizontal three-phase separator (Mhatre, 2015)

2.3 Inlet distributors and outlet geometry

Inlet distributors are essential in shaping the most important factor in gas-liquid separation, the velocity profile. In the simplest form, the inlet can be just a straight opening to the vessel without any distributor. When demands for phase separation efficiency increase, more complex inlet geometries to achieve an even flow distribution are required. According to Uki *et al.* (2012) an inlet distributor in a gas-liquid separator has three main functions:

- Reduce the momentum of the inlet stream and unify the flow profile inside the vessel
- Separate the bulk liquid phase from the gas phase
- Prevent droplet breakup and their subsequent re-entrainment

An example of poor velocity distribution due to inlet design is provided in Fig. 10.

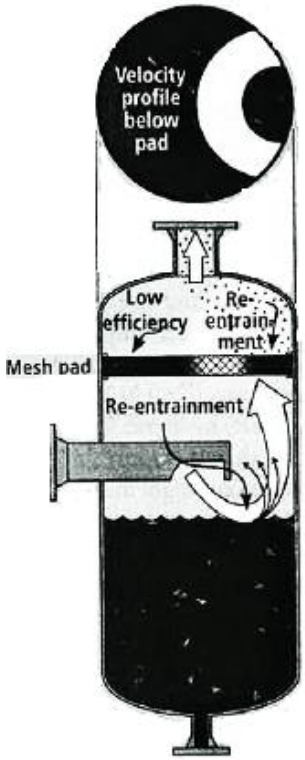

FIGURE 10. Example of poor flow velocity distribution due to inlet design in a vertical phase separator (Kalis, 2004)

Uneven flow distribution as illustrated in Fig. 10 can lead to a number of problems in the operation of the separator (Kalis, 2004):

- Re-entrainment of liquid in the gas flow due to agitation of the liquid at the bottom of the vessel.
- Less than optimal usage of demister separation capacity due to low flow velocity areas.
- Re-entrainment of liquid droplets from demister in high flow velocity areas.

A more sophisticated inlet design rectifying the mentioned shortcomings is presented in Fig 11.

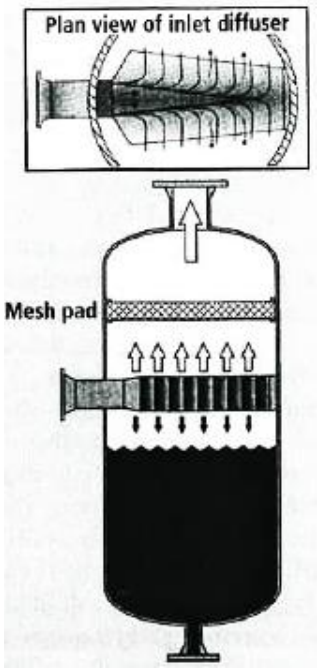

FIGURE 11. Example of an inlet distributor producing an even flow velocity distribution in a vertical phase separator (Kalis, 2004)

The advanced inlet design in Fig. 11 helps in utilizing the full potential of the demister by providing an even flowrate along the cross-sectional area of the vessel. Due to smaller openings, the pressure drop of a more complex design exceeds that of simpler design (Soares, 2002). In addition to the enhanced flow profile, inlet distributors may give additional benefits in separation. Depending on the fluid flow pattern in the distributor, strong inertial and centrifugal forces can be experienced by the droplets, which can lead to droplet coalescence. Mechanical strain on the vessel walls can also be decreased by spreading the inlet flow more evenly across the surface of the vessel. Inlet distributors, like the ones discussed above, can also be used in liquid-liquid separation. More typical, however, is to use impact and perforated baffle plates downstream of the inlet.

Flow velocity profile unification can also be conducted with the use of multiple inlets and outlets. For example, in horizontal vessels, flow can be introduced to the tank at opposite ends of the vessel with the outlet at the center of the vessel or vice versa with the stream introduced at the center of the vessel (Bahadori, 2014). Of the two outlets, the gas phase outlet design is more crucial to the operation of the phase separator in a gas-liquid separator. Sharp turns in fluid flow lead to increased flow velocity and enhanced mixing by increased turbulence. If the velocity increases in the direction opposite to gravity, re-

entrainment of droplets can occur. A selection of generally accepted simple inlet and outlet configurations for gas-liquid separators is presented in Appendix I (Kalis, 2004). Uki *et al*. (2012) introduced a way of determining the liquid outlet nozzle size through Froude number analysis. Froude number for the liquid outlet nozzle is calculated as

$$Fr = \frac{u_{0ut}}{\sqrt{gD_0}}. \quad (1)$$

Fr	Froude number
u_{out}	Liquid velocity in outlet nozzle, m/s
g	Gravitational constant, 9.81 m/s^2
D_o	Diameter of the liquid outlet nozzle, m

According to Uki *et al.* (2012) an outlet nozzle with a Froude number less than 0.31 is capable of self-venting any entrained gas left in the liquid. In the same study, the authors also stated that vortex formation is a possible reason for gas entrainment in the liquid phase. Vortex breakers are used to prevent vortex formation. Uki *et al.* (2012) suggest using two plates welded to a cross shape above the liquid outlet.

3. COMPUTATIONAL FLUID DYNAMICS

Computational fluid dynamics (CFD) is a field of engineering and science where computers are used to solve mathematically formulated problems related to fluid movement. CFD has been evolving as the combination of three existing fields of research: fluid dynamics, mathematics and computer science. At present, CFD is very much becoming a specialized field of its own. With the rise in popularity of commercial CFD programs, professionals more inclined to computer science are increasingly acting as code developers. The users of these programs include engineers and researchers from various fields. Before commercial software packages became available, the distinction between users and code creators was much shallower as users usually had to write their own programs. This is still partially the case, as the commercial programs are more or less general purpose oriented and therefore detailed research in a specific field often requires users to modify the equations to comply with given conditions. (Tu, *et al.* 2013)

Since all gases and liquids are classified as fluids, the field of application for CFD is immense. Frequent use for CFD can be found in e.g. the fields of chemical engineering (pipes and pumps), aeronautics, biomedical engineering (blood flow, breathing), environmental engineering (rivers) and energy technology (turbines, wind farms). Compared to experimental methods in these fields CFD has a few key advantages. Cost and time savings are obvious if by the use of CFD, pilot-scale modeling in development and troubleshooting can be cut down. Sometimes accurate real-life modeling can also be impractical or even impossible due to the scale of the studied phenomena or the extreme conditions. Often CFD can be seen as a complimentary approach to experiments, since interpretation of the results generated by means of CFD remains important, and false judgements on the results and their reliability can lead to disastrous consequences. Verification of suspicious results thus still remains an important field where real life experiments are needed. (Tu, *et al.* 2013)

3.1 Turbulence models

Turbulence, as described by Succi (2001), is the simultaneous presence of many active scales of motion that make the long and medium time span prediction of the fluid flow hard and computationally demanding. At a macroscopic scale, turbulence can often be visually seen in the flow streamlines. Mathematically, the various turbulent, transient and laminar regions can be identified by calculation of the Reynolds number as presented in Eq. 6. The particle diameter d represents the scale of the studied flow phenomena (Succi, 2001).

Turbulence modeling in general-purpose CFD calculations needs to be simple and robust. Some amount of accuracy can usually be sacrificed in engineering calculations over speed and applicability. (Tu *et al.* 2013) In terms of kinetic energy, turbulence can be described e.g. by terms k and ε which are commonly used in CFD-calculations. k describes fluctuation of kinetic energy in all coordinate directions while ε describes the rate of dissipation of k (García, 2008). The k-ω model substitutes the ε term for the ω term that describes the frequency of the large eddies. This leads to a turbulence model better suited for boundary layer flows near walls. The shear stress transport (SST) turbulence model combines the above mentioned models by utilizing k-ε –model at free flow and k-ω –

model near the walls. This results in better modeling of non-equilibrium boundary layer regions. All in all, no turbulence model has universal applicability. The much used k-ε – model is a good starting point, and further information on more sophisticated turbulence models should be sought, if need for their use arises. (Tu *et al.* 2013)

Various two equation turbulence models are only approximations and the most effective way to model turbulence is to directly simulate it. This approach is known as direct numerical simulation (DNS) and requires excessive computational power since eddies of all size scales need to be contained within the computational grid. A less computationally demanding way of working is to use the large eddy simulation (LES) approach. As the name indicates, only the motion of large scale eddies is directly simulated and the small scale eddies are numerically approximated. The use of LES can be justified if DNS cannot be used since the smaller scale eddies carry less energy and do not transport as much of the conserved properties as the larger eddies. For engineering work, DNS and LES are considered too accurate and therefore expensive. Their main usage is found in scientific research, upon which lighter and faster engineering tools can be constructed. (Tu *et al.* 2013)

3.2 Multiphase models

If a multiphase system needs to be mathematically modeled without resorting to a simplified single phase model, the phase volume fractions have an effect on the preferred approach. If one phase dominates the system by comprising more than 90% of the volumetric flowrate, the Euler-Lagrange approach should be considered. In one way coupled Euler-Lagrange approach, a large number of discrete phase particles are injected into the continuous phase. Only interactions from the continuous phase to the discrete phase are modeled and effects of the discrete phase on the continuous phase are neglected. This allows equations of the continuous phase to be solved completely before the discrete phase equations, making the approach less demanding for computational power. (Newton et al. 2007)

If two phases have roughly the same volumetric flowrate, the Euler-Euler approach is preferred. Both phases are modeled as continuous and interactions between the phases are

taken into account through interface exchange coefficients describing the momentum exchange. This approach demands much more computational power and thus the computational grid may need to be coarsened leading to decreased accuracy. Need for calculation power is further increased when more than two phases need to be calculated. In such a case simplification of suitable aspects should be considered. (Newton *et al.* 2007) Equipment-wise, a horizontal separator is usually employed in three-phase separation unless the gas volumetric fraction is unusually high (Monnery *et al.* 1994).

Volume Of Fluid methods (VOF) introduce a unique way of modeling multiphase systems in CFD calculations. In VOF methods, value for a specific marker function is calculated in each computational cell. This marker function indicates the volume fraction of a certain phase in a given cell. Values of 1 and 0 therefore indicate cells containing only a single phase if a two-phase system is considered. In dynamic simulations the movement of the phase interface can be tracked by monitoring the value of the volume fraction function in each cell. One problem with the VOF approach is the smearing of the phase interface, i.e. the interface grows progressively less sharp due to the calculation procedure of the marker function. This problem has been countered with the introduction of certain discretization techniques. Information on the interfacial tension between the phases is also needed in solving VOF calculations. Because of the nature of the interfacial phenomena, VOF simulations usually need to be run in three dimensions. This further increases the already high amount of computational power required in solving the VOF equations. If enough computational power is available to utilize a mesh fine enough to include small scale interfacial phenomena, VOF methods can be used to e.g. model droplet deformation. This information is crucial in accurate estimation of local mass and heat transfer coefficients. (Ranade, 2002)

Selection of multiphase model is influenced by the flow regime of the system as certain approaches are better suited for certain types of flow. In practice, the flow region often changes within the computational space, complicating the choice of the approach. Some development in CFD codes capable of detecting changes in flow regime and adapting the approach accordingly is currently conducted. (Vaittinen, 2015) Fig. 12 illustrates how flow within a single pipe can have multiple flow regions that make the simulation of such a flow accurately a very difficult task.

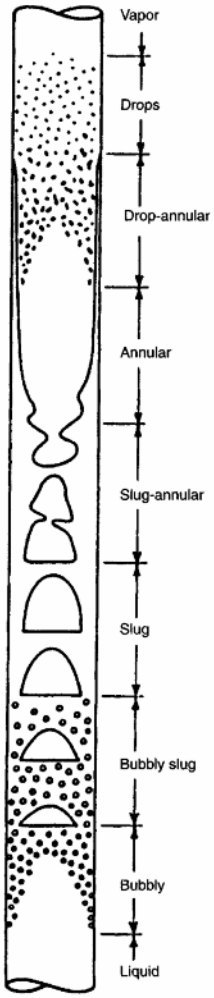

FIGURE 12. Example of pipe flow with multiple flow regions (Lyons & Plisga, 2005)

4. SIZING AND MODELING OF PHASE SEPARATORS

In this chapter, criteria concerning phase separator sizing are reviewed. First, different variables and their effect on the separation process are discussed. In the second section, commonly used sizing equations and considerations are presented. Finally, the key indicators for monitoring the performance of phase separators are reviewed.

4.1 Key variables

A number of different physical and chemical properties and process variables have an effect on the performance of phase separators. They form a basis for the selection and

design of the separator unit along with the separation criteria the unit is set to fulfill. The design and implementation of a separator unit starts with the definition of the degree of separation of the unit, i.e. what is the outlet flow from the separator. Before deciding to employ a separator unit, one should also consider the root cause behind the need for phase separation. By determining which process unit(s) causes the mixing of phases, its operating conditions (velocity, pressure, concentration etc.) can in some cases be modified to completely eliminate the need for a separator device.

4.1.1 Forces affecting a single droplet

There are three forces acting on a single free falling droplet at any given time. These forces and their directions are illustrated in Fig 13.

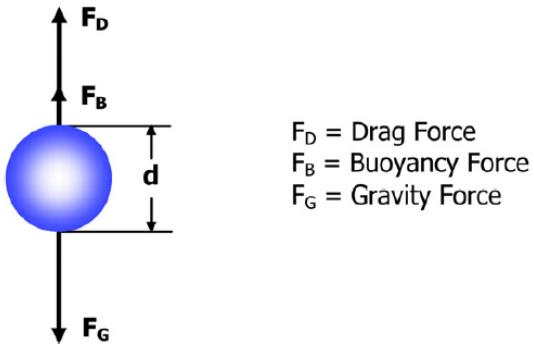

FIGURE 13. Forces affecting a single droplet in free fall (Wiencke, 2011)

In the model described by Wiencke (2011), the droplet is assumed to be spherical. Gravitational force acts in the downward direction and is defined as

$$F_G = \frac{1}{6}\pi d^3 \rho_l g. \quad (2)$$

F_G	Gravitational force, N
d	Droplet diameter, m
ρ_l	Liquid phase density, kg/m^3

Drag and buoyancy forces act in the direction opposite to gravitational force. According to Wiencke (2011) drag force is defined as

$$F_D = \frac{1}{2} C_D \left(d^2 \frac{\pi}{4} \right) \rho_g u^2. \quad (3)$$

F_D	Drag force, N
C_D	Drag coefficient (defined in Eqs. 7 and 8)
ρ_g	Gas phase density, kg/m^3
u	Droplet velocity, m/s

The buoyancy force depends on the properties of the gas phase and is defined according to Wiencke (2011) as

$$F_B = \frac{1}{6} \pi d^3 \rho_g g. \quad (4)$$

F_B	Buoyant force, N

Combining Eqs. 2-4 yields the terminal settling velocity u_t (Wiencke, 2011).

$$u_t = \sqrt{\frac{4gd(\rho_l - \rho_g)}{3C_D \rho_v}} \quad (5)$$

The terminal velocity u_t determines the maximum allowable velocity inside the separator vessel. If the velocity in the direction opposite to the settling direction is larger than u_t, settling does not occur and the particles are carried along by the continuous phase.

4.1.2 Flow region

Flow region in the separator vessel has an impact on the maximum allowable velocity by influencing the drag coefficient C_D in Eq. 5. The drag coefficient is an intricate term depending on viscosity and density of the gas phase, droplet size and particle velocity. These variables are included in the particle Reynolds number. (Wiencke, 2011)

$$Re_p = \frac{d \rho_g u}{\mu_g} \quad (6)$$

Re_p	Particle Reynolds number
μ_g	Gas phase dynamic viscosity, Pas

Depending on the flow regime, the Reynolds number has a different effect on the drag coefficient. A universal equation covering a wide Reynolds number range of $Re_p \leq 2\text{x}10^5$ is presented by Wiencke (2011):

$$C_D = \frac{24}{Re_p}\left(1 + 0.150Re_p^{0.681}\right) + \frac{0.407}{1+\frac{8710}{Re_p}}. \quad (7)$$

For laminar flow (Re_p < 0.1), the relationship between drag coefficient and Reynolds number is simpler (Wiencke, 2011):

$$C_D = \frac{24}{Re_p} \quad (8)$$

4.1.3 Temperature and pressure

Temperature affects the separation mainly by changing fluid viscosity. The dynamic viscosity μ decreases with increasing temperature (Dean, 1985). The Reynolds number in Eq. 6 is also affected by gas density, which decreases with rising temperature in constant pressure, and thus unambiguous rule on the effect of temperature is hard to define.

As with temperature, pressure has a slight effect on fluid viscosity. Pressure in the separator vessel is of importance when a demister is used. Demister pad or a vane pack in a gas-liquid separator has a certain pressure drop. Denser pads are typically more efficient, but have a higher pressure drop. If a downcomer pipe for the coalesced liquid is used, attention must be paid for the pressure drop not to create a vacuum that would suck liquid up through the pipe. (Lyons & Plisga, 2005). Sudden changes in pressure are also dangerous to the demister which can become dislodged and damaged (Kalis, 2004). In normal operation, the pressure drop across the demister is usually so low (< 250 Pa) that it is ignored in the vessel design (Moss & Basic, 2013).

4.1.4 Volume fractions

The volume fractions of the phases have an impact on both the equipment used in the separation and the methods used to model the system. Those methods are discussed in detail in section 3.2. In general practice, horizontal separator vessels are used when liquid is the dominant phase, since this minimizes fluctuation of the liquid level in the tank. Vertical vessels are preferred when gas is the dominant phase as the whole cross-sectional area of the tank is available for vapor disengagement. (Svrcek *et al.* 1993)

4.2 Sizing criteria for gas-liquid separators

The step by step procedure for the sizing of gravitational phase separators is roughly the same in many basic engineering handbooks. For example, descriptions by Bahadori (2014), Lyons & Plisga (2005), Couper *et al.* (2012), Wiencke (2011), Hall (2012) and Evans (1974) all list the same basic steps in obtaining separator vessel dimensions based on inlet stream properties and desired separation efficiency. Unless noted otherwise, the following procedure follows the descriptions by Evans (1974) and Hall (2012). The general procedure for sizing a vertical gas-liquid separator is explained first with the last sections highlighting differences when sizing a horizontal vessels and liquid-liquid separators.

4.2.1 Vessel orientation

There are two main factors to consider when deciding vessel orientation: the surge volume and the volumetric ratio of the phases. A horizontal vessel is best used when processing flows with large liquid fractions and large liquid surge volumes. The advantage of a horizontal vessel is the stability of the liquid level in the tank. With high gas to liquid ratio, a vertical vessel is preferred due to larger cross-sectional area available for vapor disengagement. A horizontal vessel is normally used in the separation of water and hydrocarbons. (Hall, 2012) In liquid-liquid separation a horizontal vessel is preferred due to shorter distance from the edges of the vessel to the phase interface (Couper, 2012).

4.2.2 Liquid surge volume

Evans (1974) provides a method for specifying separator vessel volume based on how well the process is controlled. Effective process control and monitoring systems reduce the needed tank volume because upsets in the process are identified and rectified faster. Tables II, III and IV list the factors given by Evans (1974) to describe the state of process control.

TABLE II. Instrument and labor factors affecting the necessary surge volume of a phase separator (Evans, 1974)

	Instrument Factor, F_1		Labor Factor, F_2 *		
Control Scheme	**With Alarm**	**No Alarm**	**Good**	**Fair**	**Poor**
Flow Ratio Control (FRC)	0.5	1.0	2.0	3.0	4.0
Level Ratio Control (LRC)	1.0	1.5	2.0	3.0	4.0
Temperature Ratio Control (TRC)	1.5	2.0	2.0	3.0	4.0

* Can be cut by 50 % in a competitive situation

TABLE III. External unit factor affecting the necessary surge volume of a phase separator (Evans, 1974)

Operating Characteristics	**Factor, F_3**
Good control	2.0
Fair control	3.0
Poor control	4.0
Feed to or from storage	1.25

TABLE IV. Level monitoring factor affecting the necessary surge volume of a phase separator (Evans, 1974)

Drum Level Visibility	**Factor, F_4**
Board-mounted level recorder	1.0
Level indicator on board	1.5
Gage glass at equipment only	2.0

Table II contains factors based on the controllability of the inlet flow to the vessel. When determining the factors, the control scheme is selected first. A more slowly reacting control scheme leads to a higher instrument factor, with a lack alarm further increasing it. The ability of the operators to control the inlet flow is similarly evaluated. The controllability of the outlet liquid flow is evaluated when assigning a value for the coefficient F_3 in Table III. Last, the ability of the controller to monitor the separator vessel level is considered

when determining factor F_4 in Table IV. The surge volume is then determined by the equation

$$V = 2F_4(F_1 + F_2)(Q_{in} + F_3 Q_{out}). \quad (9)$$

V	Separator vessel volume, m^3
Q_{in}	Inlet flow, m^3/min
Q_{out}	Outlet flow of heavy phase, m^3/min
$F_{1,2}$	Instrument and labor factors, min
$F_{3,4}$	External unit and level monitoring factors

The coefficient 2 in Eq. 9 is due to the surge volume being calculated based on a half full vessel. According to Hall (2012), half full refers to either half of the vessels total volume, or in case there is a high level shutoff, half of the maximum allowed liquid volume. Although the above described procedure gives good specifications for vessels with modern control systems, old rules of thumb can still be applied when needed. Couper *et al.* (2012) states that knockout drums before compressors should be sized to hold an inlet liquid flow for 10-20 minutes while half full and fired heater surge drums for up to 30 minutes. For other uses 5-10 minutes is sufficient. Typical liquid retention times inside gas-liquid separators in normal operation are in the range of 30 s to 10 min (Laleh *et al.* 2012). Gas retention times are much shorter and measured in seconds if gas is the dominant phase.

4.2.3 Gas velocity

For vessels without a demister, the gravity settling can be calculated by using Eqs. 5-8. The maximum allowable gas velocity $(u_g)_{max}$ is determined by the terminal velocity u_t of a selected size droplet.

To protect sensitive equipment such as compressors or to minimize liquid entrainment for any other reason, additional devices like demisters should be used to increase separation efficiency. Adequately designed wire mesh demister raises the separation efficiency to at least 99%. Since separation by demister is based on inertia, higher gas velocity improves separation. On the other hand, accumulated liquid in the demister pad has to be able to drain against the incoming gas flow. Hence flooding of the demister pad sets the limit to

the maximum gas velocity. Demisters are sized to a certain flooding limit same way as distillation packing. Flooding point of demister pad depends on its free volume. In practice for vessels with a demister, the following type of a short-cut equation derived from Eqs. 5-8 to calculate the demister diameter is normally used (Hall, 2012):

$$\left(u_g\right)_{max} = K\sqrt{\frac{\rho_l - \rho_g}{\rho_g}} \tag{10}$$

K maximum allowable velocity coefficient, m/s

Eq. 10 can also be used for sizing vessels without a demister if suitable *K*-values are used. The *K*-value is based on demister properties, process conditions and separation requirements. Couper *et al.* (2012) have listed typical *K*-values for separators equipped with demister pads of various efficiencies. These are presented in Table V.

TABLE V. Typical *K*-values for separator vessels fitted with wire mesh demisters (Couper *et al.* 2012)

		Specific surface area,	K, m/s	
Efficiency, %	**Density, kg/m^3**	**m^2/m^3**	**Under pressure**	**Vacuum**
Low (99.0%)	80-112	213	0.122	0.061-0.082
Standard (99.5%)	144	279	0.107	0.061-0.082
High (99.9%)	192	377	0.107	0.061-0.082
Very high (>99.9%)	208-224	394	0.076	0.061-0.082

4.2.4 Vessel and demister dimensions

The minimum cross-sectional area for the demister or the vessel is calculated based on the gas flow rate Q_g and maximum design gas velocity $(u_v)_{max}$ (Evans, 1974).

$$A_{min} = Q_g/\left(u_g\right)_{max} \tag{11}$$

A_{min} Minimum cross-sectional area of the vessel or demister, m^2

Q_g Inlet gas flowrate, m^3/s

Actual diameter of the vessel is calculated noting the liquid surge volume as calculated in section 4.2.2 and may be bigger than the demister diameter. The minimum diameter is determined through simple geometrical calculation. It should be rounded up to the next largest practical size. (Evans, 1974)

$$D_{min} = \sqrt{4(A_{min})/\pi} \tag{12}$$

D_{min} Minimum vessel or demister diameter, m

Nozzle sizes are determined using the average density variable ρ_{mix} (Evans, 1974).

$$\rho_{mix} = \frac{Q_g + Q_l}{\left(\frac{Q_g}{\rho_g}\right) + \left(\frac{Q_l}{\rho_l}\right)} \tag{13}$$

ρ_{mix} Average density, kg/m^3

According to Evans (1974), inlet nozzle maximum and minimum velocities can be estimated respectively with the empirical correlations

$$(u_{max})_{nozzle} = 30\sqrt{\rho_{mix}} \tag{14}$$

and

$$(u_{min})_{nozzle} = 18\sqrt{\rho_{mix}}. \tag{15}$$

$(u_{min})_{nozzle}$, $(u_{max})_{nozzle}$ Inlet nozzle velocities, m/s

According to Hall (2012), the inlet nozzle cross-sectional area can be determined as

$$A_{nozzle} = \frac{Q_g + Q_l}{\rho_{mix} u}. \tag{16}$$

A_{nozzle} Inlet nozzle cross sectional area, m^2

u Inlet velocity $(u_{min})_{nozzle} < u < (u_{max})_{nozzle}$, m/s

The velocity *u* should be selected so, that a practical inlet nozzle size is calculated (Hall, 2012). Position of the inlet nozzle can be determined based on the dimensions specified in Fig. 14.

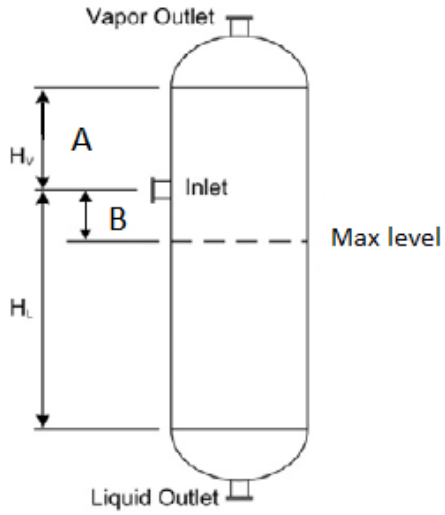

FIGURE 14. Inlet nozzle spacing in a vertical separator vessel (Hall, 2012)

Hall (2012) gives the following criteria for the inlet nozzle spacing factors A and B in Fig. 14.

A – The vertical distance between the inlet nozzle and the top of the vessel

- 910 mm + 0.5 x Inlet nozzle outer diameter
- Minimum 1220 mm

B – The vertical distance between the inlet nozzle and the maximum liquid level (Calculated based on the result of Eq. 9.)

- 300 mm + 0.5 x Inlet nozzle outer diameter
- Minimum 460 mm

Last, the total height H_v + H_l needs to be checked against the vessel diameter calculated earlier. The ratio of total height to diameter should be between 3 and 5. To bring the ratio up to 3, excess surge volume may be added to increase total height of the vessel. If the ratio is larger than 5, a horizontal vessels should be used instead. (Evans, 1974)

4.2.5 Horizontal separators

A horizontal separator vessel should be considered early on in the design process if inlet gas to liquid ratio is low and/or a large surge volume is required (Hall, 2012). This is mainly to prevent rapid rising of the liquid level during process upset conditions. Before making the final selection, a few drawbacks of a horizontal vessel should be considered (Stewart & Arnold, 2008):

- Solids removal from horizontal vessels is troublesome. Accumulated solids can easily be removed from a single outlet at the bottom of a vertical vessel, but not from the horizontal vessel.
- Horizontal vessel requires more area at plant site.
- Sized for the same steady state flow rate, a small diameter (< 1.5m) horizontal vessel has less liquid surge volume than a vertical vessel.
- Level indicators and other instruments are more closely spaced in a horizontal vessel. This can be a problem if there is turbulence on the gas-liquid interface.

Due to lack of upward drag on the droplets, the maximum design gas velocity $(u_g)_{max}$ inside a horizontal vessel can be slightly higher than in a vertical vessel (Couper *et al.* 2012). The terminal velocity u_t calculated in Eq. 5 indicates the absolute maximum value which cannot be exceeded.

Minimum cross-sectional area obtained by solving Eq. 11 corresponds to the cross-sectional area available for vapor disengagement. As a rule of thumb, the gas volume inside the vessel must be at least 20% of the vessel volume when it is full. Additionally, the gas should occupy at least 300 mm of space at the top of the vessel. Therefore the minimum total cross-sectional area for a horizontal vessel is according to Hall (2012) and Evans (1974)

$$(A_{total})_{min} = \frac{A_{min}}{0.2}. \tag{17}$$

$(A_{total})_{min}$ Minimum total cross-sectional are for a horizontal vessel, m^2

The minimum diameter D_{min} is then obtained as for vertical vessels through solving Eq. 12. The requirement for 20% gas volume in the tank needs to be also taken into account when calculating the total vessel volume by Eq. 9 (Hall, 2012).

$$V_H = \frac{V}{0.8} \tag{18}$$

V_H Total vessel volume for horizontal vessel, m^3

The length of the horizontal vessel is determined according to Evans (1974) by solving

$$L_H = \frac{V_H}{(\pi/4)D_H^2}. \tag{19}$$

L_H Length of the horizontal vessel, m

D_H Diameter of the horizontal vessel, m

The vessel diameter D_H should be determined as the next largest practical size from D_{min} . Last, the length to diameter ratio should be checked. If the L/D ratio is under 3, the length of the vessel can be increased which leads to an increased surge volume. If the ratio is over 5, diameter of the vessel can be increased which leads to a decrease in gas velocity. (Hall, 2012)

4.3 Sizing criteria for liquid-liquid separators

The typical configuration for a liquid-liquid separator is a horizontal vessel operating full of liquid. Exceptions include some low flow rate operations and very high flowrates at near atmospheric pressures as in mixer-settler units. In those cases a vertical vessel with an overflow weir can be used. The advantage of a horizontal vessel, as opposed to vertical, in liquid-liquid separation is the shorter distance the droplets have to travel in order to be separated. (Couper, 2012)

Stokes' law governs the rise and fall rates of two immiscible liquids (Stewart & Arnold, 2008).

$$u_t = \frac{5.56x10^{-10}(\Delta SG)d^2}{\mu} \quad (20)$$

u_t	Terminal settling velocity, m/s
ΔSG	Specific gravity (relative to water) difference between phases, -
d	Droplet diameter, µm
μ	Viscosity of the continuous phase, mPas

Retention time, determined by the inlet flow rate and vessel dimensions, is the single most important factor in liquid-liquid separation. The length of the horizontal separator vessel should be such that particles larger than the determined cut-off size have sufficient time to reach the phase interface. (Couper, 2012) For example in oil-water systems, the viscosity value in Eq. 20 receives different values depending on which phase is considered continuous. Therefore separation of oil droplets from water is easier than water droplets from oil. The vessel length should be selected based on the phase that has the more strict purity requirements. (Stewart & Arnold, 2008) Typical separation times for liquid systems that do not form emulsions are in the range of 5 to 10 minutes (Towler & Sinnott, 2013).

The diameter of the vessel should be such that the lateral velocity does not increase to a level where it inhibits phase separation. The hindrance caused by the lateral fluid motion can be estimated through calculation of the continuous phase Reynolds number. (Couper, 2012)

$$Re = \frac{D_h u \rho}{\mu} \quad (21)$$

D_h	Hydraulic diameter, m
u	Lateral velocity of the continuous phase, m/s
ρ	Density of continuous phase, kg/m^3
μ	Dynamic viscosity of the continuous phase, Pas

Little or no hindrance should be expected when Reynolds number is below 5 000. The negative effects increase above this value and poor separation is expected at latest when the Reynolds number reaches 50 000. (Couper, 2012) Disturbances caused by the inlet

fluid flow should be minimized by designing the inlet for a maximum velocity of 1 m/s (Sinnott, 2005).

A phase interface, where the droplets migrate towards their respective phases, is formed between two immiscible liquid phases after the initial phase separation. The design of a liquid-liquid separator should be such that the interface does not extend to the bottom or the top of the vessel. For sizing purposes, the thickness of the interface zone is usually assumed as 10% of the vessel height. (Sinnott, 2005) The accumulation of emulsion on the phase interface can over time reduce the efficiency of a liquid-liquid separator. The unseparated emulsion layer reduces the height of the other liquid layers and thus decreases retention times. The application of de-emulsifying chemicals and/or heat are the most common ways to overcome this problem. (Stewart & Arnold, 2008)

4.4 Sizing criteria for three-phase separators

Three-phase separation involving solids is not discussed in the scope of this review. Instead, three-phase separation is used to refer to a system where a gas phase and two immiscible liquid phases are separated.

A system of overflows is usually required in a three-phase separator. The separation of the two liquid phases follows the same principle as in two-phase liquid-liquid separation where retention time is the governing variable. If overflows are used, either in two-phase or three-phase separation, the retention volume used in calculation of the retention time must be specified as the volume where the liquid phases are in contact with each other. Once the liquid is directed to a separate compartment, albeit inside the vessel, it is no longer considered part of the retention volume. (Lyons & Plisga, 2005) The gas-liquid interface in three-phase separation is usually assumed to be situated at the centerline in horizontal separators to maximize the interfacial area but variation to either direction is not uncommon (Laleh, 2012).

Typical retention times for liquids in three-phase separation are in the range of 2 to 10 minutes. In crude oil processing where oil, water and gas are separated, the retention times can extend even to two hours. (Laleh, 2012)

4.5 Performance indicators

In the following subsections, the most important phase separator performance indicators are discussed. These are factors by which the performance of different separators can be compared.

4.5.1 Velocity profile

Velocity profile is usually of primary interest when visual representations of CFD-calculations are presented. Visually, the velocity profile can be assessed in two different ways. When using streamlines, the density of the streamlines in a given region typically represents the flowrate while the color of the lines represents flow velocity. Another approach to visual representation is the visualization of planes, where colors on the plane indicate velocities at different points. Planes are particularly useful when extracted at key points where velocity profile has the largest impact on the overall performance of the separator. These include e.g. demister inlets, where the velocity profile should be as uniform as possible to ensure optimal performance of the device (Kalis, 2004). In addition to the evenness of the profile, attention should also be paid to regions where the velocity exceeds critical velocity. Mathematically, the evenness of the flow profile can be described e.g. by standard deviation of velocities in a given plane represented by the equation

$$s_n = \sqrt{\frac{\sum_{i=1}^{n}(x_i - \bar{x})^2}{n}} \tag{22}$$

s_n	Standard deviation
x_i	Value at data point i
$\bar{x}$	Mean value over all data points
n	Number of data points

4.5.2 Entrainment

Ultimately, the purpose of the separator is to separate phases into their respective outlets. The success in this task is usually measured through the entrainment value which indicates

how much of the separated phase escapes through the wrong outlet. Mathematically entrainment is defined as (Sinnott, 2005)

$$\psi = \frac{flow\ of\ entrained\ component\ a}{total\ inlet\ flow\ of\ component\ a}. \quad (23)$$

ψ Entrainment value

Concentrations can also be used in place of mass flows in Eq. 23. Actual multiphase modeling of separators is complicated and computationally expensive in CFD calculations (Newton, 2007). Therefore, the indicators mentioned in the earlier chapters are more widely used as performance indicators in CFD calculations. However, entrainment value remains a valid tool for estimating the performance of separators in real-life experiments, where e.g. the moisture entrained in a gas flow can be captured by a filter and quantitatively measured.

4.5.3 Wall shear stress

Wall shear stress is defined as the force applied to wall when it is affected by a fluid moving tangentially at the wall surface. The force is proportional to the kinetic energy per unit volume of the fluid and is therefore dependent on fluid density. (Schaschke, 2014; Case *et al.* 1999)

$$\tau = F/A \quad (24)$$

τ Wall shear stress, Pa

F Force in a tangential direction to the surface, N

A Area of the surface, m^2

Wall shear stresses are useful indicators in assessing the mechanical durability of the design. High shear stress areas can indicate places of possible wear damage inside the vessel and pipes. These are also the most likely areas to experience corrosion if corrosive substances are handled by the unit.

5. LITERATURE REVIEW: CFD-STUDIES ON PHASE SEPARATORS

This chapter reviews the current state of research on the field of gravitational phase separation. Overall, vast majority of studies that utilize CFD are related to packed bed columns. Studies on reactors, e.g. fluidized bed reactors, are also abundant. Experimental studies on phase separator vessel performance are surprisingly scarce, given the possibilities CFD offers as a modeling tool. The fact that most of the vessel internal components, such as distributors, are patented solutions further decreases the public availability of related studies. Four of the most relevant studies found in the conducted literature search in the field of gravitational phase separation technology are presented in the following sections. A summary of methods used in the studies is presented in Table VI.

TABLE VI. Summary of methods used in reviewed studies

Study	Purpose	Dimensions	Steady/ Transient	Turbulence model	Single/ Multiphase	Software
Chekmenev *et al.* 2010	Comparison of internal structures of a gas-liquid separator vessel	Unspecified	Unspecified	Unspecified	Multiphase, unspecified	Star CD
Liu *et al.* 2007	Optimization of a distributor geometry in a packed bed column	3D	Transient	k-ε	Multiphase, Euler-Lagrangian	FLUENT
Wilkinson *et al.* 2000	Optimization of baffle geometry in liquid-liquid separation	2D	Steady state	k-ε	Single liquid phase	Phoenics V1.5
Al-Fulaji *et al.* 2014	Simulation of wire mesh demisters	2D	Steady state	k-ε	Multiphase, Euler-Euler	FLUENT 6.3

5.1 Study of Chekmenev *et al.*

Chekmenev *et al.* (2010) studied the effects of inlet, outlet and demister configurations on separation efficiency in a two-phase vertical separator. Using the finite element method in Star-CD program they modelled gas-liquid separation in four different configurations. Liquid droplets were modelled as “packets” with specific density and size distribution. In addition to the movement of these “packets”, gas flow rate and pressure differences inside the vessel were monitored. The studied configurations are shown in Fig. 15.

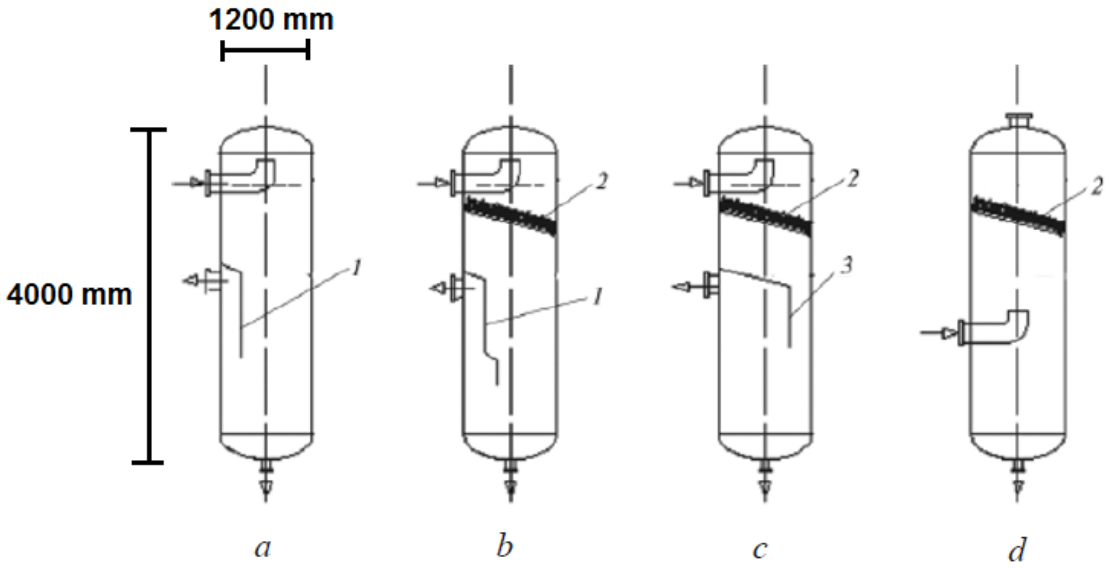

FIGURE 15. Separator configurations studied by Chekmenev *et al.* (2010)

In Fig. 15, (1) denotes a pocket for the outlet, (2) denotes the demister which was modeled as a porous media and (3) denotes a baffle which covers most of the cross-sectional area in the vessel. Contrary to general practice, flow enters the vessel at the top, except in configuration (d). Positioning of the demister at a 30° angle allows for more surface area and promotes runoff of entrained liquid droplets.

Positioning the inlet pipe to discharge the inlet flow upward was found to yield a sufficiently uniform flow profile in the demister. Outlet pocket designs in configurations (a) and (b) were found to hinder separation efficiency by creating a rarefaction zone at the outlet that draws droplets out through the gas outlet. No such effect was observed for the baffle in configuration (c). Instead, the narrowed gas flow field was found to enhance separation by increasing the velocity in the sharp turn to the outlet.

Separation efficiencies obtained for different sized droplets are shown in Table VII.

TABLE VII. Separation efficiencies obtained by Chekmenev *et al.* (2010) for different sized droplets using 85 % of the maximum allowable load for the demister

Separator design, (see Fig 15)	**Efficiency (%) of separation of particles with diameter, mm**			
	0.05	**0.5**	**0.7**	**1.0**
a	17.1	95	99	99.3
b	15.8	97	100	100
c	28.1	100	100	100
d	18.8	100	100	100

Chekmenev et al. (2010) concluded that separator design (c) with baffle and a demister was overall the most recommendable choice based on its separation efficiency. Additional remarks included positioning the inlet pipe sufficiently far (minimum 600 mm) from the demister to avoid distorting the flow profile in the demister. The recommended minimum distance between the demister and the pocket for the outlet was found to be 300 mm also for the same reason.

5.2 Study of Liu *et al.*

Liu *et al.* (2007) studied the gas-liquid flow distribution in a two directional vapor-horn distributor using a finite volume solver in FLUENT software. Two-phase modeling was conducted by employing the Euler-Lagrangian multiphase model and injecting liquid particles at the inlet. Although the study was related to packed columns, flow profile characteristics are equally important also in separator vessels.

In the study, a computational model was first created based on experimental measurements on a 1 m diameter laboratory scale column. Good agreement between experimental data and the model was observed. The model was applied to optimize various parameters of a distributor in a 7.4 m diameter commercial scale column. A schematic drawing and the computational grid of the laboratory scale distributor are shown in Figs. 16 and 17 respectively to illustrate the structure of the two directional vapor-horn.

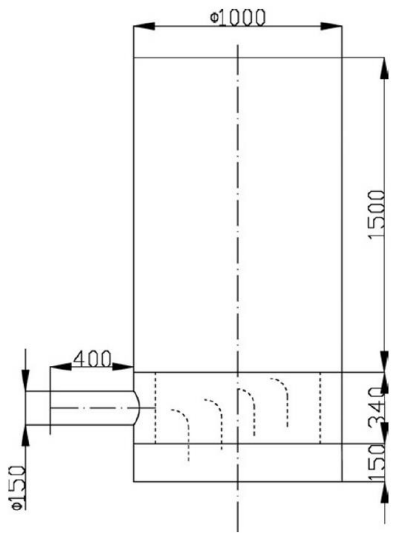

FIGURE 16. Schematic drawing of the laboratory scale two directional vapor-horn distributor, Liu *et al.* (2007)

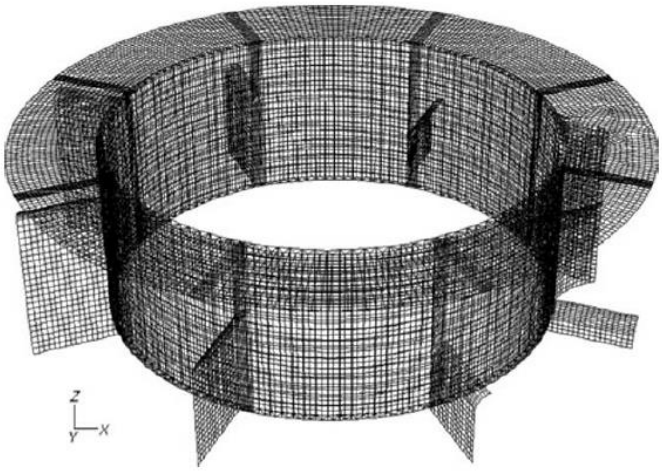

FIGURE 17. Computational grid used by Liu *et al.* (2007) to model a two directional vapor-horn distributor (8 vanes, radial slope angle 0°)

The modified parameters in the full scale design included number of vanes, radial slope angle of the vanes and space between the inside cylindrical wall and the tower wall (Δr in Fig 18). Performance indicators were maldistribution factor, entrainment rate, and pressure drop. The gas feed velocity was set to 40 m/s and the volumetric liquid to gas ratio to 1.2.

Increasing the number of vanes with 0° radial slope angle and 1.3 m between the distributor and vessel walls was observed to lead to an improved distribution and decreased entrainment rate in the 6-20 vanes region. Pressure drop was unsurprisingly increased with increasing number of vanes. Fig. 18 illustrates the effect of the radial slope angle.

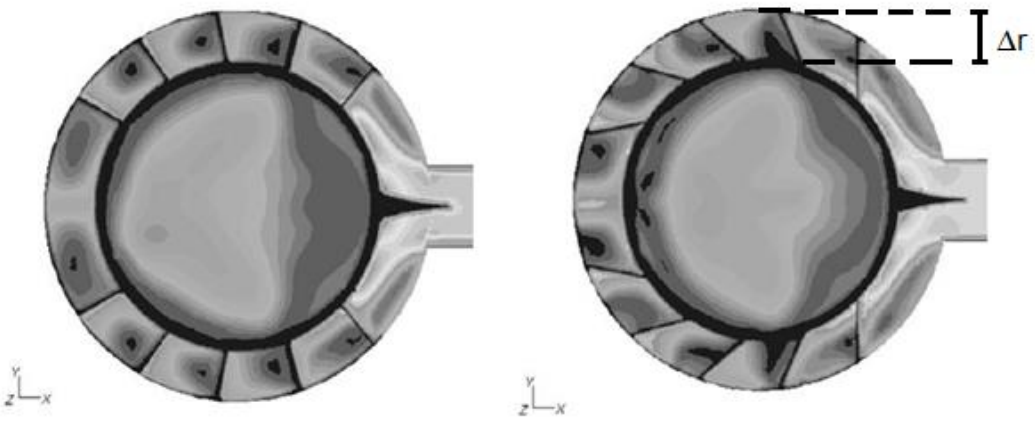

FIGURE 18. Effect of the radial slope angle on the distributor geometry with 10 vanes, 10° (left) and 45° (right), color indicates velocity profile, Liu *et al.* (2007)

With 10 vanes and 1.3 m between the distributor and vessel walls, radial slope angle of 30° was found to be optimal. In the simulation this angle led to the best flow distribution with least amount of entrainment while also yielding the lowest pressure drop.

The effect of space between the inside cylindrical wall and the tower wall was studied by varying the distance between 0.6 and 1.6 meters with 10 vanes at a 30° radial slope angle. Distribution was the most even in the region between 0.9 and 1.2 meters. Pressure drop and entrainment rate decreased as the space was increased. Therefore the authors concluded that a distance of 1.2 m is optimal between the vessel and the distributor walls in the studied configuration. The authors claim that the developed model is valid on any length scale. The model could therefore be used in designing also separation equipment that are often smaller in scale than the commercial sized column in the study.

5.3 Study of Wilkinson *et al.*

Wilkinson *et al.* (2000) studied the effect of baffle plate configurations in horizontal liquid-liquid separators. CFD-modeling was conducted using a two dimensional single phase model. The k-ε turbulence model was used because local velocities were much higher than the superficial velocity and the flow through the baffle holes was turbulent in many cases. The simulation results were compared with measured experimental data from a larger separator vessel. Flow vectors within a certain region in the separator were monitored using laser-, light- and acoustic-based Doppler measurements and compared to simulated values. Uniformity of flow was described as a good indication of appropriate separator performance since it indicates plug flow conditions inside the vessel. Two factors were considered: modifying the baffle free area and adding a second baffle at varying distances at the inlet. Schematic drawings of the CFD model and the experimental separator are presented in Figs. 19 and 20, respectively.

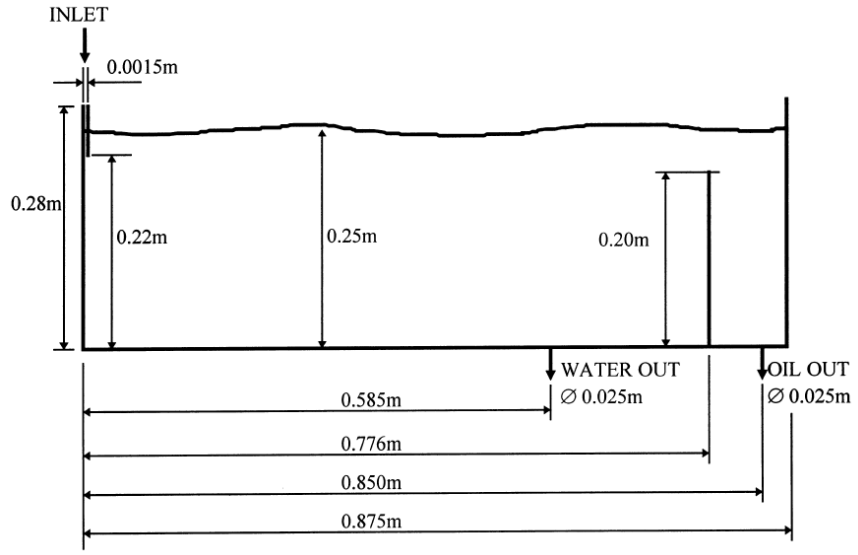

FIGURE 19. Schematic drawing of the CFD model used by Wilkinson *et al.* (2000)

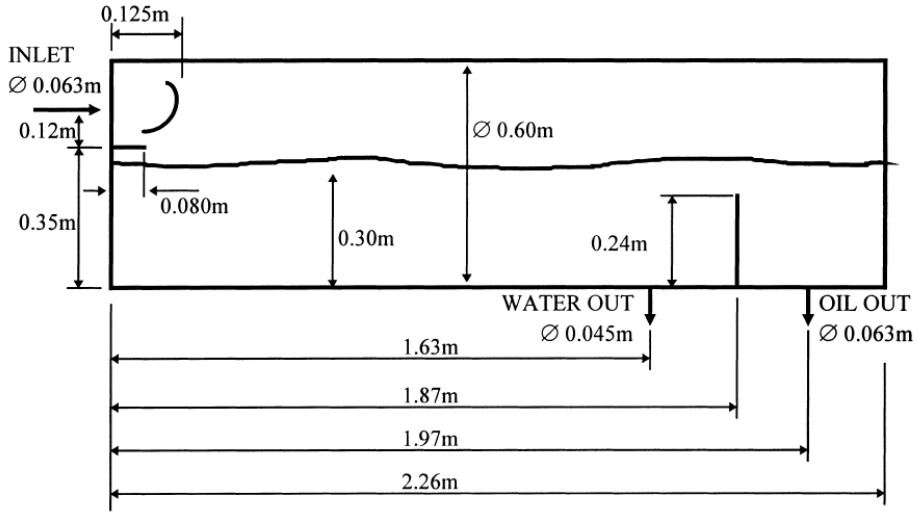

FIGURE 20. Schematic drawing of separator vessel used by Wilkinson *et al.* (2000) for experimental measurements

Baffles with varying free surface area were placed at 0.30 m from the inlet. In the multiple baffle study, the downstream baffle was placed at 0.60 m from the inlet with the additional baffle location varied between 0.10 - 0.55 m from the inlet. As seen in Figs. 19 and 20, apart from the scale, the inlet configurations also vary between the CFD model and the experimental vessel. The effect of this deviation is diminished by the fact that all experiments, excluding some reference measurements, were conducted using only a water phase.

When studying the flow field at 0.6 m from the inlet with baffles of varying free area at 0.3 m from the inlet, Wilkinson *et al.* (2000) found that experimentally a baffle with 10% free area resulted in the most uniform velocity distribution between free areas of 5, 10, 15 and 20%. In the CFD model, the best velocity distribution at 0.5 m downstream from the inlet was observed using a baffle with 20% free area. Experimental flow measurements at 0.3 m from the downstream baffle in the dual baffle measurements indicated that no significant advantage is gained from using two baffles unless they are less than 0.1 m apart.

Wilkinson *et al.* (2000) also noted that varying the hole size of a baffle with constant free area results in no significant change in flow profile even if the flow through the holes changes between laminar and turbulent. Because the CFD model and the experimental measurements failed to indicate a uniform optimal free area value, the authors believe there is limited usability for the CFD model as such in studying baffled separators.

5.4 Study of Al-Fulaij *et al.*

Al-Fulaij *et al.* (2014) studied wire mesh demisters in multistage flash desalination plants with CFD modeling using an Euler-Euler two-phase approach in FLUENT 6.3. Equations were solved using the finite volume approach and a pressure–based solver that is suitable for low speed incompressible flows.

The purpose of the demister in this case was the removal of brine droplets from fresh water vapor. The brine droplets and the gas were modelled as separate phases, each with their own set of continuum equations. The demister was modelled as both a porous media zone and a tube bank. A schematic drawing of the two 2D-models is presented in Fig. 21.

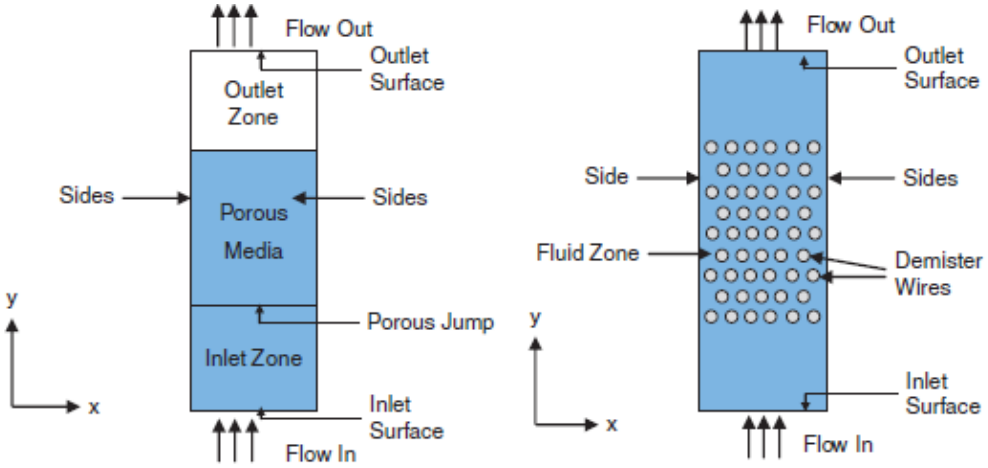

FIGURE 21. Schematic drawings of the models used by Al-Fulaij *et al.* (2014). Length in the y-direction: 150 mm, width in the x-direction: 30 mm.

The main assumption in the model of Al-Fulaij *et al.* (2014) was the inclusion of a mass sink boundary condition around the demister wires for brine droplets. This simulates the removal of the brine droplets from the fresh water vapor flow and thus it requires knowledge of the demister separation efficiency. This limits the use of this model to the study and troubleshooting of existing demisters and excludes the use in designing new units. Boundary conditions included specified flow conditions at the inlet, specified pressure conditions at the outlet and geometrical symmetry at the sides. For the porous media approach a porous jump condition was placed at the entrance of the demister. In the tube bank approach the porous jump condition was replaced by wall boundary condition at the demister wires.

Grid analysis was performed for both the porous media and tube bank models, where an optimal number of cells was obtained. The simulation of the tube bank approach included the use of a zone of triangular cells around the tubes, otherwise the cells were quadratic.

Both models were validated against experimental data from an existing multistage desalination plant. Accuracy of both models was found better than an existing empirical correlation by El-Dessouky *et al.* (2000):

$$\Delta P = 3.88178 \rho_p^{0.375798} u_g^{0.81317} d_w^{-1.56114147} \tag{25}$$

ΔP Pressure drop, Pa

ρ_p	Packing density, kg/m^3
u_g	Gas velocity, m/s
d_w	Diameter of the wire, mm

The validated model was used to study the effect of various parameters on the pressure drop across the demister. For each parameter study, vapor velocities from 2 to 6 m/s were simulated. If all other parameters remain constant, an increase in vapor velocity leads to an increased pressure drop.

A slight indirect effect of temperature change on the pressure drop was observed, where increase in temperature leads to gas expansion and thus increased velocity and pressure drop. Pressure drop was also found to increase with the decrease in face permeability, which describes the capacity of the porous media face to transport fluid. Decreasing this value leads to increased resistance on the surface and thus increased pressure drop. Finally, the effect of volume fraction of water droplets in the vapor flow was studied. The pressure drop was found to increase when the volume fraction was increased. This is due to liquid accumulation in the demister which leads to increasing resistance to the vapor flow.

EXPERIMENTAL PART

The purpose of the calculations in the experimental part was to evaluate the effect of design geometry of the separator vessel on separation efficiency. The changes in geometry included inlet distributors, vessel dimensions, demister support structures and outlet configurations. The main body of the work was conducted as steady state single phase calculations, where the separation efficiency of each configuration was evaluated based on flow velocities and flow profile uniformity. Additional dynamic simulations were performed to evaluate the amount of time based fluctuations in the solutions. Two-phase calculations were performed to obtain data on how the introduction of a second phase affects the flow inside the separator. One target for single and two-phase calculations of separators was to get experience and guidelines on how to model similar equipment in future research.

6. SOFTWARE AND COMPUTERS

A set of different software tools, each with their own specific task in the simulation process, were utilized in the experimental part. MicroStation® V8i was used in geometry creation. CFD calculations were conducted using OpenFOAM open source CFD software package. A commercial HELYX® package by Engys (http://engys.com/products/helyx), based on the OpenFOAM source code was utilized for its graphical interface and some additional computational features. Post processing and visualization of the results was mainly conducted using ParaView software.

6.1 Geometry generation

Geometry generation was conducted using Microstation® V8i version 08.11. Geometries from Microstation® were exported to OpenFOAM as STL-files which are essentially sets of triangles. Resolution of the STL-files was set high enough for edges to appear visually smooth. This was achieved by setting the maximum edge length of the triangles to 8 mm.

6.2 CFD calculations

Computational tasks were performed using OpenFOAM source code based software. OpenFOAM in itself is an open source free software package licensed and distributed by the OpenFOAM Foundation (http://www.openfoam.org/). In this work, a special commercial version of the OpenFOAM package, HELYX® by Engys was used. HELYX® contains a graphical user interface (GUI) and has some modified algorithms e.g. for mesh generation as compared to free OpenFOAM distributions. The utilized OpenFOAM versions were OpenFOAM 2.2_engysEdition-2.0 and engysEdition-2.2.

6.3 Visualization of the results

Visual data representation was performed using ParaView 4.1.0 (http://www.paraview.org/overview/). ParaView is an open source program designed specifically for large scale data analysis. It has a large selection of data visualization tools including plane view extraction, streamline generation and animation creation, among others.

6.4 Computers

Steady state CFD calculations were conducted as parallel runs using 20 cores. The cores belonged to a remotely accessed Neste Jacobs Linux cluster comprised of Opteron 6172 processors with 128 GB of RAM and Opteron 6380 processors with 512 GB of RAM.

With this parallel run setup, most steady state single phase calculations reached convergence in about an hour, after which equal amount of iterations was completed to obtain the averaged results. The single phase dynamic calculation was simulated using 44 cores and took about 2 days. The two-phase dynamic simulation progress depended heavily on the local flow velocities due to the time step length being limited by the courant number. With 88 cores the calculation times ranged up to two weeks. The figures above are rough and depend heavily on calculation parameters, but can be used for rough estimation of workloads and as reference of the current computational speed of computers.

A queue system was utilized in the resource management of the CFD cluster. It allowed the calculations to be prioritized and more urgent jobs to be run immediately, postponing less urgent calculations.

7. CASE SETUP

In the following chapters, a comprehensive description of the calculation procedure is presented. A complete list of boundary conditions for a single case in HELYX® GUI is presented as an example in Appendix II. Unless stated otherwise in the case descriptions, the geometries and computational schemes remain as they are described here for all of the cases. Unless stated otherwise, the simulations were conducted as steady state, incompressible, single phase calculations. This simplification is based on the following assumptions:

- Flow behavior is dictated by the gas phase (gas phase volume fraction ≥ 90%)
- Temperature changes are relatively small within the system (negligible buoyancy)
- Flow velocity scales remain below the compressible limit (0.3 x the speed of sound)

Motivation behind the simplification was to increase robustness of the calculation, obtain easy-to-interpret results and to decrease the need for computational power. Particularly the requirement for computational power and time constraints were limiting factors in this work. Considering the dynamic single phase simulation consumed 50 times and the two-phase dynamic simulation minimum of 170 times more resources than the steady state single phase simulations, the scope of this work would have needed to be drastically altered if only the non-simplified models had been used exclusively.

7.1 Base geometry of a gas-liquid separator

The base geometry of the studied gas-liquid separator is used as a basis for all of the other cases. Modifications to the base geometry are presented in the description of each separate case in sections 9.1-9.5. The dimensions of the cylindrical base geometry vessel are

presented in Fig. 22. The demister frame is visible in the upper part of the vessel. Dimensions not visible in Fig. 22 are:

- Inlet and outlet inner diameter: 305 mm
- Length of inlet pipe: 450 mm
- Length of outlet pipe: 1210 mm

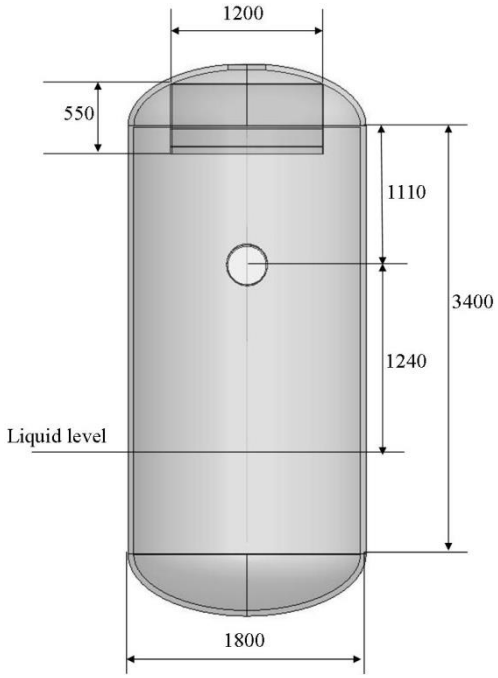

FIGURE 22. Dimensions of the base geometry vessel in millimeters, outlet pipe omitted from picture

The base geometry is based on an existing gas-liquid separator vessel and differs somewhat from the general design guidelines presented in the literature part. Main difference is the L/D ratio which in the base geometry is 1.9 as opposed to the 3-5 recommended in section 4.2.4. In engineering practice, a deviation such as this is not uncommon. Reasons for designing the vessel as short as possible may include restrictions in space and cost awareness. It is also important to note that in the computational model, the mesh is generated only in the space above the liquid level. Computationally, the space below the liquid surface is not noted. If the flow of liquid out of the vessel was to be modelled, the liquid outlet would be situated at the bottom of the vessel. In the computational model, no flow can penetrate the liquid level and thus the separated liquid

droplets in the two-phase simulation are accumulated on the surface. The base geometry is illustrated in three dimensions in Fig. 23.

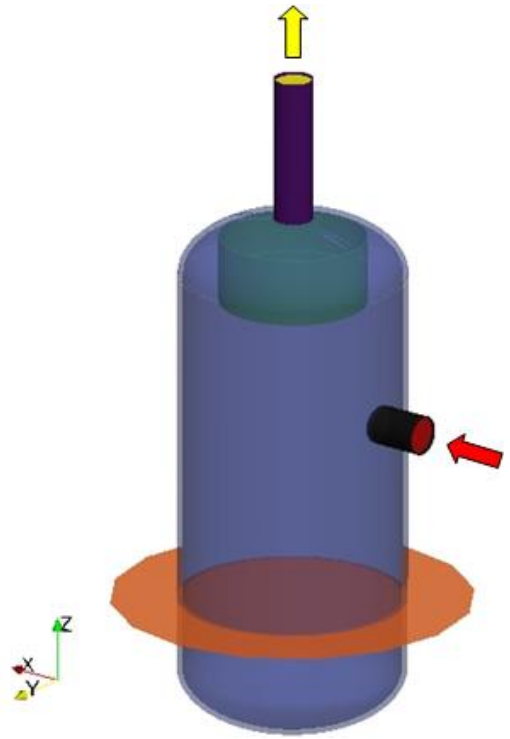

FIGURE 23. Base geometry of the studied separator vessel

In Fig. 23 the blue part represents the separator vessel. Flow enters the vessel from the horizontal inlet pipe (black) and exits through the vertical outlet pipe (purple). Computational inlet (red) and outlet (yellow) patches are located at the ends of the aforementioned pipes. The demister frame is drawn in green. For illustrative purposes, the liquid level (orange) in the tank is drawn to reach outside of the vessel walls. This is purely a visual feature and has no effect on the computation.

7.2 Feed stream properties

In the single phase calculations, only a gaseous phase was simulated. The material properties were based on earlier simulations of similar flows and were specified as follows:

- Density: 3.17 kg/m^3
- Dynamic viscosity: 0.01 mPas
- Kinematic viscosity: 3.15 x 10^{-6} m^2/s

In one specific study, two different inlet flow rates, corresponding to high and low design values, were used. Other calculations were conducted using only high design values. The gas flow rates were specified as follows:

- Mass flow rate:
  - 4.42 kg/s (low)
  - 7.37 kg/s (high)
- Volumetric flow rate:
  - 1.40 m^3/s (low)
  - 2.32 m^3/s (high)

7.3 Computational mesh

Dimensions of the computational mesh determine the maximum accuracy at which the flow phenomena can be modeled. Therefore it is important that the mesh is fine enough at key areas of the flow domain. A base mesh spacing of 3 cm was chosen for the cubic mesh based on previous experience and a mesh study conducted for different base mesh sizes.

In OpenFOAM calculations, level of refinement indicates how many times the dimensions of a base mesh element have been halved. Thus, cells of refinement level 2 have in this case a length, width and depth of 0.75 cm. With this formula, 8 elements of refinement level 1 and 64 elements of refinement level 2 are extracted from a single base mesh element. Due to this, the amount cells of refinement level 2 is high even though they are only present at the walls of key areas inside the vessel. The splitting of cells is triggered by surface curvature and it is performed gradually, thus cells of refinement level 1 are also present, even though they were not specified to any surface within the vessel before mesh generation. Side view of the mesh inside the vessel is presented in Fig. 24.

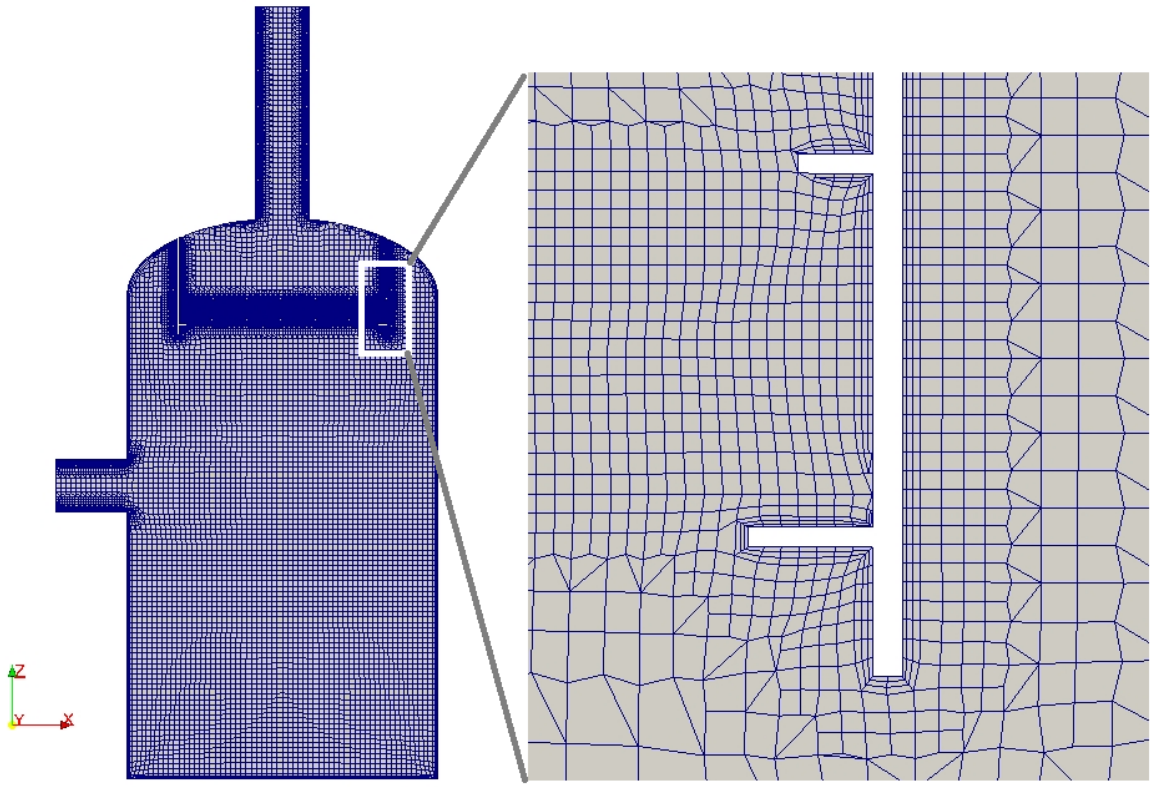

FIGURE 24. Computational grid inside a separator vessel with no inlet distributor with part of the demister frame area magnified

Three surface layers, as seen in Fig. 24, were created on all wall surfaces. The layer cells are flattened, i.e. they have less thickness measured from the surface than base mesh cells. This allows for more accurate modeling of surface interactions between the flow and the walls. The thickness of the surface layer cells is progressively diminished approaching the wall surface.

The demister pad volume, as indicated in the magnification in Fig. 24, was specified as refinement level 2. The pad thickness is 13 cm and it is situated between the two brackets. As seen in Fig. 24, the demister frame extends another 5 cm below the demister pad, forming a “lip” around it. Mesh statistics in the selected configuration of the mesh study are presented in Table VIII.

TABLE VIII. Base mesh statistics

Base mesh spacing	30 mm
Refinement levels	
All walls, incl. liquid level	0
Demister frame	2
Inlet and outlet pipes	2
Distributor	2
Demister pad	2
Cells by refinement level	
0	335 000
1	84 000
2	1 094 000
Total number of cells	1 514 000

Total number of cells between cases ranged from the *No Distributor* case's 1 514 000 cells as presented in Table VIII to 2 500 000 cells depending mainly on geometrical complexity of the distributor. The grid for the *Vane Type 2* distributor was special among all of the studied cases. It contained 35 000 000 cells as it included several refinement volumes containing cells of refinement level 4 (1.9 mm). Further details on the mesh in that particular case are given in section 9.1.4.

In the mesh study nine different meshes were created using the *No Distributor* configuration. Three different base mesh sizes (10, 6 and 3 cm) were used with each mesh created using refinement levels 2, 1 and 0 for the volume inside the demister pad. Since the performance of the demister is of special interest in this work, the aim was to model the fluid flow through it as accurately as possible. Standard deviation of the vertical velocity through a plane 5 cm below the demister pad was monitored. The results obtained with the high design values are presented in Fig. 25.

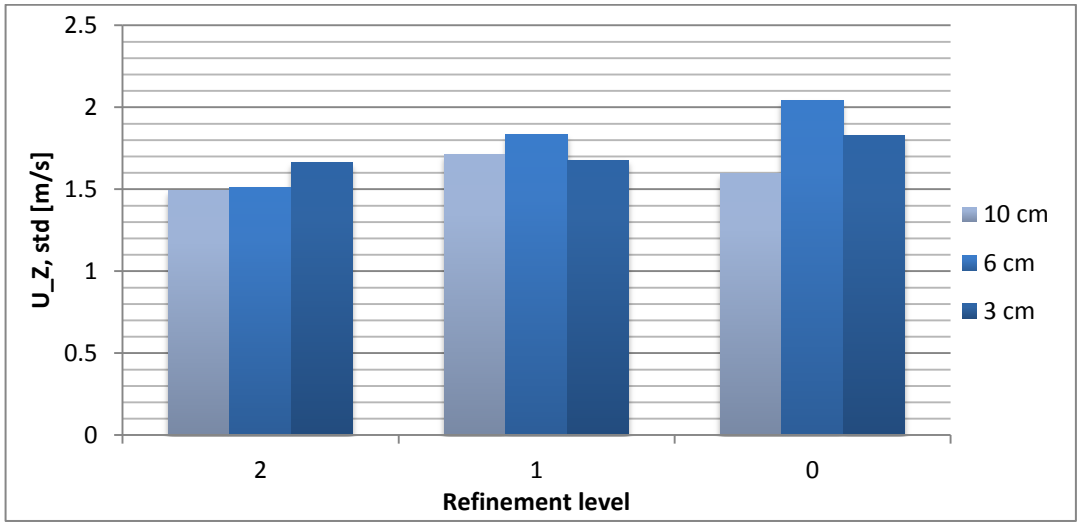

FIGURE 25. Standard deviation of vertical velocity in m/s below the demister pad with different base mesh sizes and refinement levels for the demister pad. *No distributor* configuration, high design values.

When using a constant refinement level for the demister pad, diminishing the base mesh size doesn't seem to have any straightforward effect to the standard deviation. With the exception of base mesh size 10 cm, the refinement of cells inside the demister pad yield lower values for the standard deviation. Overall, no significant effects of mesh size were observed with the studied mesh sizes. Finer base meshes were also studied, but they often resulted in the mesh escaping outside of the vessel through minute cracks in the geometry. Based on these observations a base mesh size of 3 cm with refinement level 2 inside the demister pad was chosen as a compromise between accuracy of the results, reliability in mesh generation and demand for computational power.

7.4 Boundary conditions and turbulence modeling

Turbulence was modelled using the k-ω SST –model based on its utilization in earlier simulations on similar flows. The model combines two approaches into a single model, utilizing k-ω formulation in the inner boundary layer and k-ε formulation in the free stream. (Visuri, 2012) This makes the model suitable to be used for the entire flow from the free stream all the way to the wall.

All of the wall surfaces, including the liquid level at the tank bottom were modeled as no-slip walls with no surface roughness. The no-slip condition dictates that fluid flow has zero velocity on the surface of the wall.

Inlet at the beginning of the inlet pipe was specified as a constant velocity inlet, with the velocity vector normal to the boundary patch. The velocity profile was set uniform across the inlet plane. Fully developed flow conditions were observed at the entrance to the vessel. Two different design capacities, low and high, were used in the simulations. They were implemented by specifying either an inlet velocity of 19.1 m/s or 31.8 m/s. Turbulence of the inlet flow was specified by setting turbulence intensity to 0.05 and mixing length to 0.03 m.

Outlet at the end of the outlet pipe was specified as a fixed relative pressure outlet at 0 Pa(g) and the pressure was calculated upstream across the rest of the fluid domain. In incompressible fluid modeling, the true pressure inside the vessel is not reflected in the simulation. With the given fluid density of 3.17 kg/m^3 and the flowrate of the high design value case, the actual pressure inside the vessel is around 3 MPa. Thus the simulated total pressure drop across the entire vessel is only around 0.1%.

The demister pad was modeled as an anisotropic porous medium zone using the Darcy-Forchheimer model. Experience has shown that this model is good for pressure drop and superficial velocity modeling particularly in cases where scale of the turbulent eddies is below the pore scale. (Soulaine & Quintard, 2014) Coefficients in the Darcy-Forchheimer model are presented in Table IX.

TABLE IX. Coefficients in the Darcy-Forchheimer porous medium model used in the demister pad modeling

	x	y	z
e1, m	1	0	0
e2, m	0	1	0
Viscous loss coefficient D, 1/m^2	1100	1100	1100
Inertial loss coefficient F, 1/m	100	100	100

The effect of the coefficients *D* and *F* on the source term of the momentum equation can be written as (Engys Ltd, 2015)

$$S_i = -\left(\sum_{j=1}^{3} D_{ij}\mu U_j + \sum_{j=1}^{3} F_{ij}\frac{1}{2}\rho\bar{U}U_j\right) \quad (26)$$

S_i	Source term of the ith (X, Y or Z) momentum equation
D_{ij}, F_{ij}	Porous media coefficients, 1/m^2 and 1/m respectively
μ	Dynamic viscosity of the fluid, Pas
ρ	Fluid density, kg/m^3
U_j	jth component of the (X, Y or Z) velocity vector
$\bar{U}$	Velocity magnitude, m/s

The values for the coefficients *D* and *F* were specified based on earlier simulations so that a realistic pressure drop was observed over the demister. With the given coefficients, the pressure drop across the demister pad was roughly 140 Pa.

7.5 Numerical schemes and residual control

Linear upwind second order schemes were used in calculating the derivatives of the momentum equations. Second order schemes yield more accurate results and are therefore preferred over simpler first order schemes (Siikonen, 2014). The choice between different second order schemes was done based on experience from earlier calculations on similar flows.

HELYX® default values were used as residual criteria. The default values included a value of 10^{-5} for variables *U*, *p*, *k* and *omega*. When the initial residuals of the variables reached the specified limits, the iterative calculation in the given time step was stopped and the solutions written to file. The residuals were monitored during calculation to evaluate solution convergence. Mass balance inside the vessel was also monitored to verify convergence of the solution. A solution convergence plot for a single steady state case is presented in Appendix III. Convergence parameters and criteria remained constant throughout the steady state simulations and therefore the convergence plots look almost identical for every steady state case.

7.6 Calculation procedure

Several different programs in two different operating systems were utilized during the calculation procedure. In this section a step-by-step description is given for the different steps of the calculation.

Geometries were created using Microstation® V8i in a Windows environment. For use in CFD-calculations, STL-files of the geometry elements were created. STL-files represent each surface as a set of triangles and therefore sufficient resolution needs to be used when working with curved surfaces. Each part of the separator vessel (shell, inlet/outlet pipes, demister frame, liquid surface and inlet/outlet patches) was exported as a separate STL-file, allowing separate specifications for each surface to be given in HELYX® GUI and OpenFOAM case files. After generation, the STL-files were transferred to the NJ Linux cluster machines using a file transfer program.

HELYX® GUI was utilized as the first step in the creation of a new case. Geometries were imported into HELYX® GUI using the STL import tool. Meshing parameters were specified in the user interface. When a new case is saved, HELYX® creates case description files in ASCII text format based on the OpenFOAM standard. After the mesh parameters had been specified, the case was decomposed to utilize 20 computational cores in the Linux cluster. The mesh creation utility for the created case was executed manually through a queue system which allows for advanced resource management in the Linux cluster.

The generated mesh was inspected visually using either HELYX® GUI or Paraview and by inspecting the created log file. If the quality of the mesh was sufficient, the case was opened again in HELYX® GUI for specifying of boundary conditions and solution algorithms. Minor tweaks, e.g. changing inlet velocity, were done directly in the OpenFOAM case files without the need to start the HELYX® GUI. The case was again saved and run though the queue system.

Post processing, e.g. the extraction of pictures was conducted after the calculations using ParaView. Additional Python and C++ scripts were utilized in extracting numerical data from planes within the vessel.

7.7 Data-averaging procedure

Because of the inherent unstable nature of the calculation, the solution fields never reached exactly the same values even in steady state simulations. Instead, they reached values in close proximity to a mean value which is the desired steady state solution. To remove the inaccuracy caused by using only a single solution, all monitored variables were derived from averaging of a large amount of steady state solutions. In practice, this was conducted by first running the steady state simulations for 1000 iterations. The residuals were monitored to make sure this number of iterations was adequate for them to stabilize to a low level. After the first 1000 iterations, averaging of the monitored variables was started. As a result, all the results analyzed and presented in this work are comprised of averaged values gathered from iterations 1000-2000. An example of a convergence plot as well as two flow profiles from individual iterations are presented in Appendix III. The following equation was used in obtaining an averaged value for the velocity field; the averaging was conducted similarly for the pressure and wall shear stress fields.

$$U = \frac{\sum_{i=n1}^{n2} U_i}{(n2-n1)} \tag{27}$$

U	Averaged velocity, m/s
U_i	Velocity at iteration i, m/s
n_1, n_2	First and last iterations of the averaging procedure, respectively

8. EVALUATION CRITERIA

The choice of performance indicators was governed by the simplifications implemented in the studied model. Since most of the simulations were performed as single phase steady state calculations, the movement of droplets of liquid in the separator could not be directly observed. Instead, gas velocity profiles (particularly at the demister inlet) were used as the main indicators of droplet entrainment within the vessel.

8.1 Velocity profiles

In the steady state single phase calculations the main monitored variable was the vertical velocity inside the separator vessel. It can be used to approximate the separation performance of the vessel since the vertical velocity is the most important individual contributor to droplet entrainment in vertical vessels. As described in the previous chapter, all analyzed velocity data was averaged over 1000 iterations to remove inaccuracies caused by small fluctuations in the solution fields. The two horizontal and one vertical plane where the vertical velocity was monitored are presented in Fig. 26.

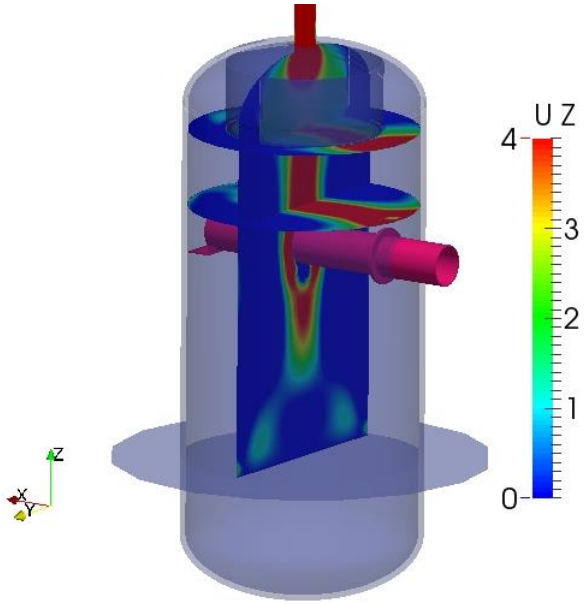

FIGURE 26. Three planes inside the separator vessel, on which the vertical velocity was monitored

The lower horizontal plane situated 30 cm above the center line of the inlet pipe was used in studying the velocity profile leaving the distributor. Comparing it with the upper horizontal plane, the change of the flow profile along the height of the vessel could be assessed. The upper horizontal plane was also crucial in determining the performance of the demister. Velocity peaks in the upper plane indicate hydraulically highest capacity areas (areas which will flood first) and low velocity areas indicate inadequate utilization of the demister capacity. Ideally, the flow profile across the demister should be uniform. The

vertical plane was used to visually inspect leveling of the flow profile and flow orientation around each studied distributor.

Numerically, the vertical velocity was studied by calculating two performance indicators from a data set extracted below the demister. This data set was created by extracting values within the circular area below the demister from the upper horizontal plane in Fig 26, hence excluding the outer region between the demister frame and the vessel walls. The main monitored indicators within this area were the maximum (indicating flooding in the demister) and the standard deviation of the vertical velocity (a numerical indicator of the evenness of the flow profile). To help visualize the magnitude of the changes, a red baseline corresponding to the results of the *Base geometry* vessel with the *Impact Plate Type 1* distributor is drawn in each graph.

Streamlines were generated to visualize the flow inside the vessel. They were mainly used for evaluating flow patterns around different distributor geometries.

8.2 Wall shear stresses

Wall shear stresses were monitored mainly to assess the mechanical durability of each design. High shear stresses indicate possible areas susceptible to erosion or corrosion-erosion damage. High wall shear stresses also indicate areas where the liquid level measurement instruments can be disturbed or damaged by high velocity flows.

As all other monitored variables, wall shear stresses were calculated as averaged values between iterations 1000-2000. Actual obtained values of the wall shear stresses in the single gas phase calculations were in the range of 0 to 10 Pa. This is very low and in large part due to excluding the heavier liquid phase in these simulations. In reality, the values are considerably larger as liquid droplets are over 300 times denser than the modeled fluid. Instead of actual values, emphasis is placed on observing the locations where the shear stresses are highest and comparing the trend between different cases. The location of these areas is not expected to depend on the fluid density and therefore the results of the cases are comparable with each other. The results of the two two-phase calculations supported this assumption. The locations of the areas with high relative shear stresses remained

largely uniform to the single phase calculations and the magnitude of the stresses increased roughly by a factor of 80.

9. SINGLE PHASE MODEL SIMULATION RESULTS

Various vessel internals and vessel geometries were simulated in different studies. Every inlet distributor (introduced in section 9.1) was simulated in the base geometry vessel (as described in chapter 7.1) in the *Distributor study*. In other studies, only selected distributors were used. Table X lists all of the studies and indicates the simulated distributors in each study.

TABLE X. Case study chart indicating distributors simulated in each study. Results presented in chapters 9.1 to 10.

	No Distributor	Half Pipe	Vane Type 1	Vane Type 2	Impact Plate Type 1	T-Junction	Impact Plate Type 2	Vapor Horn
Distributor Study	X	X	X	X	X	X	X	X
Vessel Dimension Study					X	X		
Demister Study					X	X		
Outlet Study					X			
Modified Distributor Study		X			X	X		
Dynamic Simulation					X			
Two-Phase Simulation			X		X			

9.1 Inlet distributors

The purpose of the inlet *Distributor study* was to study the effect of the inlet distributor geometry on the flow patterns inside the separator vessel. Some of the proprietary designs are claimed to have superior performance over conventional designs. This improvement is often related to first stage separation of droplets by the distributor. In the single phase simulations this aspect could not be taken into account and evaluation was conducted only based on flow profiles. Design details of the proprietary devices are not disclosed. The following distributors were simulated in the *Inlet distributor* study:

- No distributor
    - Reference case
- Half Pipe
    - Horizontal cylinder with open bottom half
    - Conventional in phase separators
- Vane Type 1
    - Designed for separation of gas-liquid mixtures in separators and distillation columns
    - Vanes direct the flow sideways out of the distributor as a series of small streams
    - Vanes provide centrifugal acceleration to promote the separation of liquid from the gas phase
- Vane Type 2
    - Improved design of Vane Type 1
    - Claimed to reduce entrainment significantly compared to conventional design and be the best radial inlet feed device
- Impact Plate Type 1
    - Vertical plate placed near the inlet suspended by an upper horizontal plate
    - Conventional in phase separators
- T-Junction
    - Standard T-shaped pipe segment placed at the inlet
    - Conventional in phase separators
- Impact Plate Type 2
    - Curved impact plate
- Vapor Horn
    - Tangential inlet surrounded by a shell with open bottom and end sections
    - Typical design for very high gas velocities

Sketches of the distributor geometries are presented collectively in Fig. 27.

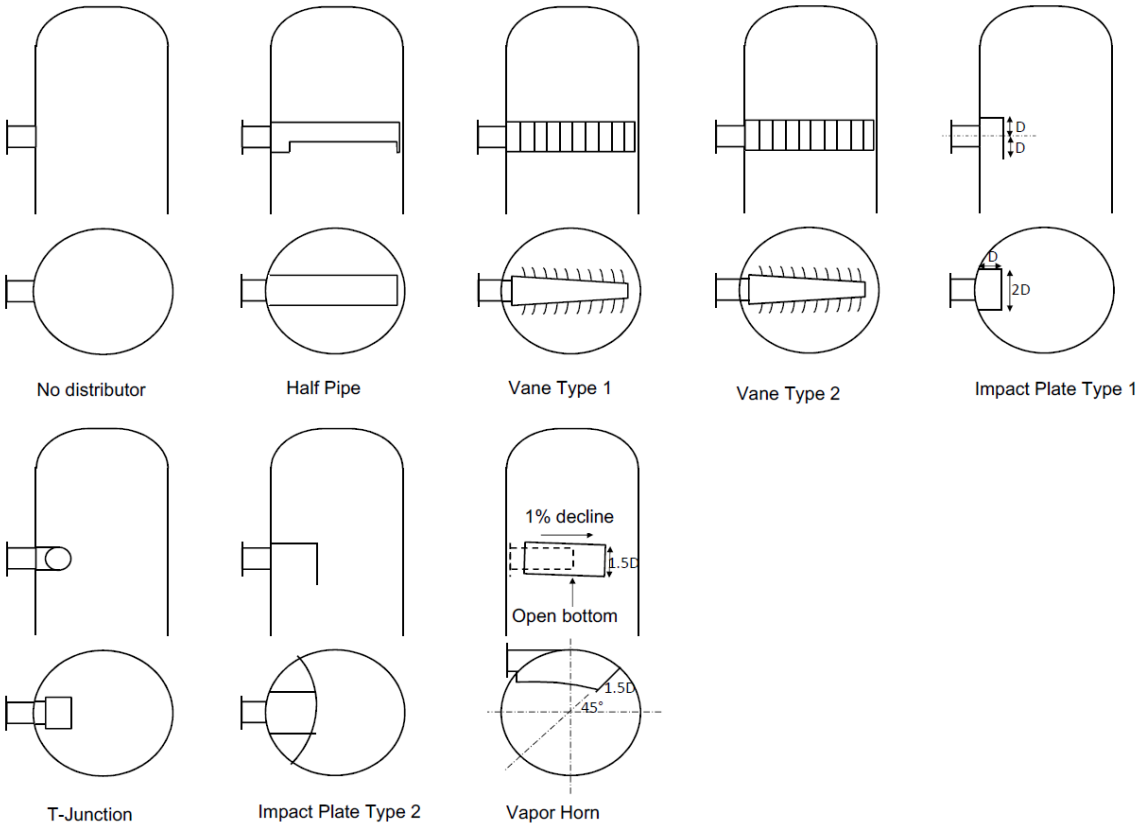

FIGURE 27. Schematic drawings of the distributors studied in the *Distributor Study*

Simulations were conducted as steady state single phase runs with both the low and high design capacities.

9.1.1 No Distributor

Although it is rarely used in practice, a reference case was calculated without an inlet distributor. The geometry with stream tracers and the shear stresses on the vessel walls are presented in Fig. 28.

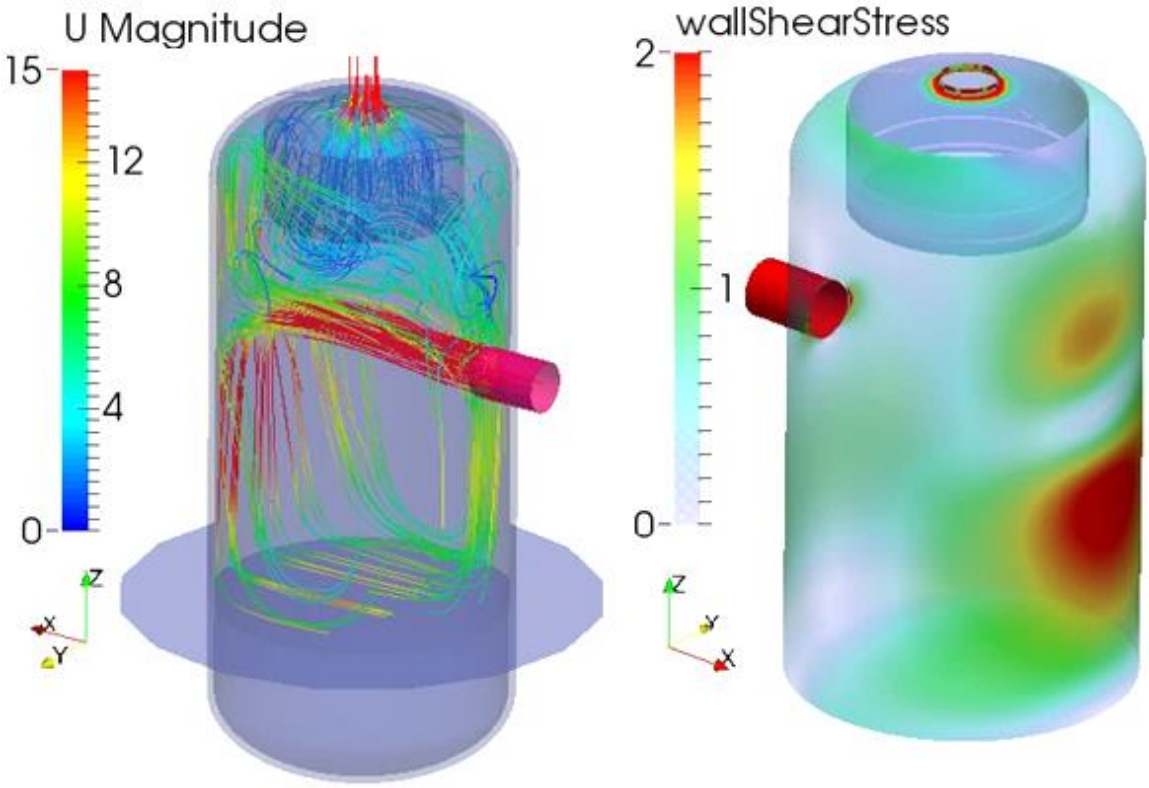

FIGURE 28. Left: *No Distributor* case geometry with stream tracers representing flow orientation (velocity magnitudes in m/s), Right: shear stresses on the vessel walls in Pascals (high design capacity, outlet pipe hidden for clarity)

Fig. 28 indicates that the stream is projected at high velocity to the vessel wall opposite to the inlet pipe. The wall shear stresses also indicate that the flow hits the opposite wall at a high velocity. This can result in possible damage at the back wall of the vessel due to erosion or corrosion-erosion.

Plane view of the vertical velocity profile 5 cm below the demister pad is presented in Fig. 41. It indicates that the flow profile in the demister is not optimal. A high velocity zone is formed along the back edge of the demister entrance. This part of the demister will flood first depending on the density of the demister.

9.1.2 Half Pipe

The *Half Pipe* distributor consists of a pipe with an equal diameter to the inlet pipe. The bottom half of the pipe is open along the width of the vessel. The geometry with stream tracers and the shear stresses on the vessel walls are presented in Fig. 29.

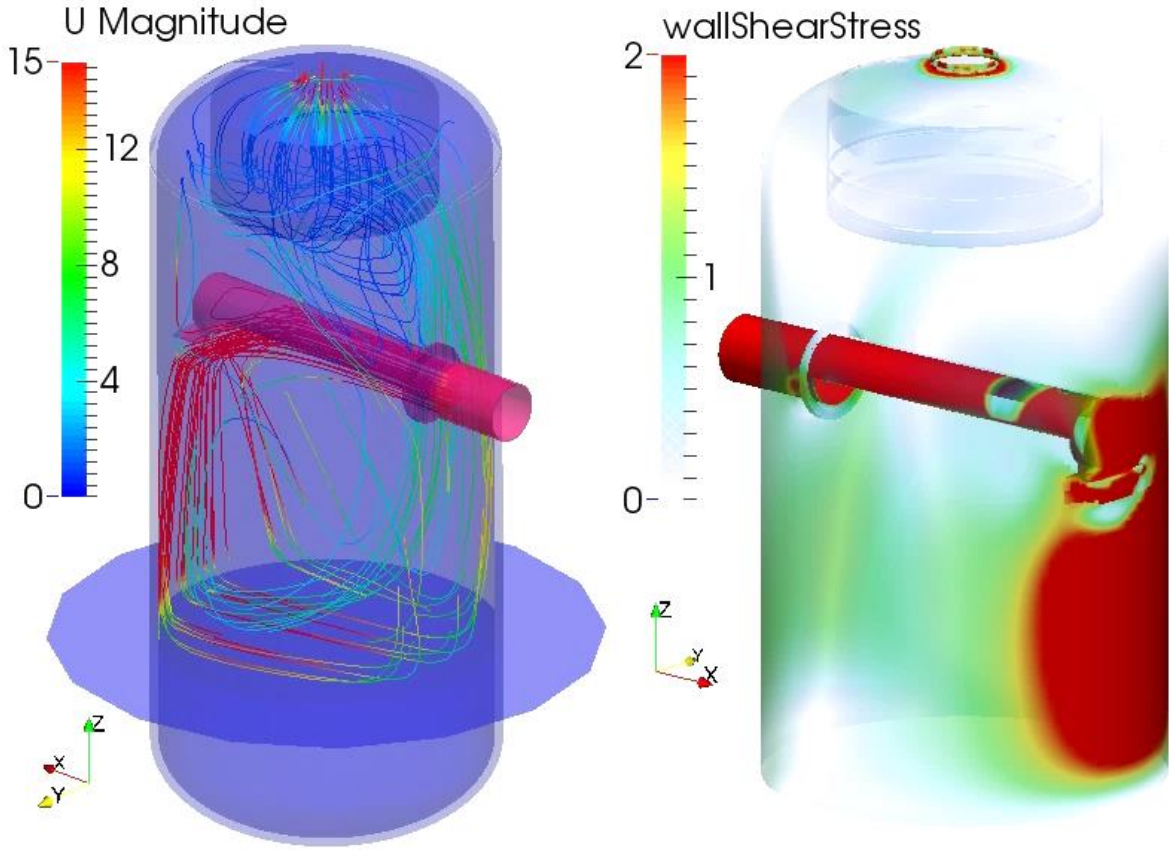

FIGURE 29. Left: *Half Pipe* case geometry with stream tracers representing flow orientation (velocity magnitudes in m/s), Right: shear stresses on the vessel walls in Pascals (high design capacity, outlet pipe hidden for clarity)

Fig. 29 indicates that much like in the *No Distributor* case, the inlet stream hits the opposite vessel wall at a high velocity. In this case, the stream cannot turn directly upwards at the opposite wall and is instead projected entirely downwards. The wall shear stresses also indicate that the flow hits the opposite wall at a high velocity. This can cause possible erosion or corrosion-erosion damage at the lower part of the back wall in the vessel.

Plane view of the vertical velocity profile 5 cm below the demister pad is presented in Fig. 41. It indicates that the flow profile in the demister is not optimal. A high velocity zone is formed above the distributor's inlet side. As seen from the streamlines in Fig. 29 this is the

result of the flow being projected from the back wall of the vessel. This part of the demister will flood first depending on the density of the demister.

9.1.3 Vane Type 1

The *Vane Type 1* distributor consists of a narrowing box structure with several outlets on each side directing the flow sideways out of the distributor. The flow is forced to make a 90° turn with the help of curved guide plates, which introduce centrifugal forces to the flow. The geometry with stream tracers is presented in Fig. 30.

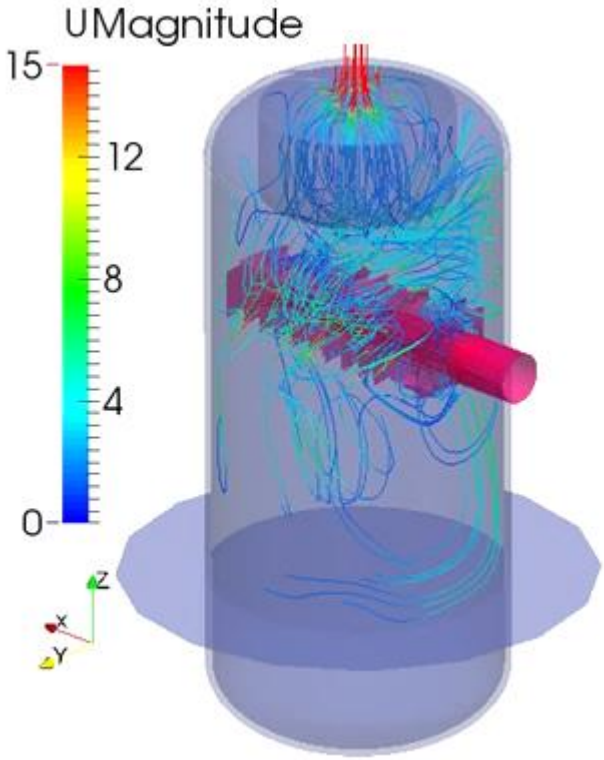

FIGURE 30. *Vane Type 1* case geometry with stream tracers representing flow orientation (velocity magnitudes in m/s)

Fig. 30 indicates that very little flow is directed to the bottom of the vessel. This is advantageous considering liquid re-entrainment from the liquid surface, but the flow profile may not have sufficient time to stabilize before the demister inlet. Flowrates out of each separate opening in the distributor are visually almost equal. Flow velocities remain relatively low compared to other distributors. The wall shear stresses are non-existent on the vessel walls with practically all the strain absorbed by the distributor. If mechanical

durability of the vessel is an issue, the *Vane Type 1* is a more viable option compared to some simpler designs.

Plane view of the vertical velocity profile 5 cm below the demister pad is presented in Fig. 41. It indicates that the flow profile in the demister is not optimal. A high velocity zone is formed above below sides of the demister. As seen from the streamlines in Fig. 30 this is the result of the flow pattern remaining mostly at the vessel walls. The high velocity parts of the demister will flood first depending on the density of the demister.

9.1.4 Vane Type 2

The *Vane Type 2* distributor, based on the *Vane Type 1*, consists of a narrowing box structure with several outlets on each side directing the flow sideways out of the distributor. In addition to the *Vane Type 1* guide plate design, the edges of the guide plates in the *Vane Type 2* have been bended. This prevents liquid re-entrainment from the edges. Cylindrical refinement volumes containing cells of refinement level 4 (side length 1.9 mm) were used in the simulation to assure accurate modeling of flow through key areas of the distributor. The geometry with stream tracers is presented in Fig. 31.

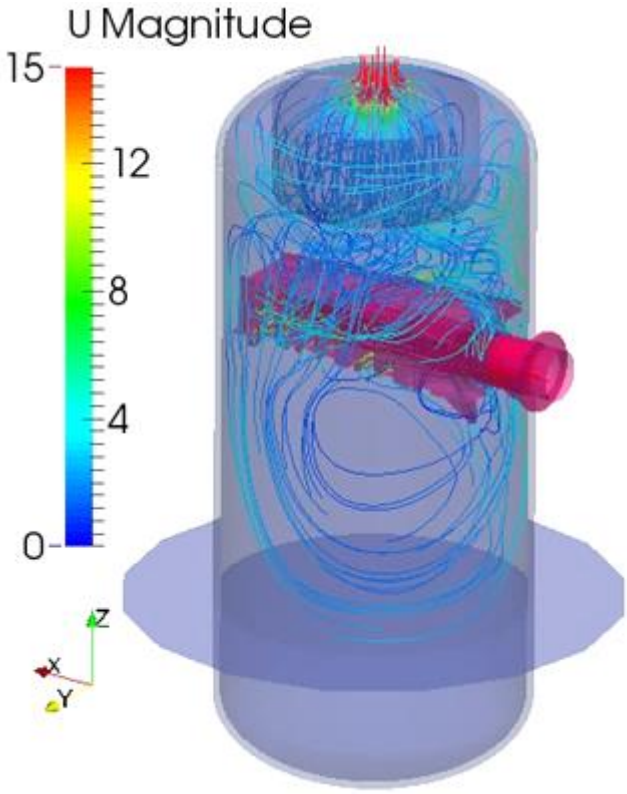

FIGURE 31. *Vane Type 2* case geometry with stream tracers representing flow orientation (velocity magnitudes in m/s)

Based on the stream tracers in Fig. 31, the *Vane Type 2* directs the flow much like the *Vane Type 1*. Very little flow is again directed to the bottom of the vessel, minimizing re-entrainment from the liquid surface but hindering velocity profile leveling. The flow seems to prefer exiting the distributor at the far side to the inlet, with the openings nearer to the inlet receiving less flow through them. Similar to the *Vane Type 1* case, the visualization of the shear stresses reveals that forces on the vessel walls are non-existent. This is good for the mechanical reliability of the design. Practically all of the shear stress is absorbed by the distributor.

Plane view of the vertical velocity profile 5 cm below the demister pad is presented in Fig. 41. It indicates that the flow profile in the demister is very similar to the *Vane Type 1* case. A high velocity zone is formed below both sides of the demister. As seen from the streamlines in Fig. 31 this is the result of the flow pattern remaining mostly at the vessel walls. The high velocity parts of the demister will flood first depending on the density of the demister. Despite the less than optimal flow profile at the demister inlet, the *Vane Type*

2, and to some extent the *Vane Type 1*, designs have other benefits. Due to the centrifugal separation being conducted at the distributor, larger droplets are removed from the stream before entering the demister. As the space beneath the distributor is relatively stagnant, these droplets have a good chance of avoiding re-entrainment and exiting the vessel through the bottom liquid outlet.

9.1.5 Impact Plate Type 1

The *Impact Plate Type 1* distributor is a plate placed one inlet pipe diameter away from the vessel wall. The width and height of the plate used here are two times the inlet pipe diameter and the design includes a top plate attaching the unit to the vessel wall. The geometry with stream tracers is presented in Fig. 32.

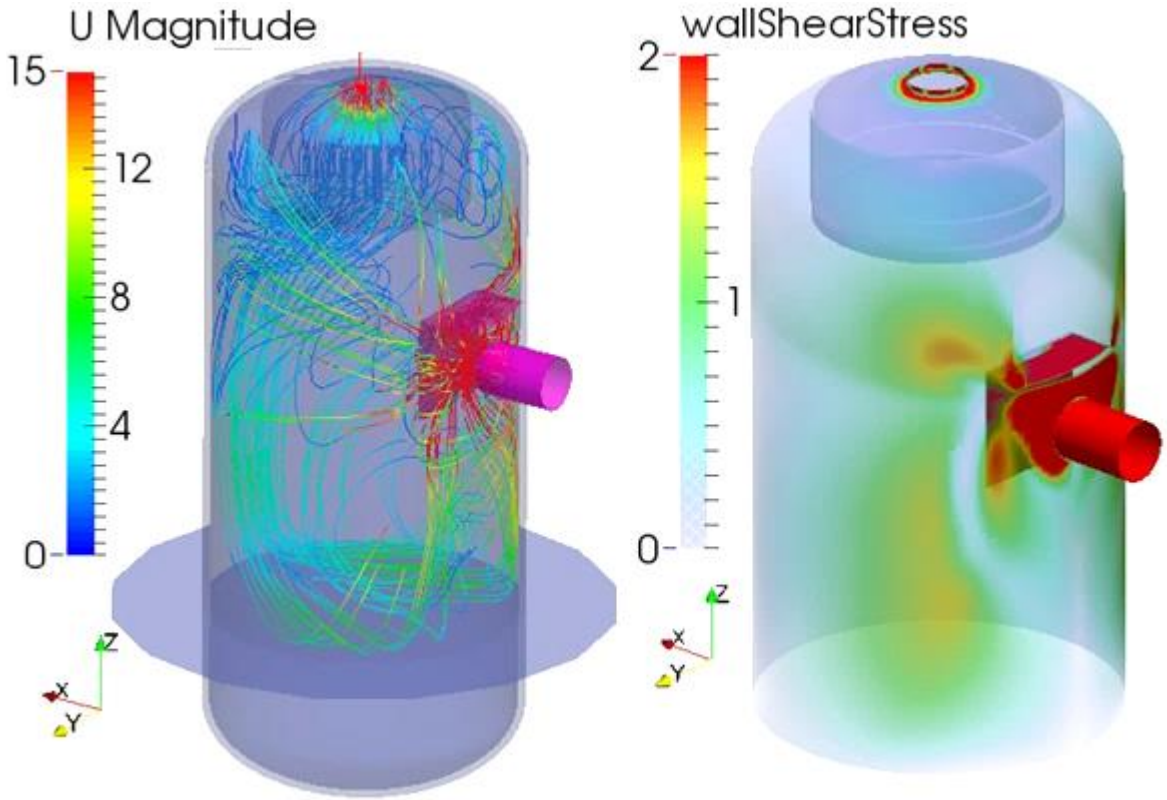

FIGURE 32. Left: *Impact Plate Type 1* case geometry with stream tracers representing flow orientation (velocity magnitudes in m/s), Right: shear stresses on the vessel walls in Pascals (high design capacity, outlet pipe hidden for clarity)

Based on the stream tracers in Fig. 32, the *Impact Plate Type 1* distributor directs the flow mostly downwards and the flow subsequently flows upward at the opposite wall of the vessel. The visualization of the shear stresses reveals that the largest shear stresses are concentrated on the distributor and the area around the inlet pipe. In addition to the mechanical durability of the distributor, attention should also be paid to the wall of the inlet if there is a risk of erosion or corrosion-erosion.

Plane view of the vertical velocity profile 5 cm below the demister pad is presented in Fig. 41. It indicates that the *Impact Plate Type 1* distributor produces a very even flow profile at the demister inlet. Presumably, as the flow travels through the bottom of the vessel, it has time to reach an average velocity by the time it enters the demister. The downside of this flow pattern is that re-entrainment of droplets from the liquid surface to the flow can occur. However, even flow distribution at the demister should ensure that the demister performs efficiently and removes the entrained droplets.

9.1.6 T-Junction

The *T-Junction* distributor used here consists of a standard T-shaped pipe part attached to the inlet pipe so that the flow is directed sideways. The angles of the T-part are rounded and the width of the distributor is approximately 1.5 times that of the inlet pipe diameter. The geometry with stream tracers is presented in Fig. 33.

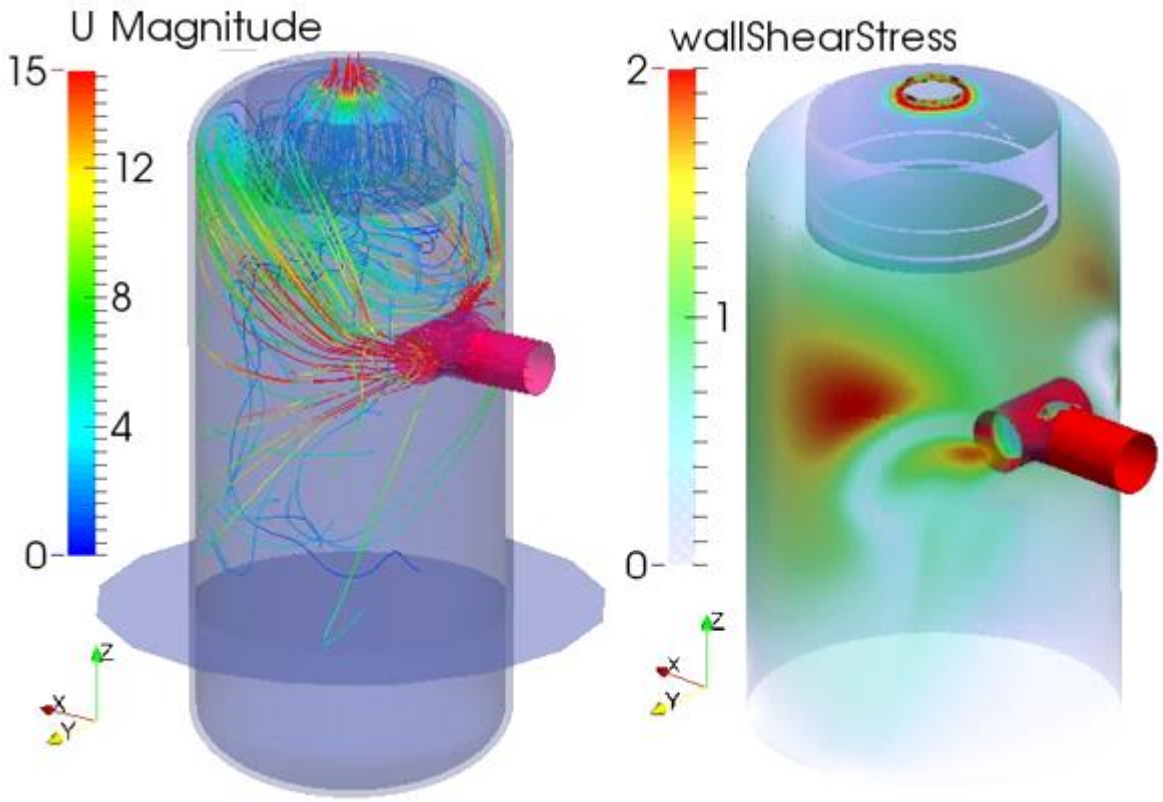

FIGURE 33. Left: *T-junction* case geometry with stream tracers representing flow orientation (velocity magnitudes in m/s), Right: shear stresses on the vessel walls in Pascals (high design capacity, outlet pipe hidden for clarity)

Based on the stream tracers in Fig. 33, most of the flow never reaches below the distributor. This reduces the time available for flow profile leveling and leads to high velocities at the demister inlet. A large portion of the flow is projected to the space between the demister frame and the vessel wall, from where it then needs to ascend again to reach the demister inlet. The visualization of the shear stresses indicates moderate stresses at the vessel sides. The distributor itself experiences high shear forces mainly on the top and around the open ends of the T-part.

Plane view of the vertical velocity profile 5 cm below the demister pad is presented in Fig. 41. It shows that the *T-Junction* produces a notably distorted flow profile at the demister inlet. What is most notable is that the flow velocity in the vertical direction is actually negative on a large surface near the demister frame. A close up of the problem area is presented in Fig. 34.

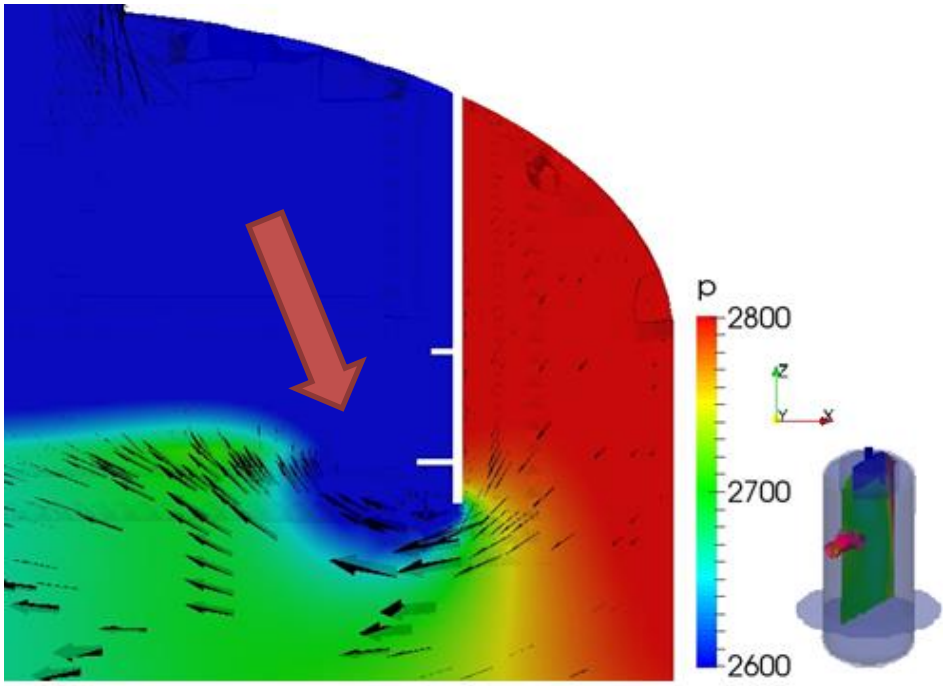

FIGURE 34. Close up of the low pressure zone (indicated by the red arrow) at the demister inlet in the *T-Junction* case, color indicates relative pressure in Pascals, arrows indicate main flow direction. Small picture indicates slice orientation.

The arrows in Fig. 34 indicate the main direction of the flow while the color indicates local pressure. The returning flow from the area between the demister frame and the vessel wall creates a low pressure zone along the lip of the demister frame. By blocking the flow into the demister in this part, the vacuum zone further increases the load at other points in the demister.

9.1.7 Impact Plate Type 2

The *Impact Plate Type 2* distributor is somewhat similar to the *Impact Plate Type 1* distributor. The vertical plate is curved and is attached from both ends to the vessel wall. The geometry with stream tracers is presented in Fig. 35.

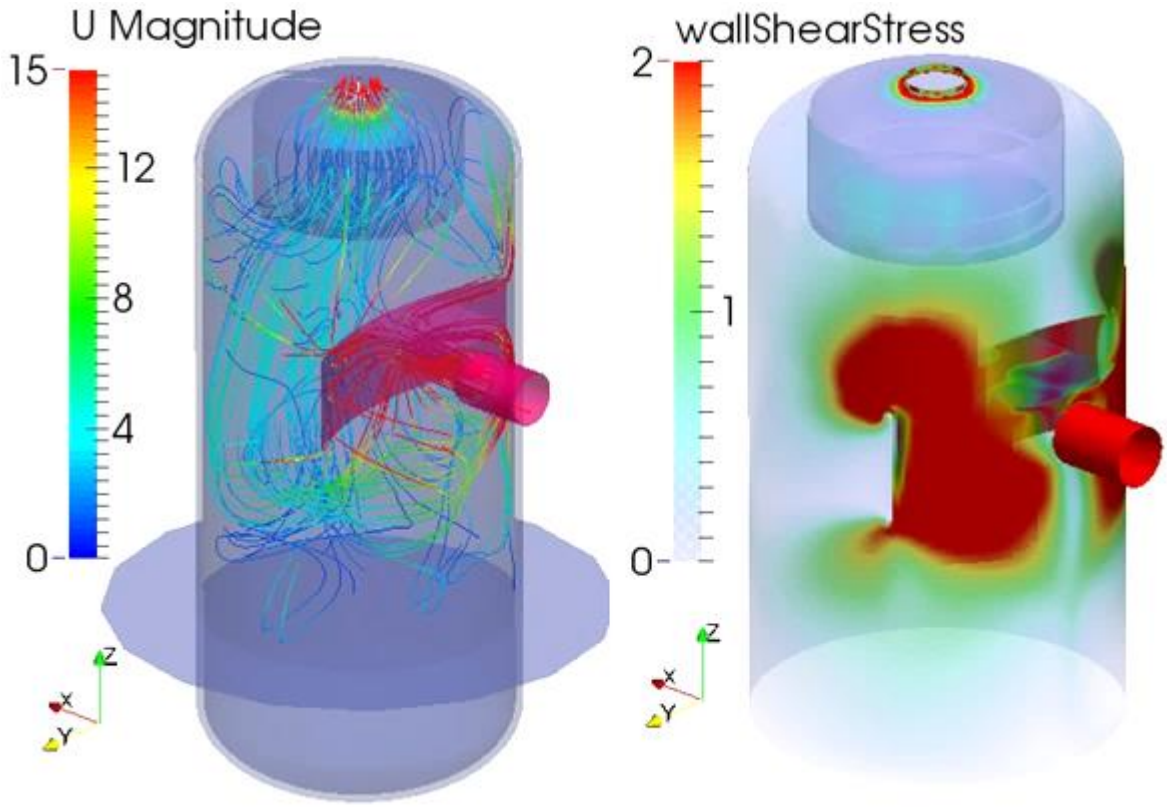

FIGURE 35. Left: *Impact Plate Type 2* case geometry with stream tracers representing flow orientation (velocity magnitudes in m/s), Right: shear stresses on the vessel walls in Pascals (high design capacity, outlet pipe hidden for clarity)

Based on the stream tracers in Fig. 35, much like the *Impact Plate Type 1*, the *Impact Plate Type 2* directs the flow mostly downwards and the flow subsequently flows upward at the opposite wall of the vessel. A detailed picture of shear stresses on the surface of the *Impact Plate Type 2* distributor is presented in Fig. 36.

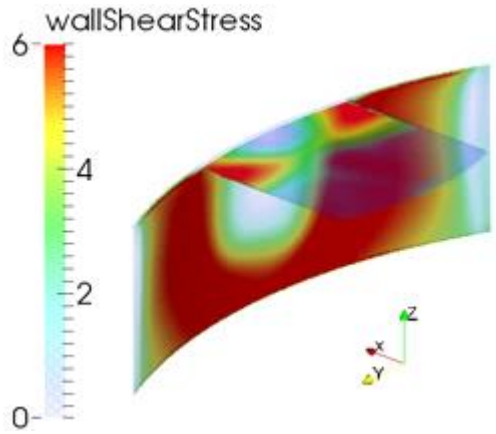

FIGURE 36. Shear stresses on the distributor in Pascals in the *Impact Plate Type 2* case. NOTE! modified scale

The visualization of the shear stresses in Figs. 35 and 36 reveals that the largest shear stresses are concentrated on the distributor and areas at the left and right sides of the inlet pipe. The vertical part of the distributor is the subject of the most amount of mechanical strain.

Plane view of the vertical velocity profile 5 cm below the demister pad is presented in Fig. 41. It indicates that the *Impact Plate Type 2* distributor produces a very even flow profile at the demister inlet similar to the *Impact Plate Type 1* distributor. Within the calculation accuracy, it can be stated that both the *Impact Plate* distributors perform equally well and produce the most even flow profiles amongst all of the distributors inside the studied vessel geometry.

9.1.8 Vapor Horn

The *Vapor Horn* distributor differs from all of the other studied distributors in that it has a tangential inlet. This allows centrifugal forces to be exerted on the flow. The width and height of the distributor used here are both 1.5 times the diameter of the inlet pipe. These are typical dimensions for tangential inlet devices. The bottom and the downstream end of the distributor are both open and the distributor is placed at a 1% decline. The geometry with stream tracers is presented in Fig. 37.

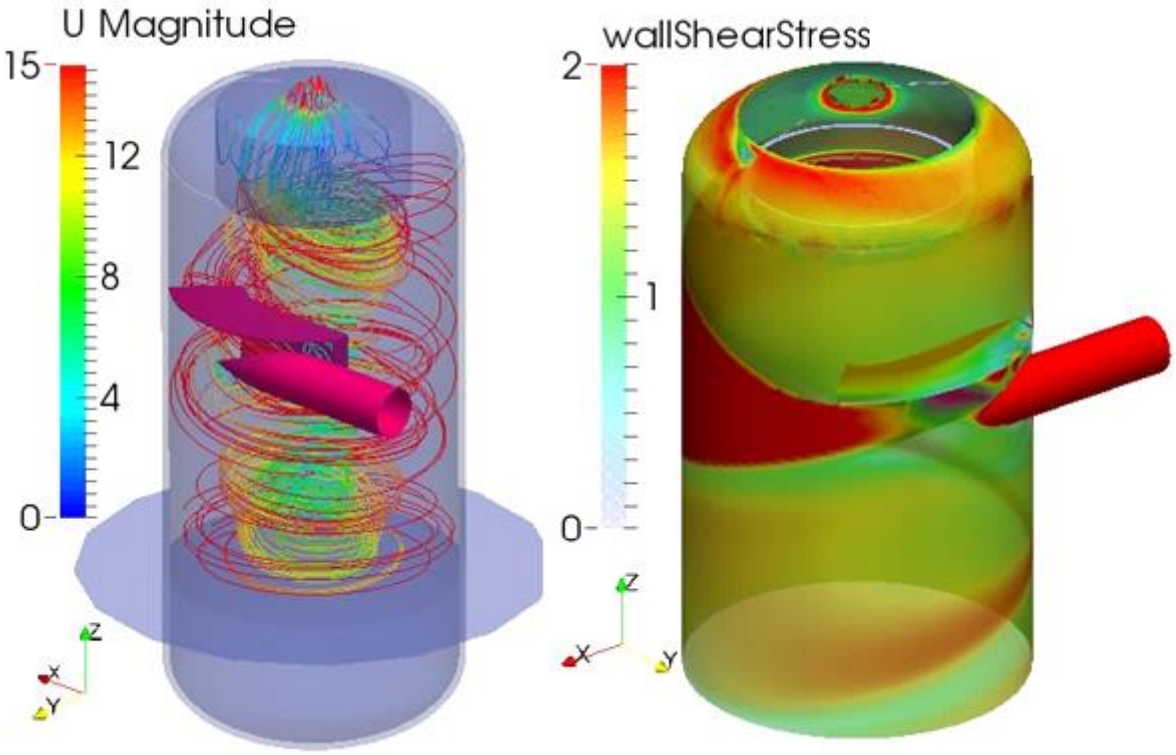

FIGURE 37. Left: *Vapor Horn* case geometry with stream tracers representing flow orientation (velocity magnitudes in m/s), Right: shear stresses on the vessel walls in Pascals (high design capacity, outlet pipe hidden for clarity)

As intended, the *Vapor Horn* design forms two vortices: an outer vortex where the flow is directed mainly downwards and an inner one where the flow moves towards the gas outlet. Even though the distributor is placed at a 1% decline, some of the inlet flow is directed upwards which may contribute to the uneven flow profile. Shear stresses are mainly concentrated on the vessel wall where contact is made with the inlet flow. Wear in this area can occur especially if there are solid particles or corrosive materials in the stream. Typically tangential inlet devices are coupled with wear plates to minimize this risk.

Plane view of the vertical velocity profile 5 cm below the demister pad is presented in Fig. 41. Even though the numerical value for the standard deviation of the vertical velocity is only moderate compared to other distributors, the *Vapor Horn* produces large zones of very high velocity and zero velocity at the demister inlet. Fig. 38, which contains the vertical plane presented in Fig. 26, explains the formation of these zones.

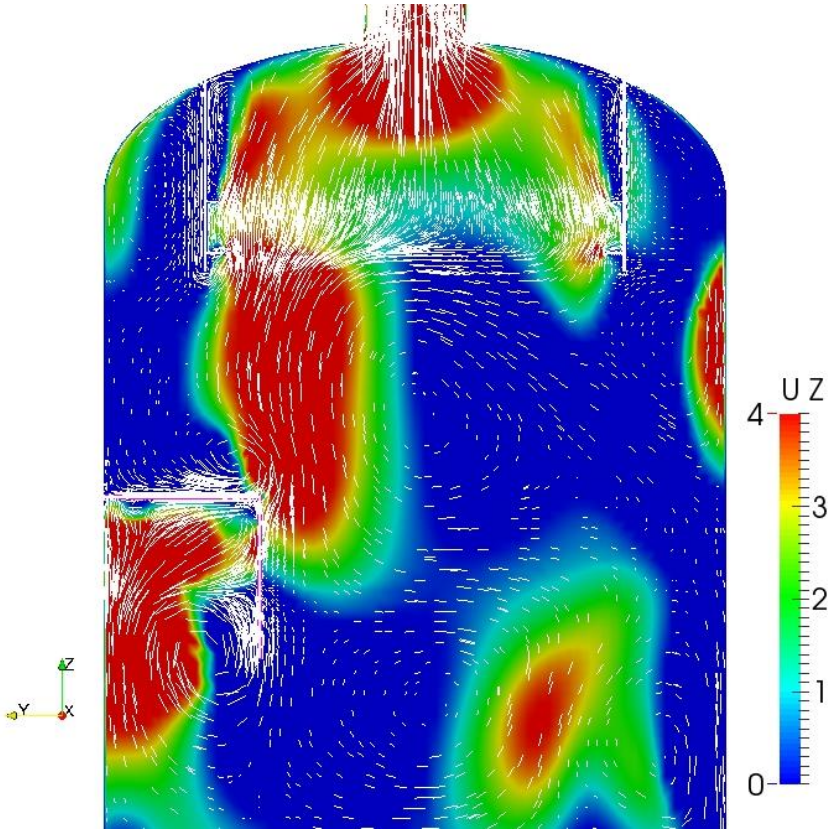

FIGURE 38. Vertical plane view of the *Vapor Horn* case at high design capacity, lines represent main flow direction, color represents vertical velocity in m/s (Refer to Fig. 26 for plane location)

Fig. 38 indicates that by reducing the available cross sectional area in the vessel, the plates of the *Vapor Horn* distributor accelerate the flow in the vertical direction. The flow is accelerated to such an extent that it cannot entirely pass through the demister pad. Some of the flow is pushed horizontally along the underside of the demister creating a zone of negative or zero vertical velocity. This makes the demister extremely ineffective as it is both flooded at some areas and working below the optimal capacity at others.

9.1.9 Conclusions on distributors

The maximum and the standard deviation of the vertical velocity through the plane 5 cm below the demister pad are presented in Figs. 39 and 40, respectively. Although interpretation of the results is always necessary, good distributor performance is generally indicated by low values in both categories. Graphically, the vertical velocities at the

demister inlet are presented in Fig. 41 arranged by increasing maximum vertical velocity in the high design value case. The two additional velocity planes introduced in chapter 8.1 are presented in Appendices IV and V for each distributor. The vertical velocity profiles at the demister inlet in the low design value cases are presented in Appendix VI for each distributor.

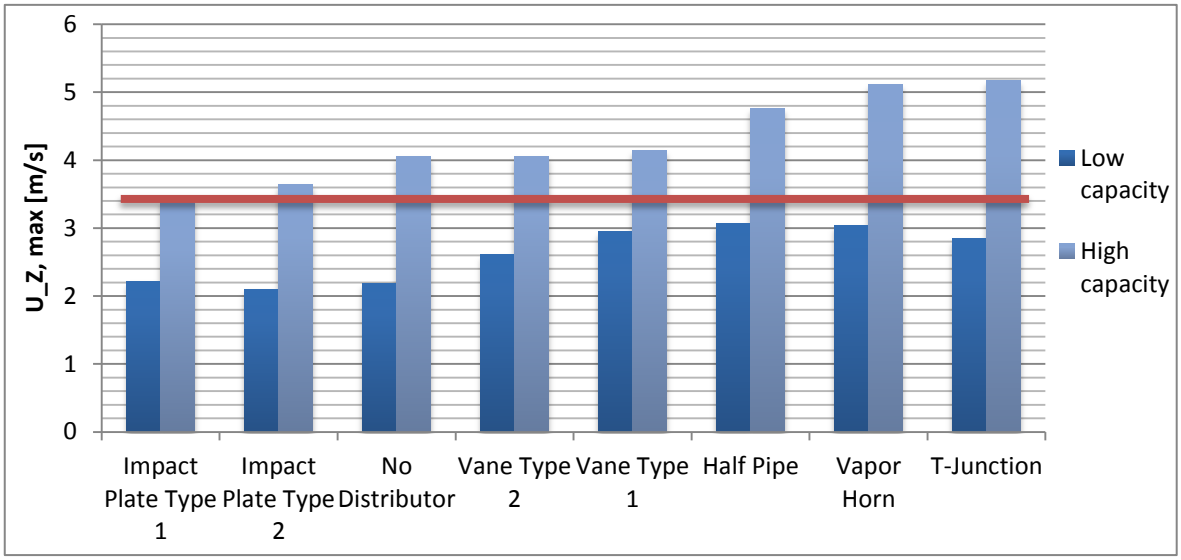

FIGURE 39. Maximum vertical velocity in m/s through a plane 5 cm below the demister pad with different inlet distributors at two different design capacities

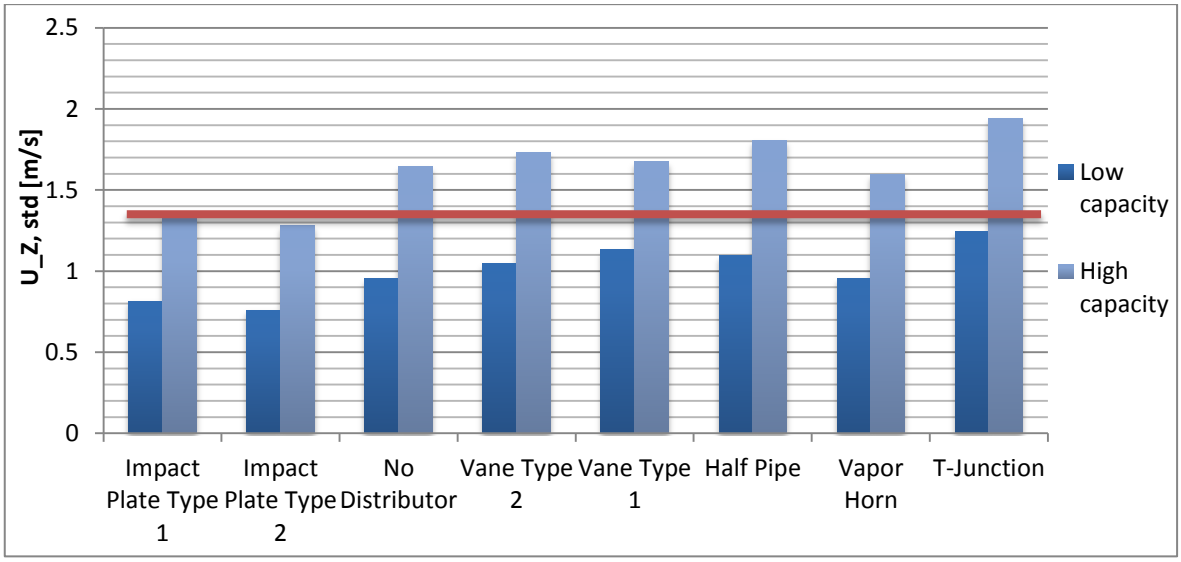

FIGURE 40. Standard deviation of vertical velocity in m/s through a plane 5 cm below the demister pad with different inlet distributors at two different design capacities

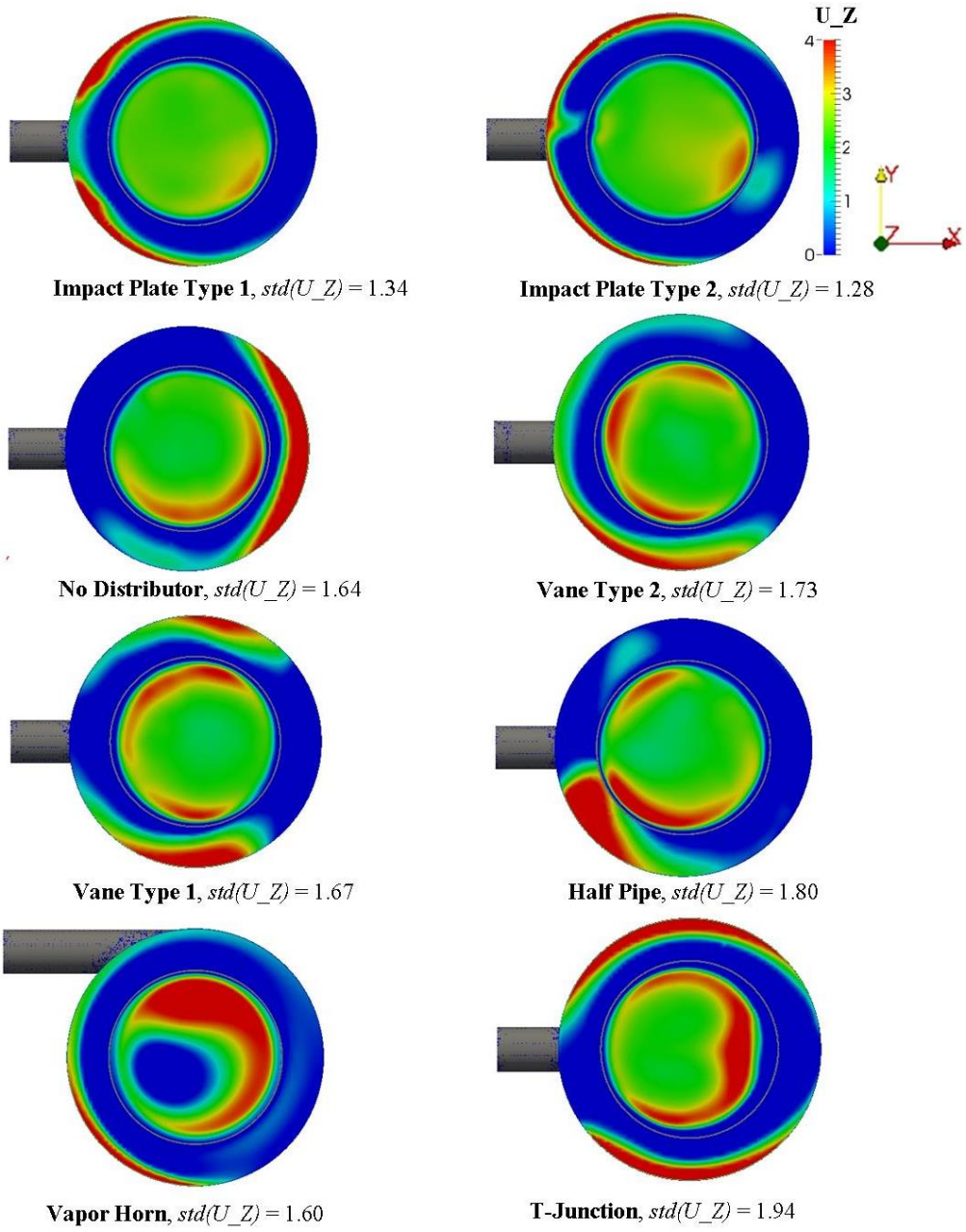

FIGURE 41. Vertical velocities in m/s 5 cm below the demister inlet for different distributor geometries at high design capacity, *std*-value calculated within demister frame (Refer to Fig. 26 for plane location)

Based on numerical and visual analysis of the simulation results, the *Impact Plate* distributors, which direct the flow mostly downwards, are the most ideal units inside the studied vessel geometry with respect to velocity profile at the demister inlet. They yield the lowest maximum and standard deviation values for the vertical velocity below the demister in Figs. 39 and 40, respectively. This indicates good utilization of full demister capacity with no flooding areas. Considering the accuracy of the results, no definitive preference

between the *Impact Plate* distributors can be made. Interestingly, the *Half Pipe* distributor, which also projects the flow downwards, gives worse results than the *No Distributor* reference case with respect to velocity profile at the demister inlet. With the low design capacity, the reference *No Distributor* -configuration achieves as low values for maximum vertical velocity below the demister as the *Impact Plate* distributors. As the capacity increases, however, the *No Distributor* designs performance is weaker compared to the two best distributors and is equal to the *Vane Type* distributors.

Precision engineered designs like the *Vane Type* distributors can have other benefits besides the flow profile enhancement, which are undetectable with the approach of this *Distributor study*. The phenomenon of first stage separation of the liquid droplets from the gas flow is obviously not present in the single phase calculations. This aspect is investigated in the two-phase simulations reported in Chapter 10.

The distributors that project the flow horizontally (like the *Vane Types*, *Vapor Horn* and *T-Junction*), perform the least efficiently inside the studied vessel. One possible cause is that when using these distributors, the flow needs more space for the flow profile to become more uniform across the vessel cross-section. The residence time evaluation performed in the dynamic single phase simulation in Chapter 9.6 supports this observation and indicates that the average residence time is smaller than what is to be expected based on vessel volume.

The sensitivity of each distributor to the flowrate inside the vessel was evaluated based on differences observed between the low and high design value cases. The largest relative drop in maximum horizontal velocity between the high and low design capacity cases was observed for *No Distributor* and *T-Junction* distributors: -46% and -45%, respectively. Especially the *T-Junction* presents itself as a viable option at lower flowrates, even though it has the poorest performance among the high design value cases. The change in standard deviation of velocities at the demister inlet is roughly the same for all of the distributors as seen in Fig. 40. Full summary of vertical velocity profiles at the demister inlet for all of the distributors with low design capacity is presented in Appendix VI. Generally, it can be stated that the importance of distributor design increases as the flow rate and capacity increase.

The effect of each distributor on the liquid surface inside the vessel was also evaluated. Although no liquid layer was introduced to the bottom of the vessel in the simulations, the pressure inflicted on the liquid surface patch by the fluid flow can provide estimation on how the liquid surface would behave in a real-life situation. High pressure gradients indicate that the surface can become agitated. This can lead to liquid re-entrainment into the gas stream, but also complicate the operability of the vessel by disturbing level indicators if wave formation occurs.

Full summary of relative pressure profiles on the bottom of the vessel for each of the distributors in the *Distributor study* is presented in Appendix VII. Liquid level agitation is most likely to occur with the *Vapor Horn* distributor as it has the largest pressure gradients on the bottom of the vessel. The probability of the phenomena is hard to judge based on steady state simulations, but it is safe to say that other distributors should not significantly disturb the liquid surface with the simulated inlet flow.

As concluded later in Chapter 9.3, no distributor can be declared universally inferior to any other based on a single study alone. Performance of the separator vessel as a whole is always dependent on more things besides just the inlet distributor, and different combinations of components can lead to flow behavior not easily predicted by earlier studies.

9.2 Vessel dimensions

The purpose of the *Vessel dimension* -study was to evaluate the effect of changing vessel dimensions on fluid flow within the vessel. The geometries of the two vessel dimension cases alongside the base geometry are presented in Fig. 42. In the *Modifications 1A* and *1B,* the vessel inner diameter was set to the same as the demister diameter: 1200 mm. Liquid residence time in the vessel was kept the same as in the base case so the vessel length increased and the distance from the feed inlet nozzle to the liquid level also increased. Length to diameter ratio moved closer to the recommended ratio of 3-5 as discussed in section 4.2.4.

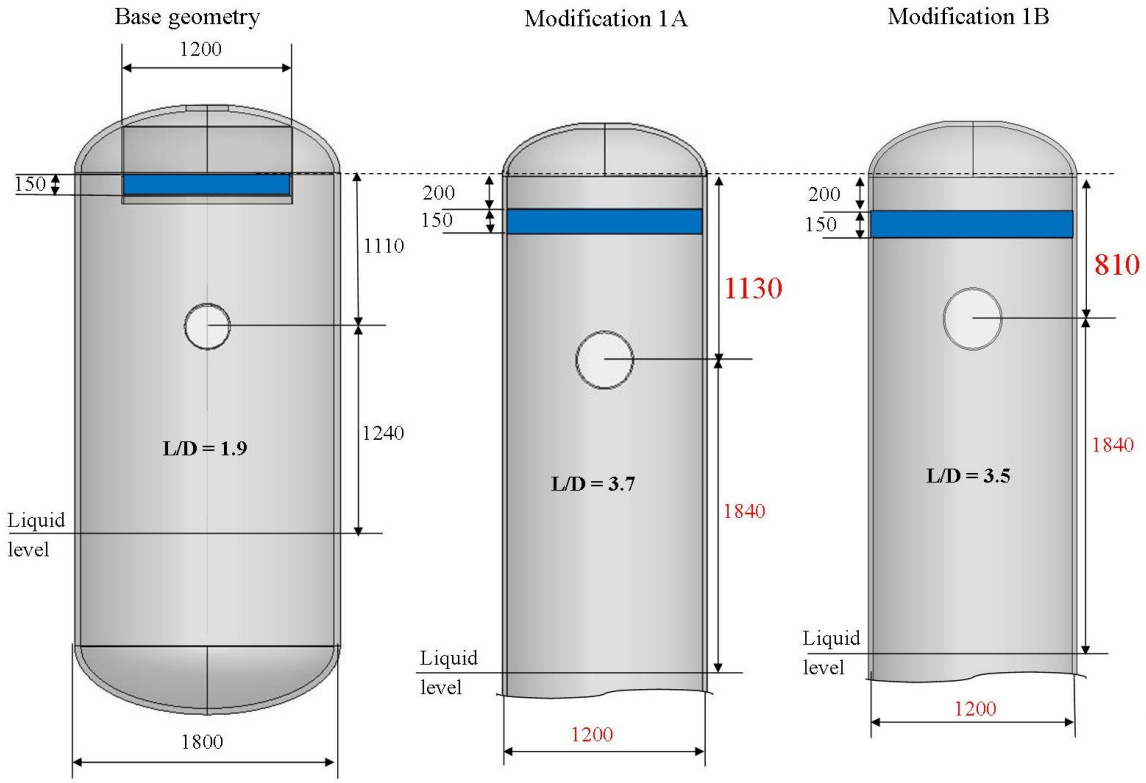

FIGURE 42. Vessel dimensions in millimeters in the two vessel dimension modification cases, base geometry shown on the left as reference. Demister pad illustrated in blue. Images are not in scale.

The demister pad in the modified configurations stretches all the way across the vessel without any external frame. The only modified variable between *Modifications 1A* and *1B* is the distance from feed nozzle to demister as highlighted in Fig. 42. These dimensions resulted in L/D ratios of 3.7 and 3.5 for *Modifications 1* and *2*, respectively. These ratios are calculated based on actual vessel dimensions which are not presented below the liquid level for the modified geometries in Fig. 42 due to illustrative purposes. As with the base geometry, it is worth noting that the liquid level is modelled as a wall like the rest of the vessel and therefore the space below the liquid level has no effect on the simulation results. To slightly lower the velocities, the inlet and outlet pipe inner diameters were increased from 305 mm by two inches to 337 mm. The sizes of the two studied distributors, the *Impact Plate Type 1* and the *T-Junction*, were scaled up with the same ratio as the inlet pipe diameter. The maximum and standard deviation values for the vertical velocity in each *Vessel dimension* -case are presented in Figs. 43 and 44, respectively.

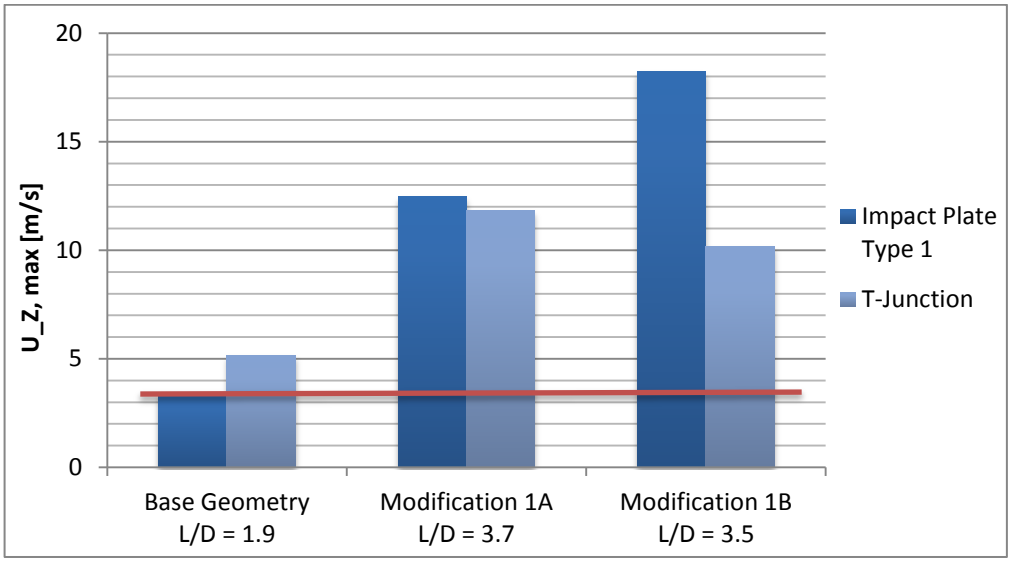

FIGURE 43. Maximum values for vertical velocity 5 cm below the demister pad in m/s in two modified *Vessel dimension* -cases with two different inlet distributors with high design capacity. Base geometry case results presented as reference.

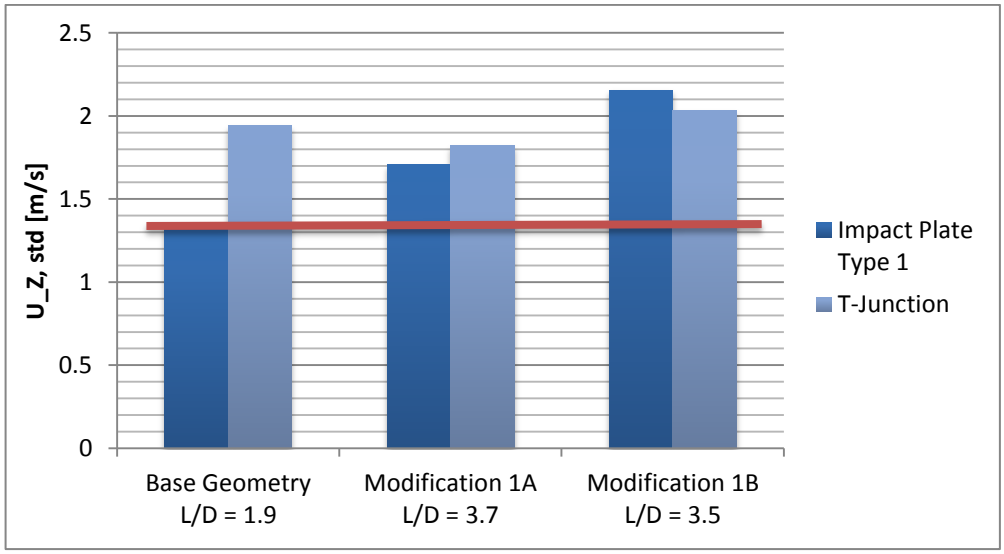

FIGURE 44. Standard deviation of vertical velocity 5 cm below the demister pad in m/s in two modified *Vessel dimension* -cases with two different inlet distributors with high design capacity. Base geometry case results presented as reference.

As expected, the thinner vessel leads to higher maximum velocities at the demister inlet as illustrated in Fig. 43. The scale of the graph in Fig. 43 is substantially larger than in the maximum velocity graphs of other studies. This indicates that the effect of changing vessel dimensions is significantly larger than any of the internal component modifications investigated in the other studies.

While the mean values of the vertical velocities at the demister inlet increase roughly inversely proportionally to the decrease in cross-sectional area, the maximum values increase much more dramatically. A summary of vertical velocity planes 5 cm below the demister pad for each *Vessel dimension* -case is presented in Fig. 45.

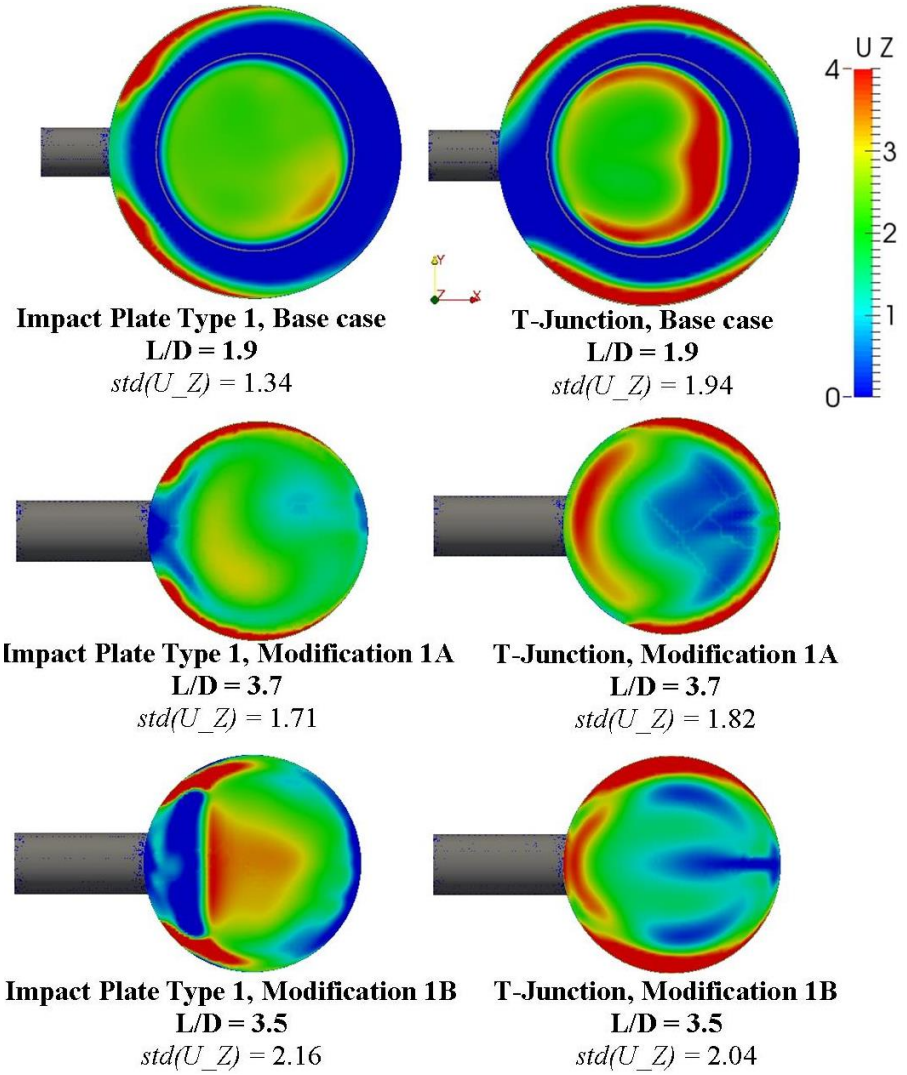

FIGURE 45. Vertical velocity profile 5 cm below the demister inlet in m/s in each modified *Vessel dimension* case. Base case presented as reference, high design capacity in all cases.

The flow profiles in Fig. 45 indicate that the smaller demister frame diameter of the base geometry is beneficial in creating an even flow profile across the demister. When the frame is excluded, and the demister pad stretched across the entire cross-section of the vessel, the high velocity flow at the edges of the vessel is directed through the demister. This leaves some of the middle parts of the demister without sufficient flowrate and thus the demister

is both flooding and working below its capacity at different points of the unit. Low flowrate areas are further magnified as the distance between the inlet and the demister is decreased. Particularly with the *Impact Plate Type 1* distributor, the horizontal plate of the distributor creates a large no-flow zone, effectively blocking the flow through a large portion of the demister. Comparison between *Modifications 1A* and *1B* indicates that increasing the distance between the inlet and the demister allows the flow velocity profile to become more uniform.

9.3 Demister configurations

The purpose of the *Demister configuration* -study was to evaluate the effect of different demister support structures on the flow profiles inside the separator vessel, particularly at the demister inlet. Three different support structures were studied, one of which was the reference demister frame of the base geometry. The structures are presented collectively in Fig. 46.

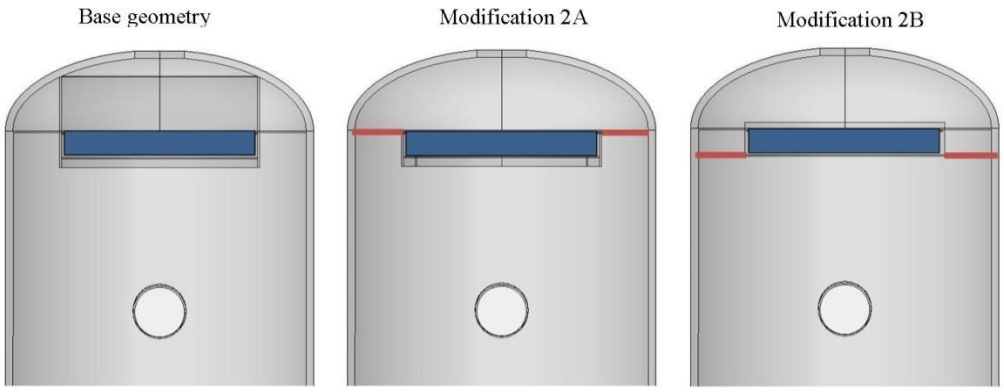

FIGURE 46. Three demister support structures studied in the *Demister configuration* -study. Refer to Fig. 22 for dimensions. Demister pad illustrated in blue, horizontal plate in red.

In the *Demister configuration* -study two different modifications to the base geometry were studied. *Modification 2A* includes a horizontal plate placed at the same elevation as the upper edge of the demister pad. *Modification 2B* has the horizontal plate placed at the elevation of the lower edge of the demister pad. The plate is ring-shaped and extends from the demister frame to the vessel wall. In every case, the demister pad is held in place by a 30 mm wide upper support ring and a 50 mm wide lower support ring. The demister frame

extends 50 mm below and above the demister pad in *Modifications 2A* and *2B*, respectively. Two inlet distributors were used in the *Demister configuration* –study, the *Impact Plate Type 1* and the *T-Junction*. Only high design values were simulated. The maximum and the standard deviation of the vertical velocity at the demister inlet for each support structure and inlet distributor are presented in Figs. 47 and 48, respectively.

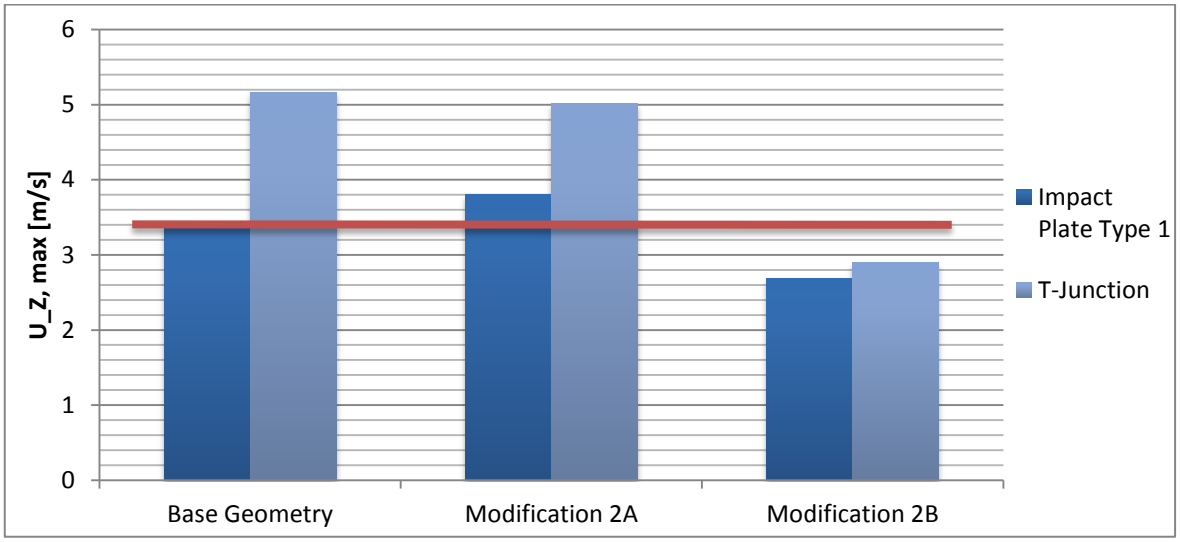

FIGURE 47. Maximum values for vertical velocity 5 cm below the demister pad in m/s in two modified *Demister configuration* -cases with two different inlet distributors with high design capacity. Base geometry case results presented as reference.

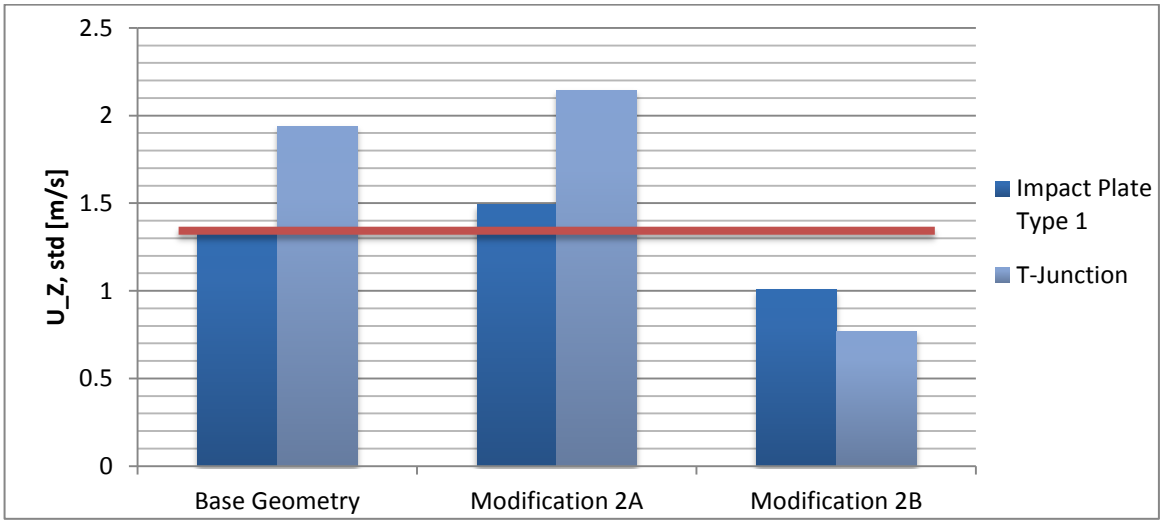

FIGURE 48. Standard deviation of vertical velocity 5 cm below the demister pad in m/s in two modified *Demister configuration* -cases with two different inlet distributors with high design capacity. Base geometry case results presented as reference.

Modification 2A does not significantly change the values of maximum velocity and standard deviation at the demister inlet. Both indicators obtain slightly inferior values as compared to the *Base geometry*, with the exception of maximum velocity for the *T-Junction* which is slightly improved. The effects of *Modification 2B* are much more dramatic. Flow uniformity as well as the maximum velocity values are clearly improved for both distributors. Most notably, the *T-Junction* which produces a markedly inferior flow profile with the *Base geometry* actually produces a more uniform pattern than the *Impact Plate Type 1* with the *Modification 2B*. A summary of vertical velocity planes 5 cm below the demister pad for each *Demister configuration* case is presented in Fig. 49.

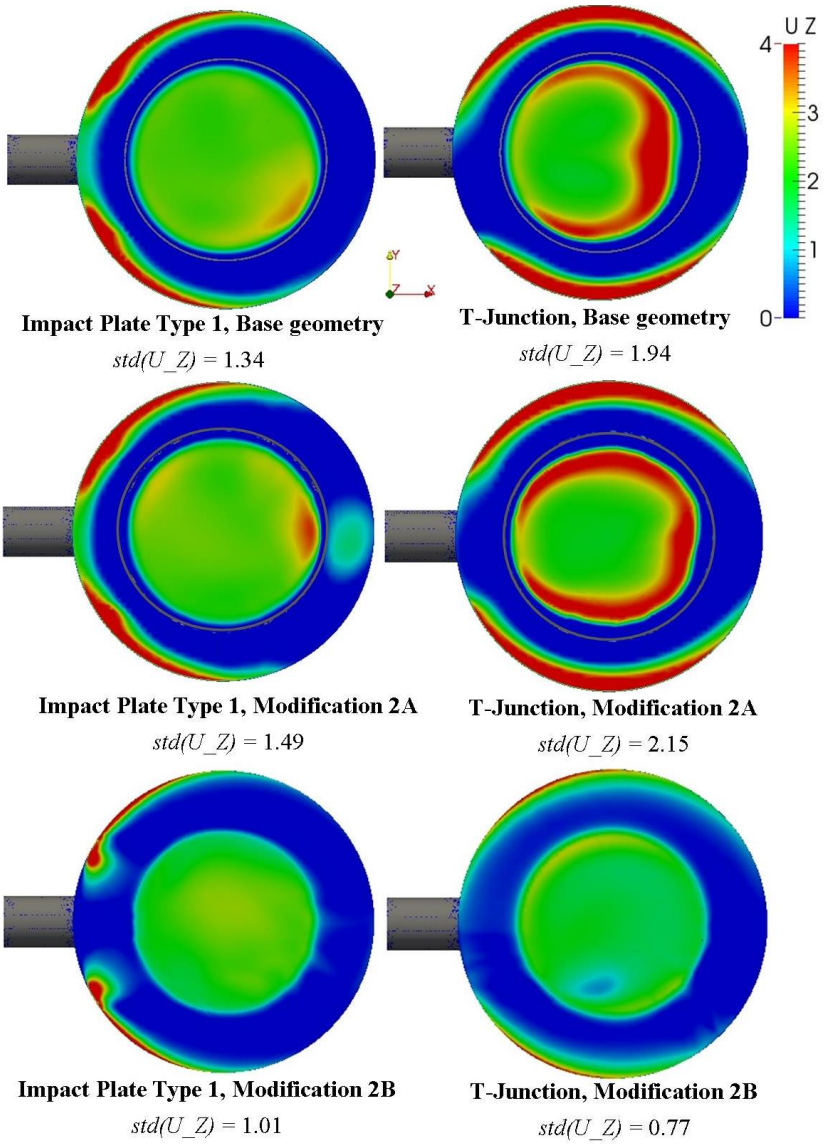

FIGURE 49. Vertical velocity profile 5 cm below the demister inlet in m/s in each modified *Demister configuration* case. Base geometry results presented as reference, high design capacity in all cases.

Fig. 49 reveals that *Modification 2A* amplifies problems around the demister frame already encountered with the *Base geometry*. This problem is described in Chapter 9.1.6 concerning the *T-Junction* distributor and is caused by the returning flow traveling downwards near the lip of the demister. As illustrated in Fig. 34, this creates a vacuum zone around the outer edge of the demister that blocks flow through that particular part of the demister. No such problem exists with *Modification 2B* because the horizontal plate prevents the flow from looping around the demister frame. Since there is no "lip" below the demister pad in the *Modification 2B*, the effect of the sharp angle of the demister frame is not visible on the plane in Fig. 49. Although the *T-Junction* produces a very even flow profile 5 cm below the demister inlet, the sharp edge of the demister frame causes local velocities to increase on direct contact with the demister.

The velocity acceleration due to the demister frame and the vertical velocity profiles on a plane in direct contact with the demister pad are presented in Fig. 50. This phenomenon has a strong effect on the demister inlet velocity profiles of the *Modification 2B* configurations, where the velocity increases right at the entrance to the demister. The effect on the *Right Angle* distributor is not as strong as on the *T-Junction*: the velocity increases around the same region, but the local velocities do not exceed 4 m/s. The horizontal planes are best compared with Fig. 49 to see how much the flow profile changes in the last 5 centimeters before entering the demister in each configuration.

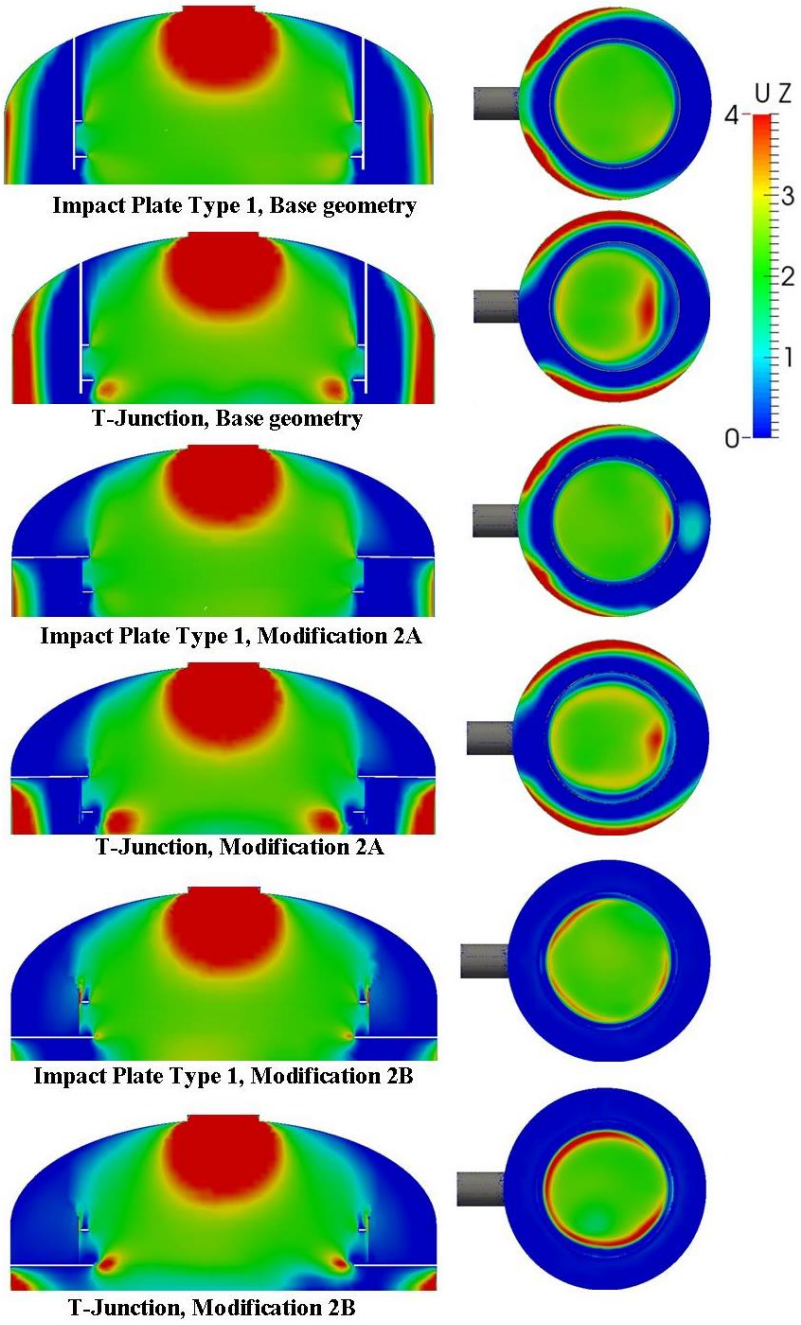

FIGURE 50. Acceleration of flow velocity due to demister design in the *Demister configuration* cases. Left: Horizontal plane, Right: Velocity profile at demister inlet level. Refer to Fig. 26 for plane locations.

In general, sharp corners should be avoided especially around key areas like demisters since they have the capability to accelerate flow velocities if the flow is forced to turn around the corner. The problem becomes more manageable if the flow is only traveling past the corner without having to change direction.

The *Modification 2B* seems to improve the flow profile produced by the *T-Junction* more than by the *Impact Plate Type 1*, to the point where the flow profile produced by the *T-Junction* is actually more uniform of the two studied distributors. This advantage is lost if the entrance to the demister is not rounded since the flow created by the *T-Junction* needs to make a sharp turn to enter the demister. Provided that the flow acceleration problems are addressed either by rounding of the demister entrance or by distributor design, the *Modification 2B* seems to be the best option among the studied *Demister configurations*. Along with leveling the flow profile, it prevents the formation of the no-flow zone along the demister frame. The extent of this benefit is uncertain though, because the demister support rings always restrict the flow along the outer edge inside the demister.

These results show that no distributor can be declared universally inferior to any other design as the overall performance of the separator unit is always dependent on all of the components inside (and often also upstream of) the vessel. Different combinations of structural components can result in flow behavior that is not always readily predicted if only a single component such as an inlet distributor or a demister is considered.

9.4 Outlet configurations

The purpose of the *Outlet study* was to evaluate the effect of changing gas outlet configuration to fluid flow mainly around the demister area. Three different outlet configurations were simulated: an outlet with rounded edges, a round solid plate placed below the outlet and a square perforated plate placed below the outlet. According to generally used friction loss charts, rounding the outlet with an *r/D* ratio of 0.15 reduces the friction loss coefficient *K* by 92% from 0.50 to 0.04 as compared to a sharp edged design. Sketches of the mentioned modifications are presented graphically in Fig. 51.

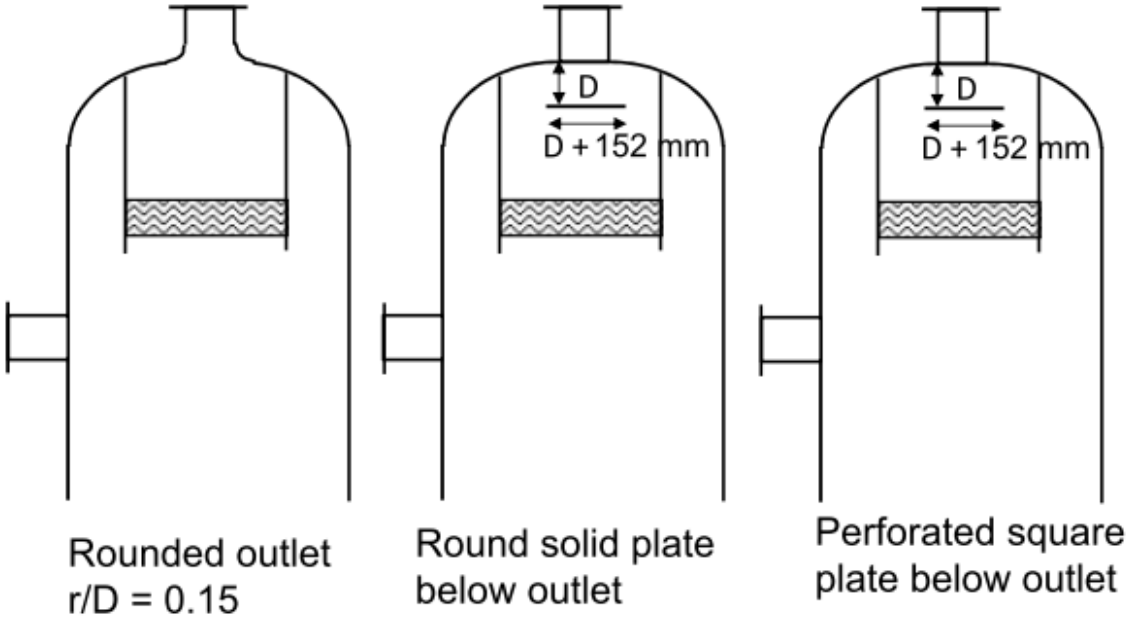

FIGURE 51. Schematic drawings of the three different configurations studied in the *Outlet study*. Roundness of the outlet exaggerated for illustrative purposes.

The configuration of the holes in the *Perforated plate* case is presented in Fig. 52.

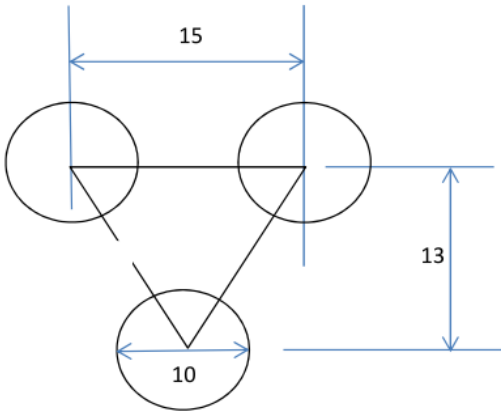

FIGURE 52. Positioning of the holes in millimeters in the *Perforated plate* case

Only the *Impact Plate Type 1* distributor and the high capacity design values were used in modeling of the cases in the *Outlet study*. Maximum and standard deviation values of vertical velocity across a plane 5 cm below the demister pad are presented in Figs. 53 and 54, respectively.

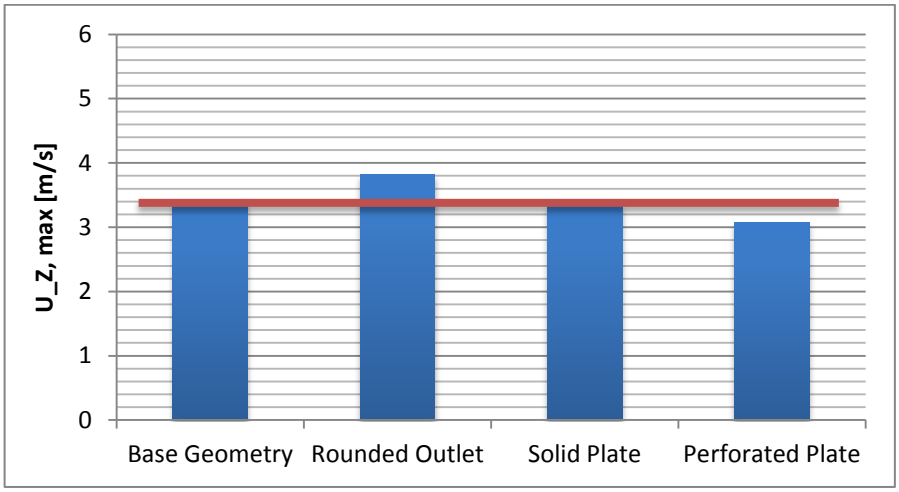

FIGURE 53. Maximum values for vertical velocity 5 cm below the demister pad in m/s in three modified *Outlet configuration* -cases with high design capacity. *Base geometry* case results presented as reference.

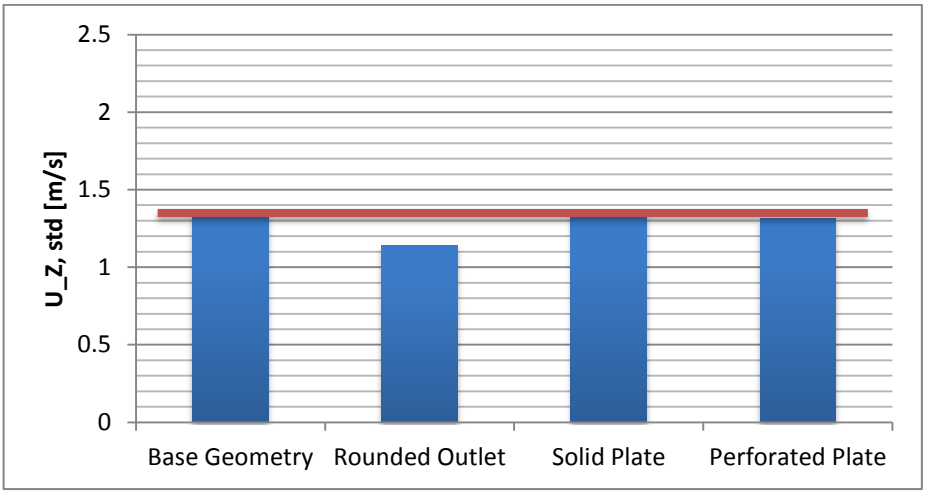

FIGURE 54. Standard deviation of vertical velocity 5 cm below the demister pad in m/s in three modified *Outlet configuration* -cases with high design capacity. *Base geometry* case results presented as reference.

Figs. 53 and 54 indicate that the *Rounded outlet* has the biggest impact on fluid flow among the *Outlet configurations*. Rounding the outlet increases the fluid maximum velocity at the demister inlet slightly as seen in Fig. 53. This is due to absence of resistance caused by sharp angles to the outlet fluid flow. The uniformity of the flow profile at the demister inlet is increased with the *Rounded outlet* as seen in Fig. 54. Even though the peak velocities can increase slightly, overall the Rounded outlet produces a smoother flow profile at the demister inlet compared to other *Outlet configurations*. Based on basic fluid

dynamics principles, the effect of the *Rounded outlet* should be more pronounced with liquid flows, since they experience higher friction forces at sharp corners due to higher viscosities. Close up views of the vertical velocities in the outlet area on a vertical plane for each *Outlet configuration* are presented in Fig. 55.

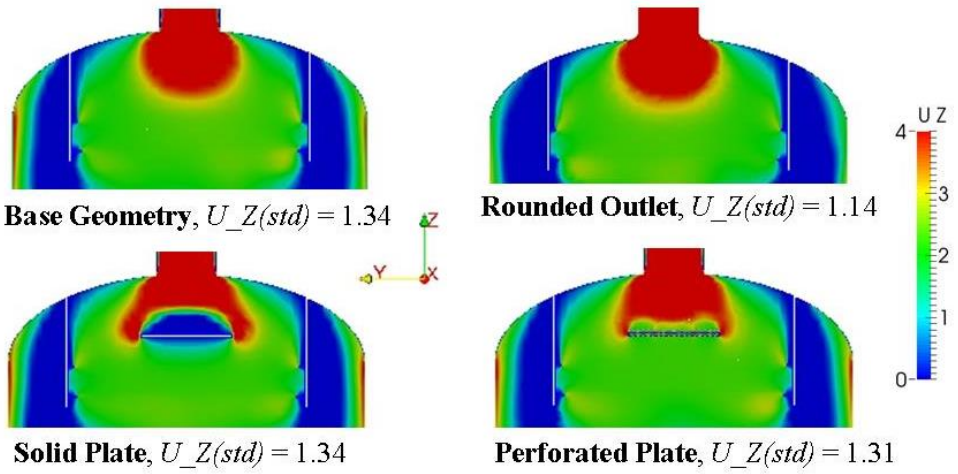

FIGURE 55. Vertical velocity profile on a vertical plane in each *Outlet configuration* case. Standard deviation value calculated across demister inlet. Refer to Fig. 26 for plane location. High design capacity, *Impact Plate Type 1* distributor.

Fig. 55 confirms that the solid and perforated plates function as expected. It also confirms that the *Rounded outlet* enhances flow through the outlet. This is seen as reduced flow velocity outside of the demister frame. A summary of vertical velocity planes 5 cm below the demister pad for each *Outlet configuration* case is presented in Fig. 56.

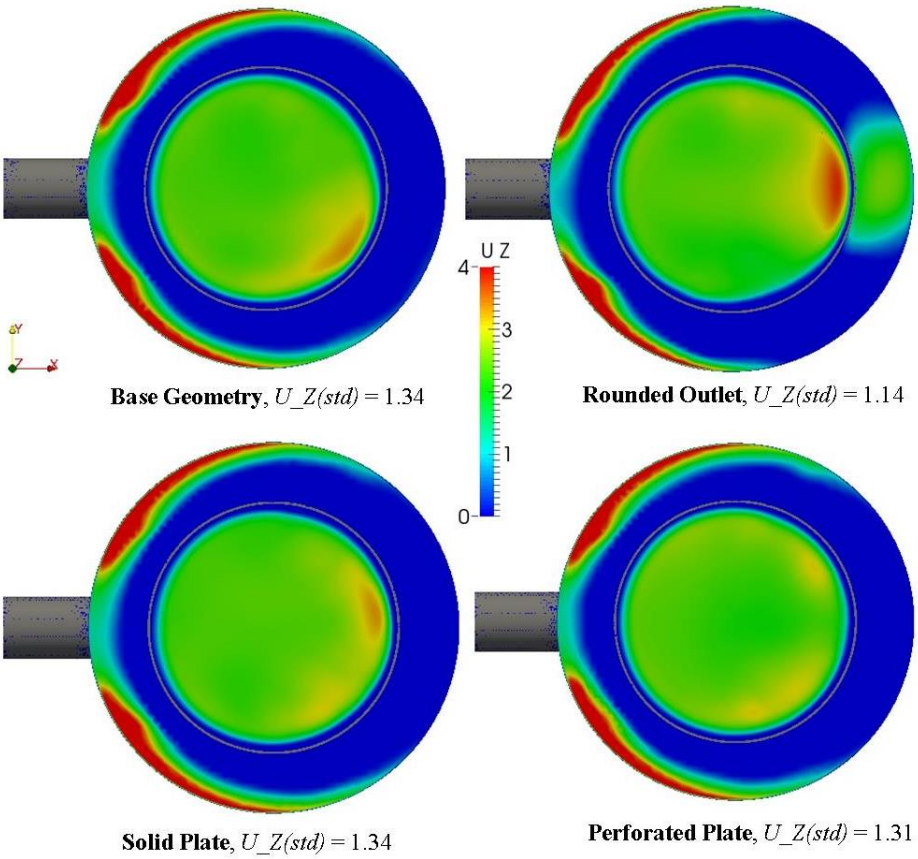

FIGURE 56. Vertical velocity profile 5 cm below the demister inlet in m/s in each modified *Outlet configuration* case. Base case presented as reference. High design capacity, *Impact Plate Type 1* distributor.

Visually, all of the flow profiles in Fig. 56 exhibit acceptable evenness. The *Rounded outlet* stands out with a slightly lower standard deviation among the *Outlet configurations* despite the formation of a small high velocity zone near the back wall of the vessel. Based on this, it can be deduced that the low standard deviation value is the result of the whole flow field obtaining velocities very close to the mean velocity at the demister inlet with the exception of the high velocity zone. In actual operation of the separator, this type of uniformity does not yield any additional benefits as long as the maximum velocities remain below the acceptable limit. To more closely study the effects of the outlet configurations, vertical velocity planes were also extracted at two locations inside the demister frame. The lower plane was extracted 5 cm above the demister pad and the upper 5 cm below the plate. These planes are presented in Fig. 57 for all of the *Outlet study* cases with only the area inside the demister frame included in the pictures.

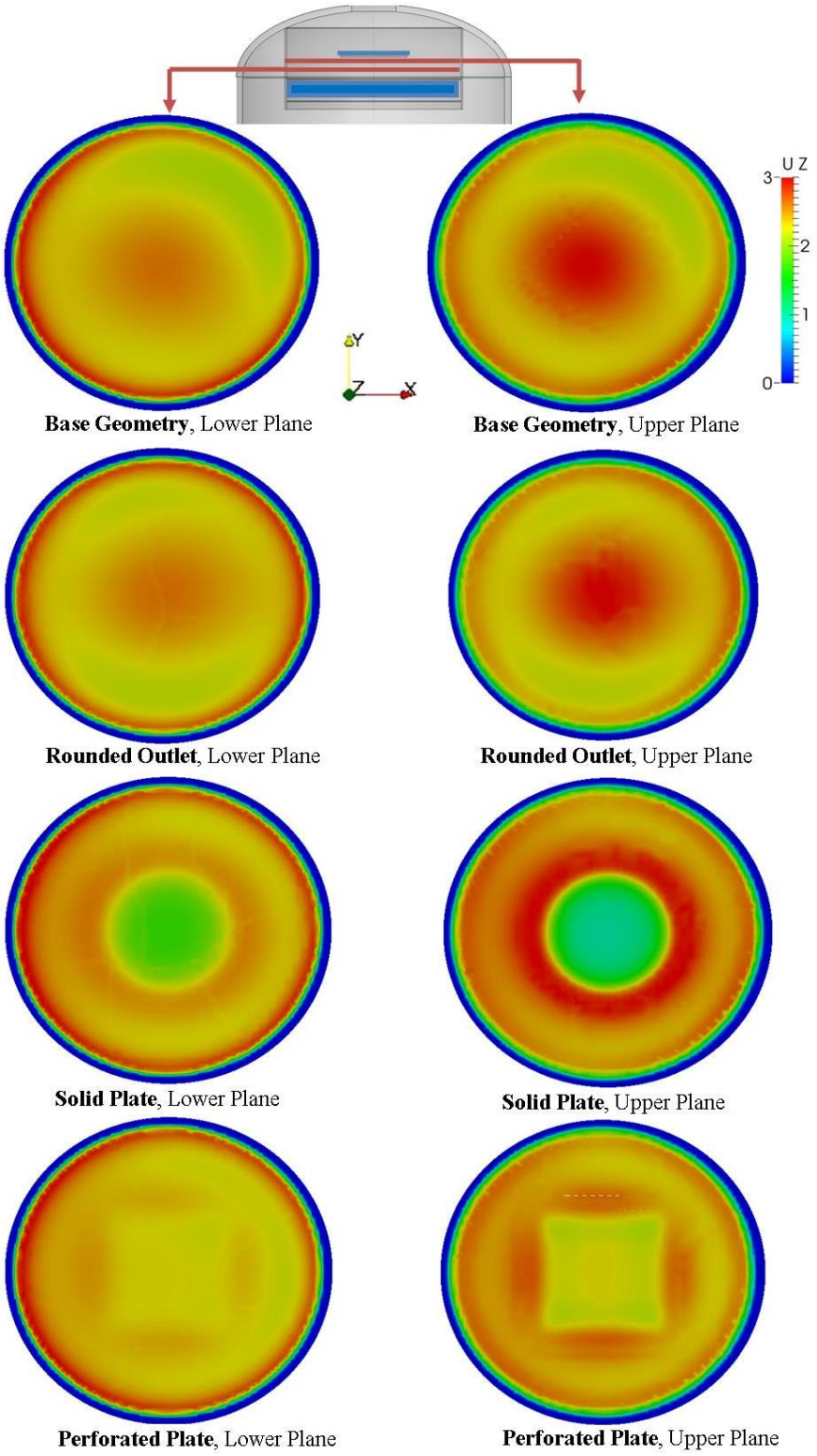

FIGURE 57. Vertical velocity on two planes inside the demister frame in the *Outlet study* cases. Only area inside demister frame is presented. Top picture indicates plane locations (in red) between demister and the plate (in blue). High design values. NOTE! Different color scale compared to other velocity figures.

Fig. 57 indicates that the rounded outlet does not significantly change the flow profile inside the demister frame. The maximum velocities on these two planes also remain unchanged for the *Rounded outlet* as compared to the *Base geometry*. The effects of the plates are as expected: The solid plate obstructs the fluid flow efficiently while the perforated plate lets part of the flow pass through, creating a more shallow aerodynamic shadow. If the velocity increases dramatically downstream of the demister, it can lead to flooding similarly than as a result of upstream velocity increase. In the calculated cases, the maximum velocities downstream of the demister remain at 3 m/s which is the same as for the *Base geometry*. Therefore it is unlikely that any of these modifications will contribute to flooding of the demister.

Overall, it can be concluded that none of the *Outlet configurations* can be declared best when employing the well performing *Impact plate* distributor. Further studies should be conducted to determine the possibilities of improving flow with outlet modifications when using distributors with worse performance characteristics.

9.5 Modified distributors

The purpose of the *Modified distributors* study was to obtain information on how changes in the design of some key distributors affect the flow profile inside the vessel. Three distributors were studied: *Half Pipe, Impact Plate Type 1* and *T-Junction*. The *Modified Half Pipe* distributor is based on an existing configuration and was modelled to determine how much narrowing the width of the opening changes the flow compared to the "actual" *Half Pipe*. The width of the opening is typically calculated based on design values for the separator, for the *Modified Half Pipe* it is set to 100 mm. *Impact Plate Type 1* and *T-Junction* were selected for the *Modified distributors* study based on their good and bad performance in the original *Distributor study*, respectively. Schematic drawings of all of the distributors studied in the *Modified distributors* study are presented in Fig. 58.

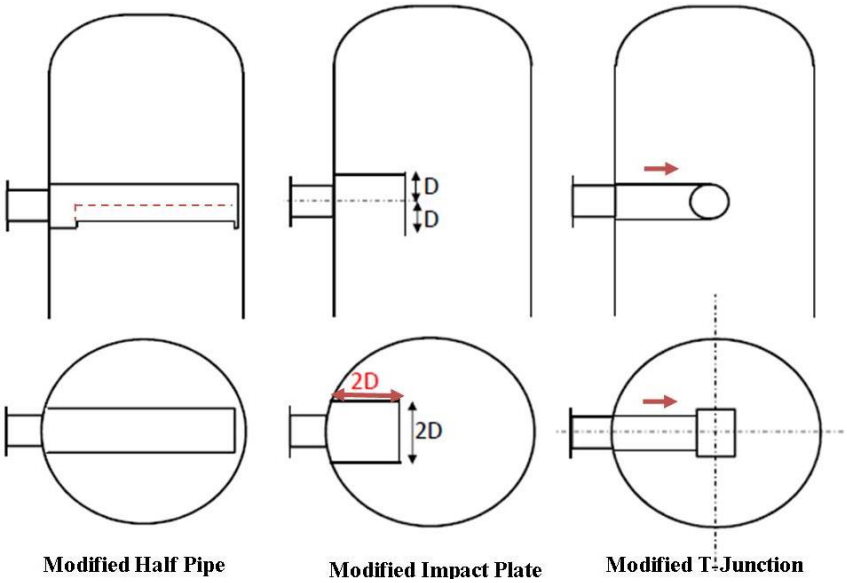

FIGURE 58. Schematic drawings of the distributors studied in the *Modified distributor study*, changes to *Distributor study* configurations highlighted in red

Only high design capacities were studied in the *Modified distributors* study. Maximum and standard deviation values of vertical velocity across a plane 5 cm below the demister pad are presented in Figs. 59 and 60, respectively.

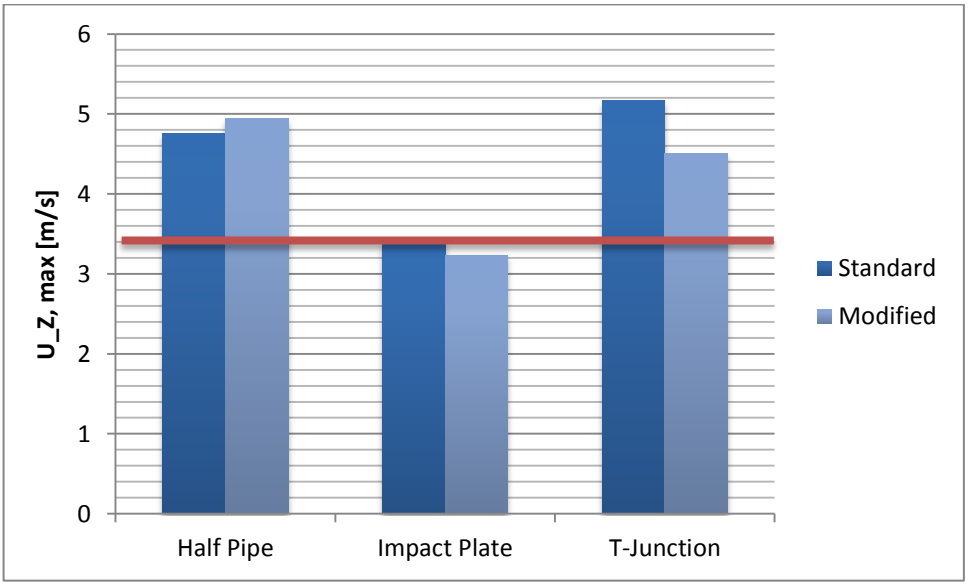

FIGURE 59. Maximum values for vertical velocity 5 cm below the demister pad in m/s in three *Modified distributor* -cases with high design capacity.

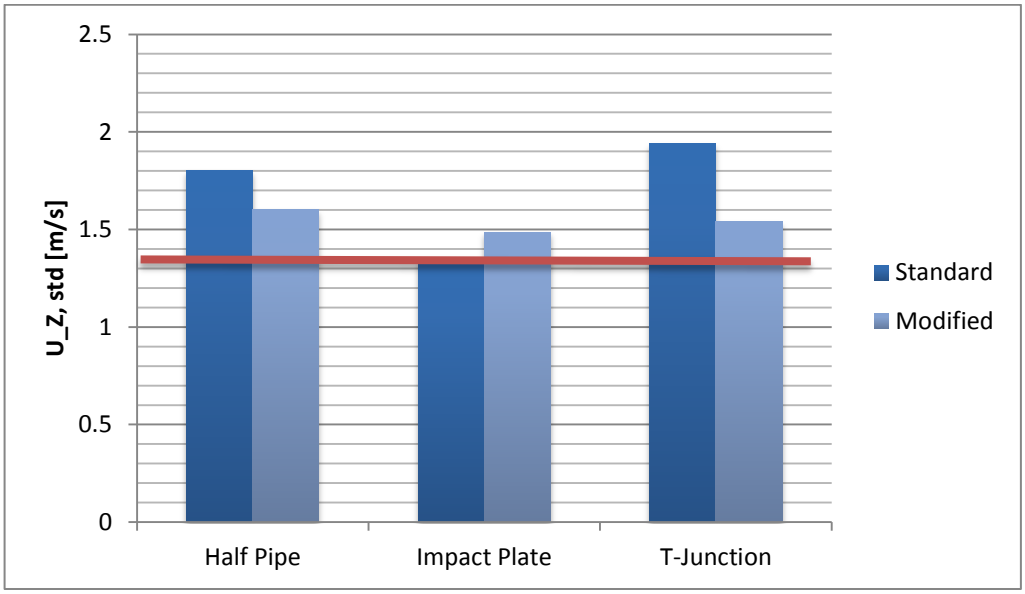

FIGURE 60. Standard deviation values for vertical velocity 5 cm below the demister pad in m/s in three *Modified distributor* -cases with high design capacity.

The most considerable effect on performance is observed for the *T-Junction* distributor. Where the *Standard T-Junction* creates clearly the most uneven flow profile among the distributors in the *Distributor study* (see Fig. 41), the *Modified T-Junction* has the third lowest standard deviation value for the vertical velocity at demister inlet right after the *Impact Plate* distributors. The vertical flow profiles at demister inlet compared between the *Standard* and *Modified* configurations are presented in Fig. 61.

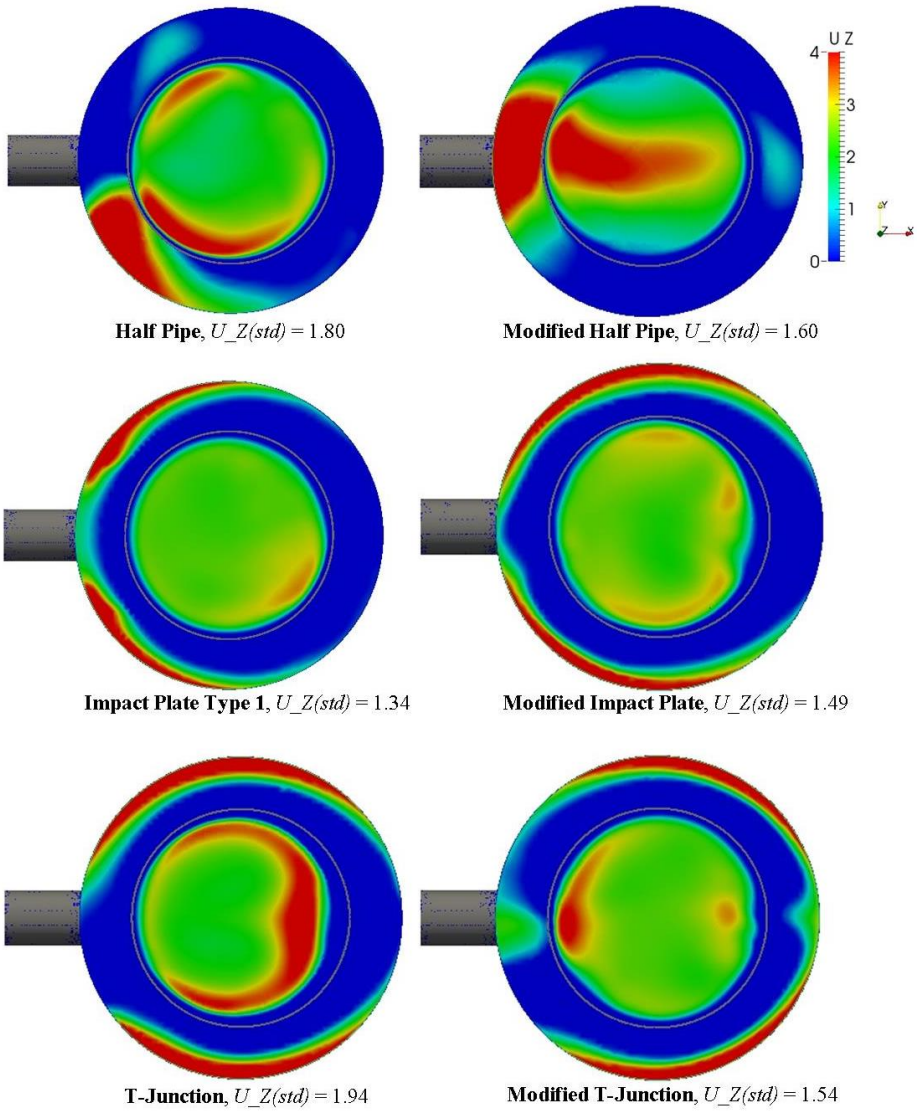

FIGURE 61. Vertical velocity profile at demister inlet in m/s in each *Modified distributor* case (right) compared to standard design from the *Distributor study* (left). High design capacity.

Again, the most interesting comparison can be made between the *T-Junction* –distributors. The *Modified T-Junction* produces a notably better flow profile than the *Standard T-Junction*. Most apparent improvements are the diminished size of the high velocity flow area and the absence of the large no-flow zone of the *Standard T-Junction* (see Fig. 34). If large amounts of liquid are present in the inlet stream, splashing of the liquid due to high velocity impact to the vessel wall can cause entrainment problems. For the *Standard T-Junction*, this problem is unlikely since the flow exits the distributor almost tangentially to the vessel wall. The asymmetry which is especially noticeable in the *Half Pipe* flow profile is not an uncommon phenomenon and is addressed in detail in Chapter 11.2.

9.6 Dynamic simulation

As described earlier in Chapter 7.7, each iteration for an already converged case in the steady state calculations produces a slightly different solution field. To obtain a better view of the inherent unstableness of the flow phenomena, a dynamic simulation was conducted. In this chapter, the amount of time-based fluctuation in the simulations is assessed for both the *Steady state* and *Dynamic simulations*.

The time-dependent simulation, referred to as *Dynamic simulation* was conducted with the *Impact Plate Type 1* configuration of the *Distributor study*. The dynamic simulation was started at time point 0 with an empty vessel. The evaluated data presented in this work was gathered between time points 6 - 12 s. This was done to assure fully developed flow profile within the vessel. The residence time of flow within the vessel is roughly 3 seconds, based on the volumetric flow and the vessel computational volume (excluding volume below the liquid level). The dynamic simulation is compared in this chapter against the identical steady state *Impact Plate Type 1* case of the *Distributor study* which is referred to in this chapter as the *Steady state simulation*. For both of these simulations, only high design values are considered.

OpenFOAM provides an option to evaluate time-based fluctuation through calculation of the *UPrime2Mean*-variable.

$$UPrime2Mean = (U - Umean)^2 \tag{28}$$

U	Momentary velocity at point i, m/s
Umean	Mean velocity over all time steps / iterations at point i, m/s

The *UPrime2Mean*-variable is calculated independently for all of the velocity components (x, y and z) as well as the possible cross-combinations. As the vertical velocity (z) is of primary interest in this work, only its variance is considered and referred to simply as *UPrime2Mean*. The location where the amount of fluctuation was monitored was the demister inlet (upper horizontal plane in Fig. 26). By modifying Eq. 28, the average amount of time-based velocity variation at demister inlet can be calculated by

$$\frac{U-Umean}{Umean} = \frac{\sqrt{UPrime2Mean}}{Umean}. \tag{29}$$

Eq. 29 yields average time-based velocity variance values of 92% and 61% at the demister inlet for the *Dynamic simulation* and the *Steady state simulation*, respectively. This indicates that the nature of the flow is highly unstable in both simulations. Hence it justifies the implementation of the averaging procedure described in Chapter 7.7. Because momentary / single time step values are compared with the time-averaged *Umean*-variable, the results discussed here are dependent, although not significantly, on the studied time step / iteration. In the *Steady state simulation* it is the iteration number 2000 and in *Dynamic simulation* time step 12.00 s.

When post-processing the data, it was observed that the average streamline spent around 1.5 seconds before reaching from inlet to outlet. This value is considerably lower than the computational volume -based residence time of roughly 3 seconds and indicates that the flow does not fully utilize the entire vessel volume. So long as the velocity profiles at the outlet remain acceptable, this is not a problem. However, with distributors that create a more uneven flow profile, longer residence times inside the vessel may help in developing a more uniform flow profile closer to the outlet.

When averaged through time steps or iterations and compared at the at the demister inlet, the obtained values are quite similar for both the *Dynamic* and the *Steady state simulation*. Time- and iteration-averaged velocity profiles at the demister inlet can be compared in Appendix III between the two simulations. They confirm visually that the obtained results are similar with both approaches. The maximum and the standard deviation values of the vertical velocity at the demister inlet are presented in Table XI for both simulations.

TABLE XI. Comparison of time- and iteration-averaged velocity variables at demister inlet in the *Steady state* and *Dynamic simulations*

	U_Z, max [m/s]	U_Z, std [m/s]
Steady state	3.40	1.34
Dynamic Simulation	3.41	1.48

Table XI indicates that the obtained value for the standard deviation in the *Steady state* model is slightly lower than in the *Dynamic simulation*. This is logical since the *Steady state* model aims to find a steady solution which is more likely to have a uniform flow profile as opposed to the *Dynamic simulation*, which only considers momentary velocities. Therefore the *Steady state* model has an inherent tendency to create more unified solution

fields. Keeping this in mind, the faster *Steady state* approach can be utilized in place of the more computationally demanding *Dynamic* model when an engineering accuracy is sufficient. Calculation through 12 seconds of fluid flow inside the vessel consumed about 50 times more computational resources than calculating 2000 iterations in a similar steady state simulation, thus making running all of the cases as dynamic an unviable option.

The time- and iteration-based fluctuations are best visualized through animations which cannot be presented here. In Appendix III, velocity profiles of individual iteration results are presented for a single steady sate case. Two velocity profiles are also presented from two time steps of the *Dynamic simulation*.

10. TWO-PHASE MODEL SIMULATION RESULTS

To further justify the use of the simplified single phase model, the *Base geometry* with two distributors, *Impact Plate Type 1* and *Vane Type 1*, was simulated using a two-phase dynamic model. The *Impact Plate Type 1* distributor was chosen as the reference configuration because of its good performance in the earlier studies. The *Vane Type 1* distributor was selected because it is specially designed to perform first stage separation of the liquid droplets from the gas stream. The results were studied to find out whether this phenomenon can be seen in the two-phase model.

10.1 Case setup

Since the two-phase calculations are computationally very heavy compared to other simulations in this thesis and due to limited time available, the emphasis of the two-phase simulations was placed on obtaining as much usable results as possible. Time spent in defining model parameters was kept to a minimum. This leaves a lot of possibilities for future work in model validation.

An Euler-Euler multiphase model was used because of the small liquid droplet sizes. The other possible alternative, the Volume of Fluid (VOF) model was deemed impractical because it would have required a too fine base mesh size to accurately track the phase interface. Material properties of the two phases were specified based on earlier simulations

on similar flows. Material properties are presented in Table XII, the gas phase material properties are equal to those used in the single phase simulations.

TABLE XII. Material properties of the phases in the two-phase simulations

	Gas	Liquid
Density, kg/m^3	3.17	774.00
Dynamic viscosity, mPas	0.01	2.86
Kinematic viscosity, m^2/s	3.15 x 10^{-6}	3.70 x 10^{-6}

A constant diameter model was used in specifying the droplet sizes for both phases. The droplet sizes were set to 1000 µm and 350 µm for the gas and liquid phases, respectively. With certain drag model settings in OpenFOAM, droplet diameters for both phases need to be specified to model also regions where phase inversion occurs. The specified liquid phase droplet size was chosen in order to see a distinct difference between the behaviors of the phases. A reference case was simulated with a liquid droplet size of 150 µm using the *Impact Plate Type 1* distributor but no significant change in behavior was observed. The effect of the droplet size therefore remains an area where further investigation is required.

Schiller-Naumann drag model was used in the two-phase calculations. The specified droplet sizes have an impact on the drag interactions between the phases. The definitions of the drag model were not optimized with respect to the simulated flow conditions, which leads to uncertainty in the results concerning interaction between the phases.

High design capacity values were used in the simulation. Inlet flow velocity was specified as 31.8 m/s for both phases. Outlet was again specified as a fixed relative pressure outlet at 0 Pa(g). Volumetric phase fraction of the liquid phase was set to 10% at the inlet with the rest of the volume occupied by the gas phase. This value was selected in order to generate results where some amount of accumulation and individual phase behavior could be observed.

The simulation was initialized with a vessel completely filled by the gas phase. 4 seconds of the simulation was run before gathering of data was started to introduce liquid flow into the vessel and reach quasi-steady flow conditions. The gathering of averaged data was started at 4 seconds of run time and carried on until the end of the simulation at 10 seconds. The averaged variables included pressure, wall shear stress, (averaged and

individual phase) velocity and the phase fractions. The time step length in the simulations was limited by the Courant number *Co*, which is specified according to Siikonen (2014) as

$$Co = \frac{\Delta t U}{\Delta x}. \tag{30}$$

Co	Courant number
⊿t	Time step length, s
U	Local velocity, m/s
⊿x	Local cell length, m

In two-phase simulations, all monitored data was averaged between time steps 4-10 seconds with the criteria $Co_{max} < 2$. Essentially this means that fluid flow at any given point inside the vessel will not travel further than the length of two computational cells during a single time step. Accuracy and stability of the solution increase as the Courant number is decreased and the time step length is decreased proportionally. The areas where the Courant number reaches its maximum value are very small and the average Courant number inside the vessel with the $Co_{max} < 2$ criterion was in the range of 0.1 to 0.2. The average time step lengths with this criterion were about 0.00008 s and 0.00004 s for the *Impact Plate Type 1* and *Vane Type 1* distributors, respectively. Slightly larger maximum Courant numbers were used during the "fill up time" of the first 4 seconds. Linear upwind 2nd order schemes were used in calculation of all the solution fields.

With the criteria specified above, the calculation of 10 seconds of flow inside the vessel using the *Impact Plate Type 1* distributor consumed about 170 times more computational resources than the same case modelled as a single phase steady state calculation. The *Vane Type 1* two-phase simulation consumed even more as the mesh was denser due to more complex geometry and time steps were shorter due to higher local velocities.

10.2 Results

Flow profiles between the two-phase calculations and the corresponding single phase calculations were compared at the demister inlet. Even though the liquid droplet size 350 µm was selected in order to see differences in phase behavior, the liquid and gas phase

velocity profiles are almost identical in the two-phase simulations. Figs. 62 and 63 show comparisons of maximum and standard deviation of the gas phase vertical velocity at the demister inlet between the single and two-phase simulations.

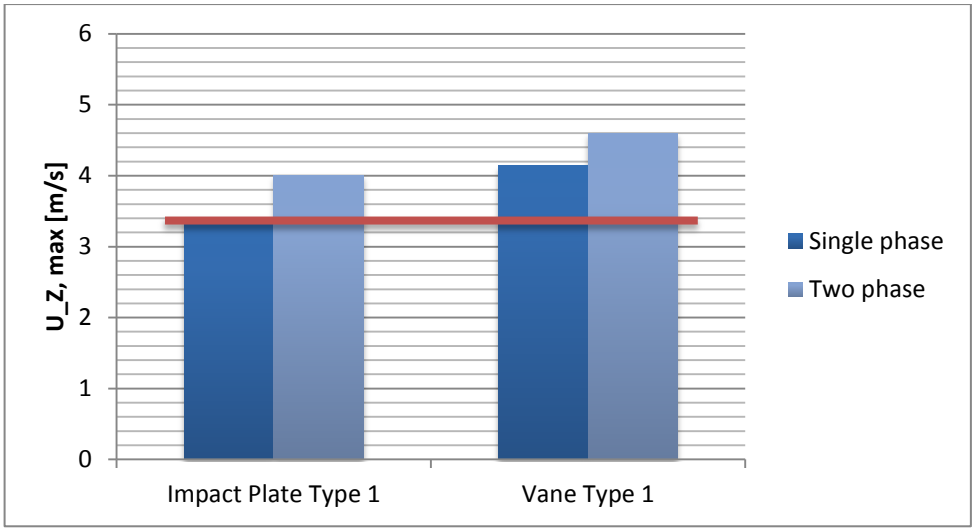

FIGURE 62. Maximum gas-phase vertical velocity on a plane 5 cm below the demister pad in the single and two-phase simulations. High design values.

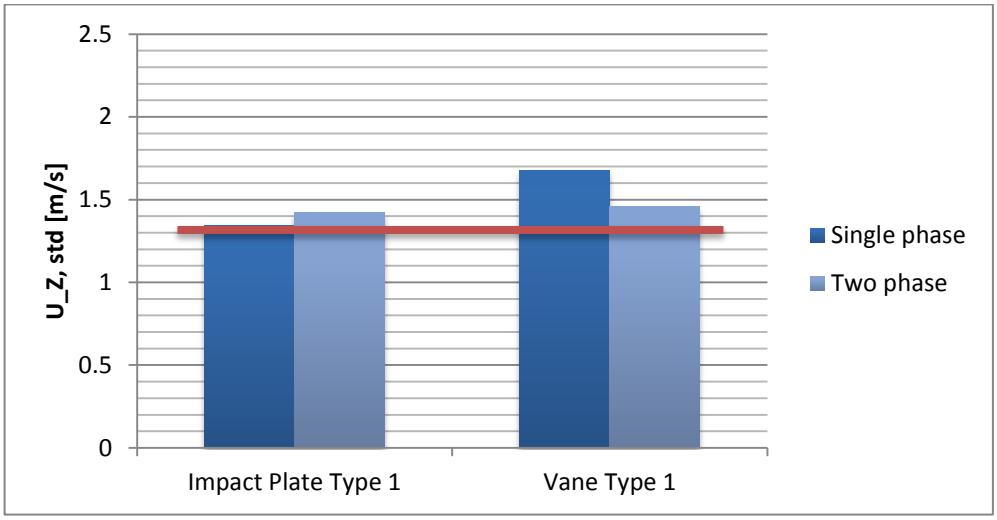

FIGURE 63. Standard deviation of the gas phase vertical velocity on a plane 5 cm below the demister pad in the single and two-phase simulations. High design values.

The gas phase maximum velocity in Fig. 62 increases from the single to the two-phase model. This increase is caused by existence of liquid in the two-phase model since the volume flux is equal between both models. The standard deviation of the gas phase vertical velocity at the demister inlet in Fig. 63 is slightly increased for the *Impact Plate Type 1*

distributor but decreased for the *Vane Type 1* between the single and two-phase simulations. This can be due to the optimized design of the *Vane Type 1* distributor which is specially designed for gas-liquid separation. The gas phase vertical velocity profiles at the demister inlet are presented collectively in Fig. 64.

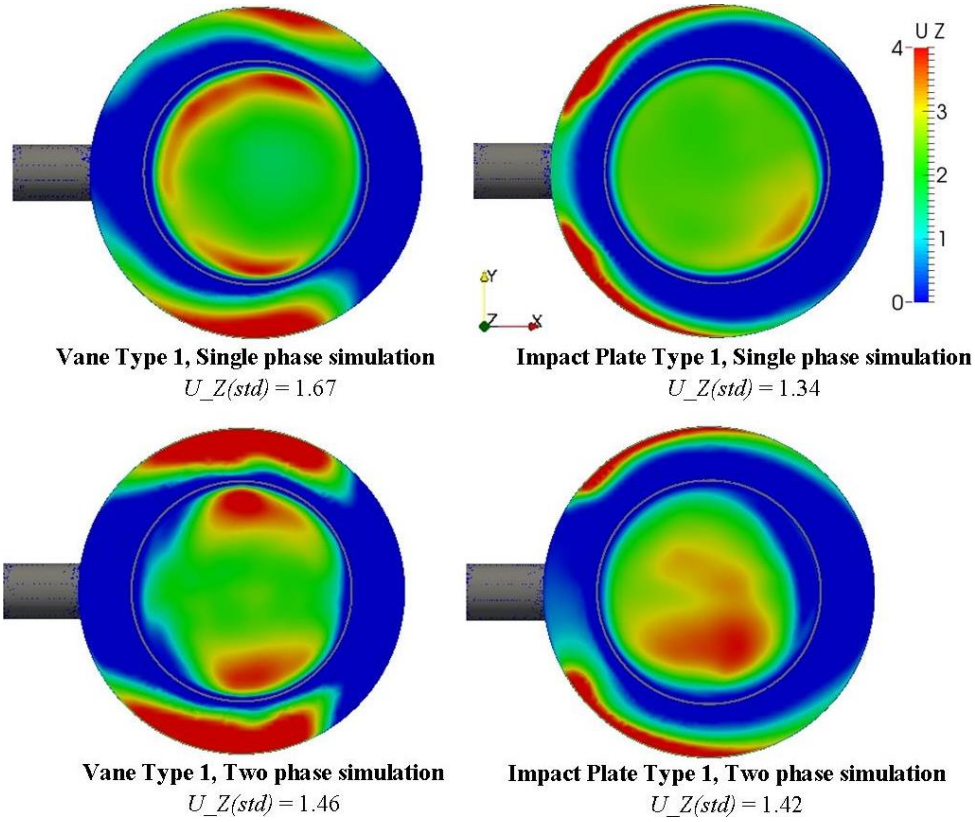

FIGURE 64. Gas phase vertical velocity 5 cm below the demister inlet in m/s in the single- and two-phase simulations. High design values.

It is evident that the two-phase model amplifies the no-flow zone effect which is caused by the formation of a low-pressure zone along the outer edge of the demister. The no-flow zone effect was illustrated in Fig. 34 concerning the *T-Junction* distributor. Presumably, the low pressure zone is more easily formed in the two-phase calculations as the denser liquid phase causes greater pressure gradients to occur inside the vessel. Since majority of the flow arrives to the demister along the back wall of the vessel with the *Impact Plate Type 1*, that side of the demister is particularly vulnerable to the formation of large pressure gradients. The liquid streamlines along with contours of high liquid concentration areas are presented in Figs. 65 and 66 for both of the studied distributors.

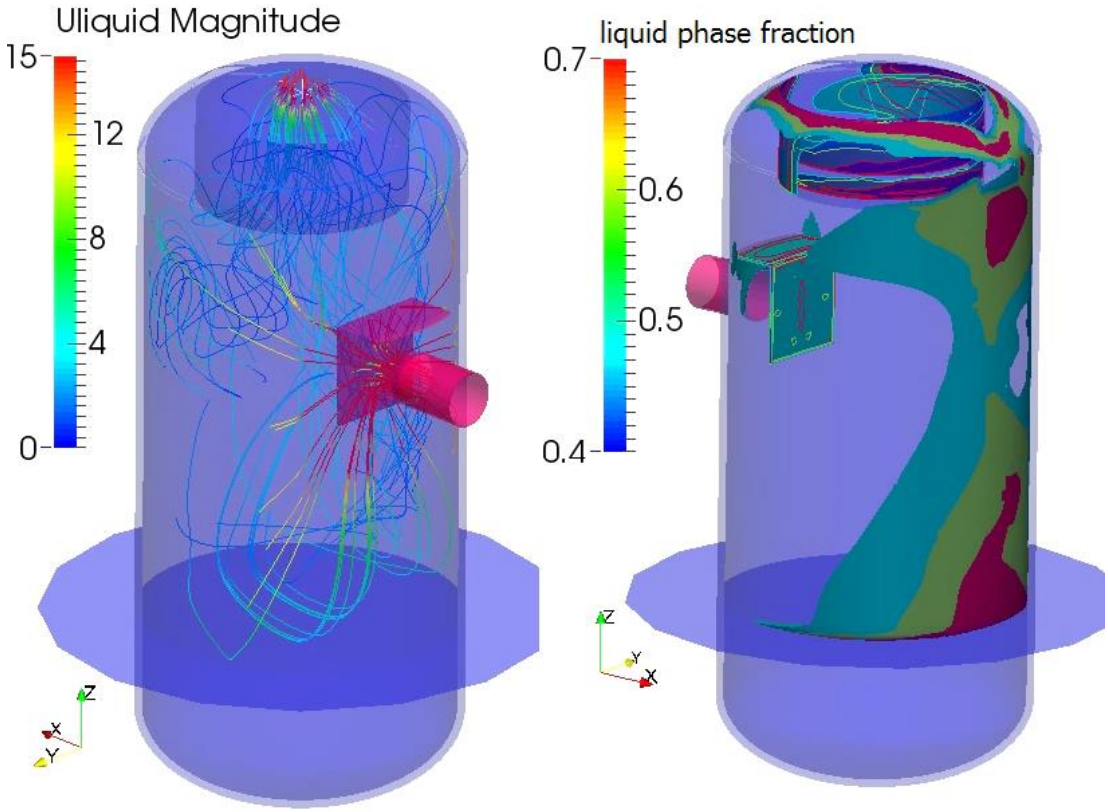

FIGURE 65. Left: Liquid streamlines representing flow orientation (velocity magnitude in m/s), Right: Contour plot of areas with liquid volume fraction over 0.5. *Impact Plate Type 1* distributor, high design values.

With the *Impact Plate Type 1* distributor, the flow is concentrated on the back wall of the vessel. This is seen as increased liquid concentration in the right side of Fig. 65. No liquid surface formation was observed during the 10 s simulation time.

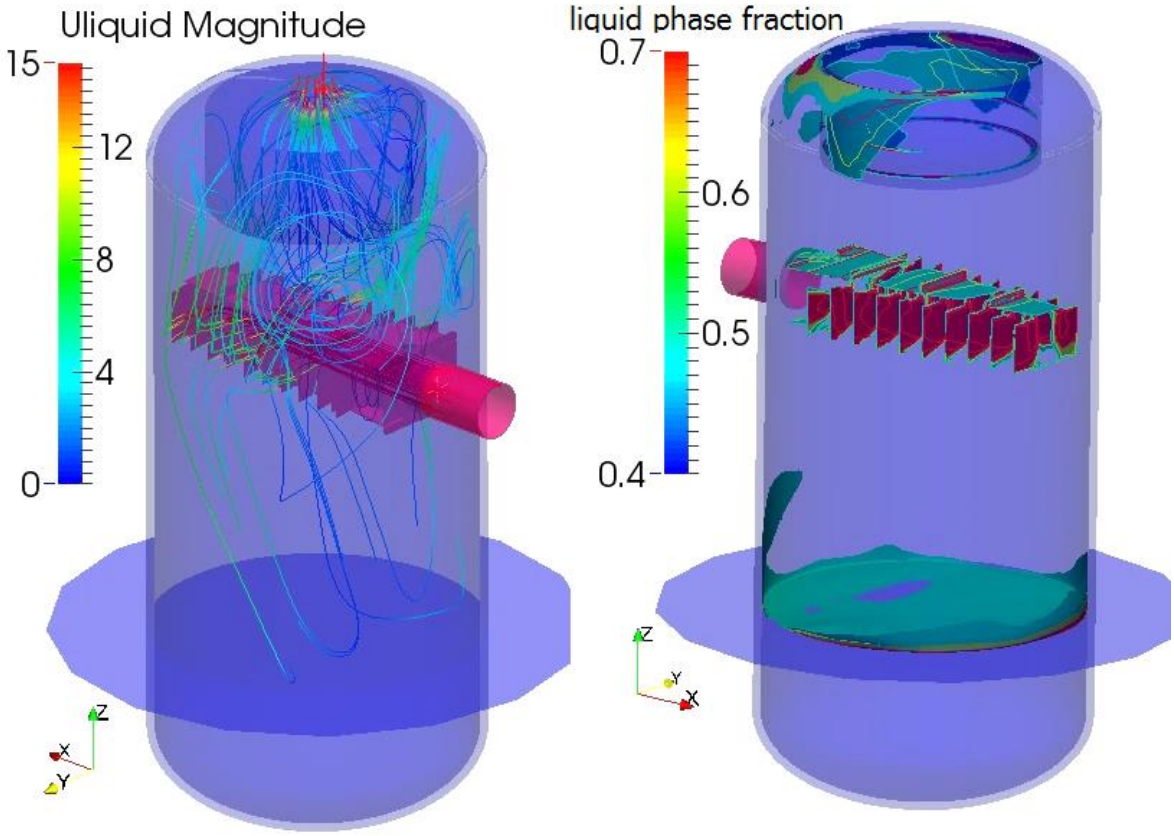

FIGURE 66. Left: Liquid streamlines representing flow orientation (velocity magnitude in m/s), Right: Contour plot of areas with liquid volume fraction over 0.5. *Vane Type 1* distributor, high design values.

As in the single phase calculations, the flow leaving the *Vane Type 1* distributor is directed to the sides of the vessel where it travels upwards. This leaves the underside of the distributor relatively stagnant and allows the liquid droplets to fall to the bottom of the vessel, forming a shallow liquid surface during the 10 s simulation time. Due to high flowrates, the upper part of the vessel also receives increased liquid concentrations. The liquid fraction is also increased inside the distributor. This needs to be taken into account in the sizing, as the accumulated liquid can partially block the openings and therefore increase local velocities. Liquid concentrations were also monitored at the demister inlet. The liquid concentration planes 5 cm below the demister pad are presented in Fig. 67 for both distributors.

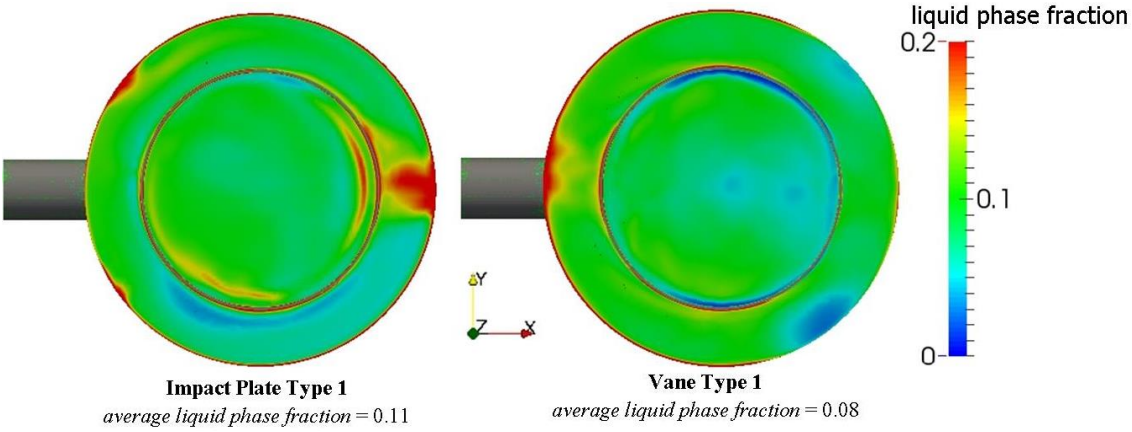

FIGURE 67. Liquid volume fractions 5 cm below the demister pad in the two-phase simulation cases. High design values. (Refer to Fig. 26 for plane location)

The differences in the liquid concentrations in Fig. 67 are subtle but clear. Both distributors produce a flow with a liquid volume fraction of around 10% across most of the cross-section. But where the *Vane Type 1* creates areas with lower concentration, the *Impact Plate Type 1* creates zones of high concentration along the outer edge of the demister. The average liquid phase fractions at the demister inlet are 8% and 11% for the *Vane Type 1* and *Impact Plate Type 1* distributors, respectively.

During the simulated 10 seconds, The *Vane Type 1* distributor accumulates more liquid into the vessel than the *Impact Plate Type 1*. The simulated outlet flow average liquid volume fractions for both distributors are 6.9% and 7.2%, respectively. According to formulas provided by Perry (1984), the maximum gas velocity in which a 350 µm liquid droplet can still descend with the given flow conditions and vessel geometry is 1.05 m/s. This is a rough estimate, but supports the observation that there are zones of low enough gas velocity inside the vessel to facilitate the descent of droplets. In reality, the demister pad significantly enhances separation by coalescing liquid droplets. In this model, as in the previous single phase calculations, the demister pad generates only a small pressure drop but otherwise does not interfere with either liquid or gas flow. The vertical plane views of the gas phase vertical velocities in Fig. 68 give indications of several regions within the vessel where the gas velocities are low enough for the 350 µm droplets to settle.

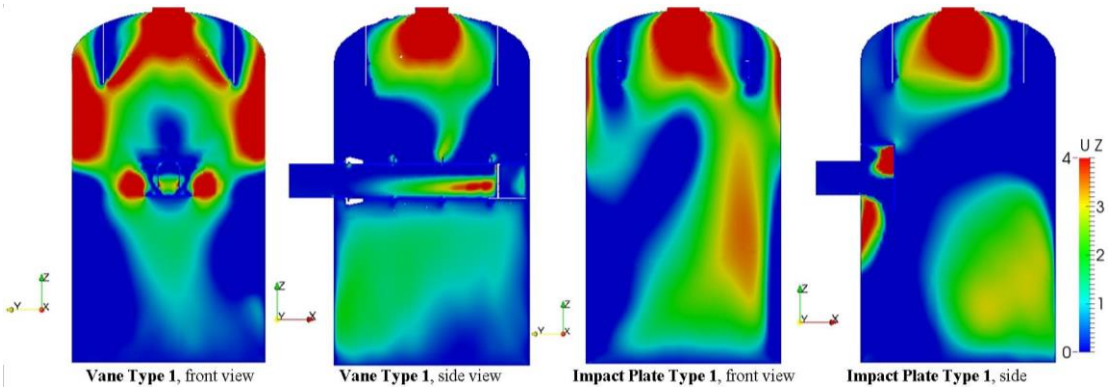

FIGURE 68. Vertical gas phase velocity profiles on vertical planes in the two-phase simulations. High design values.

Fig. 68 confirms that there are stagnant zones present below the *Vane Type 1* distributor. This and the smaller no-flow zone formation discussed earlier are factors which lead to the better performance of the *Vane Type 1* distributor over the *Impact Plate Type 1* in the two-phase simulations.

Without any experimental references to compare to, the results of the two-phase simulations seem reasonable and logical. The most significant possible error source is the Schiller-Naumann drag model, exact parameters of which were not optimized with respect to the simulated flow conditions. Due to time restrictions, no reference calculations were conducted concerning drag-model optimization. Therefore the amount on uncertainty in the results remains unclear.

With the limited number of two-phase calculations conducted here, the results are somewhat contradictory between the single phase and the two-phase calculations. The single phase calculations indicate a preference for the *Impact Plate* distributors based on the even flow profile observed at the demister inlet. In the two-phase simulations, the preference shifts to the *Vane Type 1* distributor based on liquid separation phenomena and pressure effects at the demister inlet. Although no other distributors were studied using a two-phase model, it can be concluded that both of these distributors are good initial choices when designing a separator vessel.

Further studies should always be conducted to help with the final choice between the initial options. In the two-phase model, particular attention in further studies should be paid to the formation of the no-flow zone due to the pressure effects at the demister inlet. In the

conducted simulations, the pressure effects cannot accurately represent the real phenomena, since the demister pad model provides no coalescing effect, only a pressure drop.

Based on the limited amount of comparable data gathered in the conducted studies, it can be tentatively concluded that the single phase steady state model can be used as an engineering tool in place of the more rigorous two-phase model. This is particularly justifiable if the flow behavior of a multi-phase system is dictated by a single phase. As of now, the availability of computational resources and tight schedules usually prevent the use of multi-phase models in everyday engineering activities. Even though two-phase systems can be approximated using a single phase model, the user should preferably always be aware of how the model selection influences the results. With the advent of easier-to-use CFD software requiring less theoretical expertise, this requirement is not fulfilled by default anymore.

11. CONCLUSIONS

In the experimental part of this thesis, the effect of several different design features on the flow inside gas-liquid separator vessels was studied. These features included inlet distributor configurations, vessel dimensions, demister support configurations and gas outlet configurations. Majority of the simulations were conducted as steady state single-phase calculations, assuming that the flow behavior inside the separator vessel is dictated by the gas phase. Additional simulations were performed as single- and two-phase dynamic calculations. The purpose of these simulations was both to obtain novel results and justify the use of the steady state single phase model which was employed most importantly due to the limited schedule of the work. Overall, the purpose of the simulations was to systematically gather reliable data to help in making design decisions in the future.

11.1 Results

Several design features were found to be superior to others within the used boundary conditions and model setup:

- **Distributor Study**: *Impact Plate Type 1* and *2* distributors when judged purely by the evenness of the flow profile
- **Vessel Dimension Study**: *Base geometry*
- **Demister Study:** Lower support plate configuration (*Modification 2B*)
    - Attention should be paid in avoiding sharp turns in fluid flow at demister inlet
- **Outlet study:** No definite preference

The dynamic simulation results supported the use of the steady state approach. The two-phase simulations partially supported the use of the single phase steady state approach, but also introduced new phenomena that affect the results. More two-phase calculations are needed in order to draw definitive conclusions.

Although the performance of the separator unit can in a real situation be something other than purely the sum of its components, these results give usable information on what options to consider when designing such a unit. The results are particularly useful for an experienced designer who can interpret them and use them in conjunction with practical experience from the field.

11.2 Error sources and reliability

Comparability between the results obtained in this thesis is good. However, one must be careful when comparing the results with those obtained from different studies. Factors that remained constant in the calculations of this thesis but can have a significant impact on the results include

- Inlet flow conditions and composition
- Structure of the computational mesh
- Physical models: drag, turbulence etc.

At the early stages of the simulation process, the effect of inlet flow on the results was investigated. It was noted that the flow profile at the inlet has a very prominent impact on the resulting flow profile inside the separator vessel. Particularly eddies caused by bends and restriction orifices in the inlet pipe often lead to asymmetrical and irregular flow

profiles. To remove these effects, a fully developed ideal flow profile was used in the calculations.

Still, some of the results exhibit asymmetry despite the symmetrical inlet flow profile, geometry and averaging of the results. Most notable example of this is the *Half Pipe* flow profile in Fig. 41. According to CFD experts, this is not an uncommon phenomenon as the solution fields are often unstable in a symmetrical solution. Small triggers such as mesh irregularities or rounding errors can cause the solution to divert to a more stable asymmetric solution. (Schumacher, 2015) All things considered, the asymmetry has no significant impact on the comparability of the results, at least within this thesis.

11.3 Further studies

Due to limited computational resources and time, prioritization and simplification were necessary when deciding the scope of this work. This left several aspects open for possible future research. Deeper validation of the used models presents at least an equal amount of work as the experimental part of this thesis. Validation of the used models, if done thoroughly, includes a sensitivity analysis. This provides information on how much different variables affect the final solution. To estimate reliability, simulation results need to be validated against either existing or gathered experimental data from the field.

Although gases and liquids both exhibit fluid behavior, gas-liquid and liquid-liquid separations differ in flow phenomena as well as the used equipment. Higher viscosities in all-liquid flows lead to different flow patterns inside the separation vessels. In addition, liquid-liquid separators are usually horizontal vessels. The simulation of horizontal vessels, even with the same stream compositions as used in this thesis, would provide useful reference material for designers to utilize in their work.

The two-phase gas-liquid simulations of this thesis provide plenty of starting points for future research. The gas-liquid interactions could be studied further to determine whether re-entrainment of already separated droplets occurs either from the walls or the liquid surface at the bottom of the vessel. The model could also be complemented with the addition of a demister model capable of inducing droplet coalescence. Due to its complexity, the two-phase model in particular is sensitive to input parameters. One known

example is the inlet droplet size. In reality, it is generally a distribution of different sizes, exact values of which are often unknown. This uncertainty makes it even more important to know how much the error caused by estimation of the particle size affects the final solution.

Other influential factors include the selection of drag and turbulence models. The effect of the turbulence model is most likely diminished by the data-averaging procedure which decreases the effects of time-based fluctuations on the results. But the drag model can have a significant impact on the flow fields in the two-phase calculations. Had the schedule allowed, the evaluation and optimization of the drag model with respect to the simulated flow would have been conducted as the next step in this thesis.

REFERENCES

Al-Fulaij, H. *et al*. 2014. Eulerian-Eulerian modelling and computational fluid dynamics simulation of wire mesh demisters in MSF plants, *Engineering Computations*, vol. 31(7), p. 1242-1260

Bahadori, A. 2014. Pollution Control in Oil, Gas and Chemical Plants, New York: Springer

Case, J. *et al.* 1999. Strength of Materials and Structures (4th edition), London: Arnold

Chekmenev, V.G. *et al.* 2010. Analysis of the Operation of Two-Phase Vertical Separators, *Chemistry and Technology of Fuels and Oils*, vol. 46(4), p. 259-261

Cooper, C. Alley, F. 1986. Air Pollution Control: A Design Approach, Prospect Heights: Waveland Press

Couper, J. *et al*. 2012. Chemical Process Equipment - Selection and Design (3rd edition). Oxford: Elsevier, p. 655-675

Dean, J.A. 1985, Lange's Handbook of Chemistry (13th edition), New York: McGraw-Hill

El-Dessouky H.T. *et al.* 2000. Performance of wire mesh mist eliminator, *Chemical Engineering and Processing*, vol. 39(2), p. 129-139

Engys Ltd, HELYX Core User Reference Guide, HELYX Release v2.3.x, 28.4.2015

Evans, F.L. 1974. Equipment Design Handbook for Refineries and Chemical Plants, Vol 2. Houston: Gulf Publishing Company, p. 153-165

Fabian, P. *et al.* 1993. Demystifying the Selection of Mist Eliminators. *Chemical Engineering*, vol. 100(11), p. 148-156

García, M.H. 2008. Sedimentation Engineering: Processes, Management, Modeling and Practice, Reston: American Society of Civil Engineers

Hall, S. 2012. Rules of Thumb for Chemical Engineers (5th edition), Oxford: Butterworth-Heinemann

Kalis, B. 2004. Cure Liquid Carryover from Compressor Suction Drums. *Hydrocarbon Processing*, vol. 83(10), p. 77-84

Laleh, A.P. *et al.* 2012, Design and CFD Studies of Multiphase Separators – a Review, *The Canadian Journal of Chemical Engineering*, vol. 90(6), p. 1547-1560

Liu, D. *et al.* 2007. CFD Simulation of Gas-Liquid Performance in Two Direction Vapour Horn, *Chemical Engineering Research and Design*, vol. 85(10), p. 1375-1383

Lyons, W.C. Plisga, G.J. 2005. Standard Handbook of Petroleum and Natural Gas Engineering (2nd edition), Burlington: Gulf Professional Publishing

Mhatre, S. *et al*. 2015. Electrostatic phase separation: A review. Chemical Engineering Research and Design, vol 96, p. 177-195

Monnery, W.D. Svrcek, W.Y. 1994. Successfully Specify Three-Phase Separators. *Chemical Engineering Progress*, vol. 90(9), p. 29-40

Moss, D.R. Basic, M. 2013, Pressure Vessel Design Manual (4th edition), Oxford: Butterworth-Heinemann

Newton, T. *et al.* 2007. Tools to Model Multiphase Separation, *Chemical Engineering Progress*, vol 103(6), p. 26-31

Perry, R.H. 1984. Perry's Chemical Engineers Handbook (6th edition). New York: McGraw-Hill

Ranade, V. 2002. Computational Flow Modeling for Chemical Reactor Engineering, San Diego: Academic Press

Schaschke, C. 2014. A Dictionary of Chemical Engineering, Oxford: Oxford University Press

Schumacher, T. 2015, Engys Ltd. Asymmetrical results with symmetrical geometries, e-mail communication, t.schumacher@engys.com, 2.7.2015

Siikonen, T. 2014. Virtaussimulointi, Course material, Aalto University, School of Engineering, Department of Applied Mechanics, available at http://wwwcfdthermo.hut.fi/Teaching/Ene-39.4054/ (referred on 10.8.2014)

Sinnott, R.K. 2005. Coulson & Richardson's Chemical Engineering Volume 6 (4th Edition): Chemical Engineering Design, Oxford: Elsevier Butterworth-Heinemann

Soares, C. 2002. Process Engineering Equipment Handbook. New York: McGraw-Hill

Soulaine, C, Quintard, M. 2014, On the use of a Darcy-Forchheimer like model for a macro-scale description of turbulence in porous media and its application to structured packings, *International Journal of Heat and Mass Transfer*, vol. 74, p. 88-100

Stewart, M. Arnold, K. 2008. Gas-Liquid and Liquid-Liquid Separators, Burlington: Gulf Professional Publishing

Succi, S. 2001. The Lattice Boltzmann Equation for Fluid Dynamics and Beyond, Oxford: Oxford University Press

Svrcek, W.Y. Monnery, W.D. 1993. Design Two-Phase Separators Within the Right Limits. *Chemical Engineering Progress*, vol. 89(10), p. 53-60.

Towler, G. Sinnott, R. 2013, Chemical Engineering Design: Principles, Practice and Economics of Plant and Process Design, Oxford: Butterworth-Heinemann

Trambouze, P. 2000, Petroleum Refining, Volume 4: Materials and Equipment, Paris: Editions Technip

Tu, J. et al. 2013, Computational Fluid Dynamics: A Practical Approach, Oxford: Butterworth-Heinemann

Uki, T. *et al.* 2012, Design of Gas-Liquid Separator for Complete Degasing, *International Journal of Chemical Engineering and Applications*, vol. 3(6), p. 477-480

Vaittinen, J. 2015, Neste Jacobs Oy, *Oral communication*

Visuri, O. 2012, Experimental Validations of CFD Simulations and Models in Chemical Applications, Doctoral dissertation, Aalto University, Department of Biotechnology and Chemical Technology

Wiencke, B. 2011 Fundamental principles for sizing and design of gravity separators for industrial refrigeration. *International Journal of Refrigeration*, vol. 34(8), p. 2092-2108.

Wilkinson, D. et al. 2000. Baffle Plate Configurations to Enhance Separation in Horizontal Primary Separators, Chemical Engineering Journal, vol. 77(3), p. 221-226

APPENDICES

APPENDIX I, 1(1)

Generally accepted inlet and outlet configurations for gas-liquid separators (Kalis, 2004)

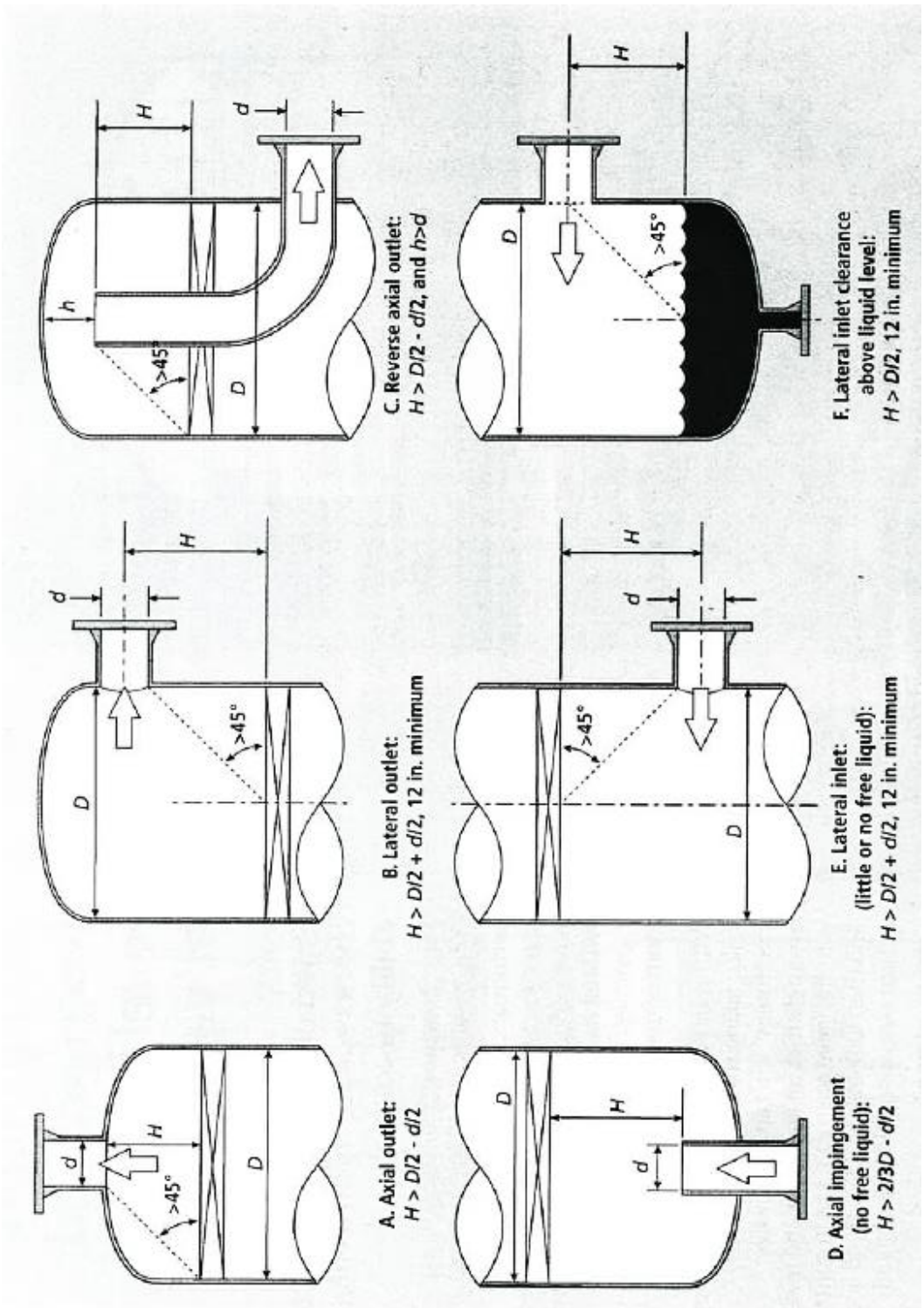

APPENDIX II, 1(1)

HELYX® boundary conditions for selected base configuration in mesh study

Base Mesh			**Solution Modelling**		
Base Mesh Type	Automatic		Time	Steady	
Base Mesh Spacing	0.03	m	Flow	Incompressible	
Geometry			Turbulence Model	k-ω SST	
Vessel			**Materials**		
Refinement level	0		**Fluid**		
Number of layers	3		Density	3.17	kg/m^3
Layer Stretching	1.25		Dynamic Viscosity	0.00001	Pas
Final Layer Thickness	0.4		Kinematic Viscosity	3.15E-06	m^2/s
Liquid level			**Boundary Conditions**		
Refinement level	0		**Inlet**		
Number of layers	3		Patch Type	Inlet	
Layer Stretching	1.25		Type	Velocity	
Final Layer Thickness	0.4		Specification Method	Normal To Boundary Patch	
Demister frame			Velocity Magnitude	High design values --> 31.8	m/s
Refinement level	2		**Outlet**		
Number of layers	3		Patch Type	Outlet	
Layer Stretching	1.25		Type	Pressure	
Final Layer Thickness	0.4		Specification Method	Fixed Pressure	
Inlet pipe			Fixed Pressure	0	m^2/s^2
Refinement level	2		**Others**		
Number of layers	3		Patch Type	Wall	
Layer Stretching	1.25		Wall Type	No-slip	
Final Layer Thickness	0.4		**Cell Zones**		
Outlet pipe			**Demister pad**		
Refinement level	2		CellZone Type	Porous Media	
Number of layers	3		Model	Darcy-Forcheimer	
Layer Stretching	1.25		e1	1 0 0	m
Final Layer Thickness	0.4		e2	0 1 0	m
Inlet			Viscous Loss Coefficient, d	1100/1100/1100	$1/m^2$
Refinement level	0		Inertial Loss Coefficient, f	10/10/10	1/m
Number of layers	0		**Numerical Schemes**		
Outlet			U	Bounded Linear Upwind - 2nd Order	
Refinement level	0		k	Linear Upwind -2nd Order	
Number of layers	0		omega	Linear Upwind -2nd Order	
Demister pad			Non-orthogonal correction	0.333	
Surface refinement level	0		**Solver Settings**		
Number of layers	0		**Residual Control**		
Zones:			U	0.00001	
Type	Internal		p	0.00001	
Face Zone Name	demisterZone		k	0.00001	
Cell Zone	Yes		omega	0.00001	
Cell Zone Name	demisterZone		**Relaxation Factors**		
Level	2		U	0.7	
Baffle Check	Yes		p	0.3	
Material Point			k	0.7	
Position	0 0 0		omega	0.7	
			Fields Initialisation		
			U		
			Type	Potential Flow	
			Initialise Boundaries	Yes	
			p		
			Type	Potential Flow	
			k		
			Type	Default	
			omega		
			Type	Default	

APPENDIX III, 1(1)

Convergence plot and examples of single iteration and time step flow profiles in the *Impact Plate Type 1* case (High design values)

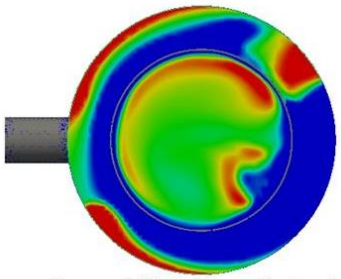

Impact Plate Type 1, steady state, iteration number 1000

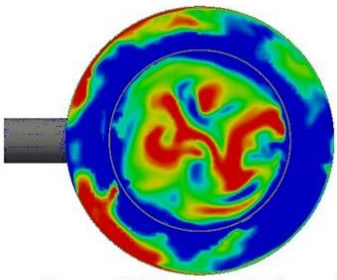

Impact Plate Type 1, dynamic simulation, time step 9.00 s

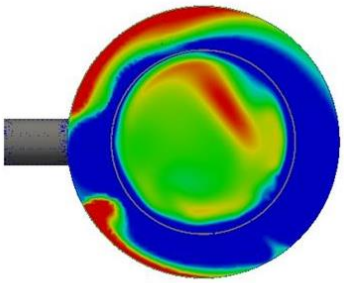

Impact Plate Type 1, steady state, iteration number 2000

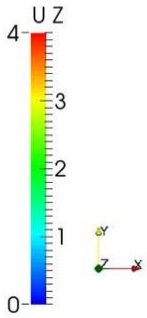

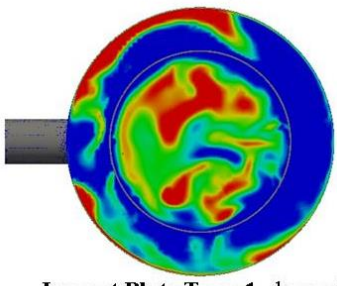

Impact Plate Type 1, dynamic simulation, time step 12.00 s

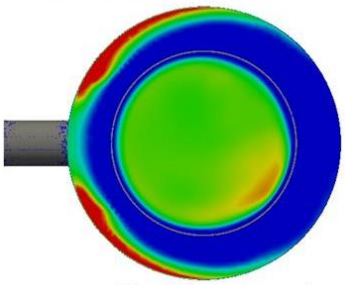

Impact Plate Type 1, steady state, averaged over iterations 1000-2000

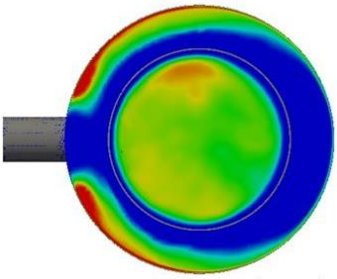

Impact Plate Type 1, dynamic simulation, averaged over time steps 6-12 s

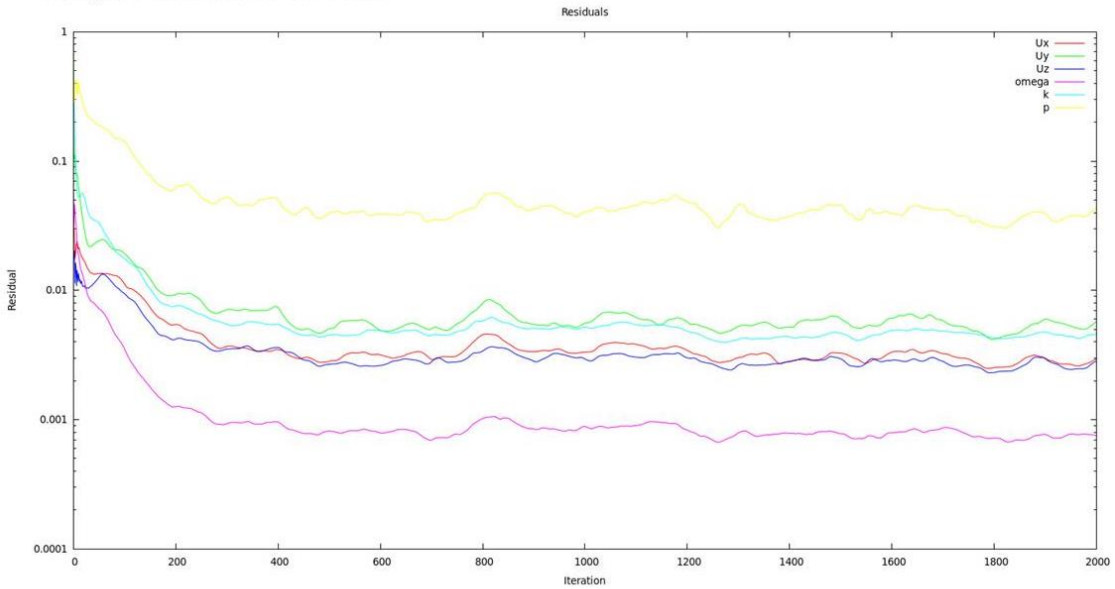

Impact Plate Type 1, example residual plot of a steady state simulation

APPENDIX IV, 1(1)

Vertical velocity profiles 30 cm above the inlet centerline in the distributor study (High design values)

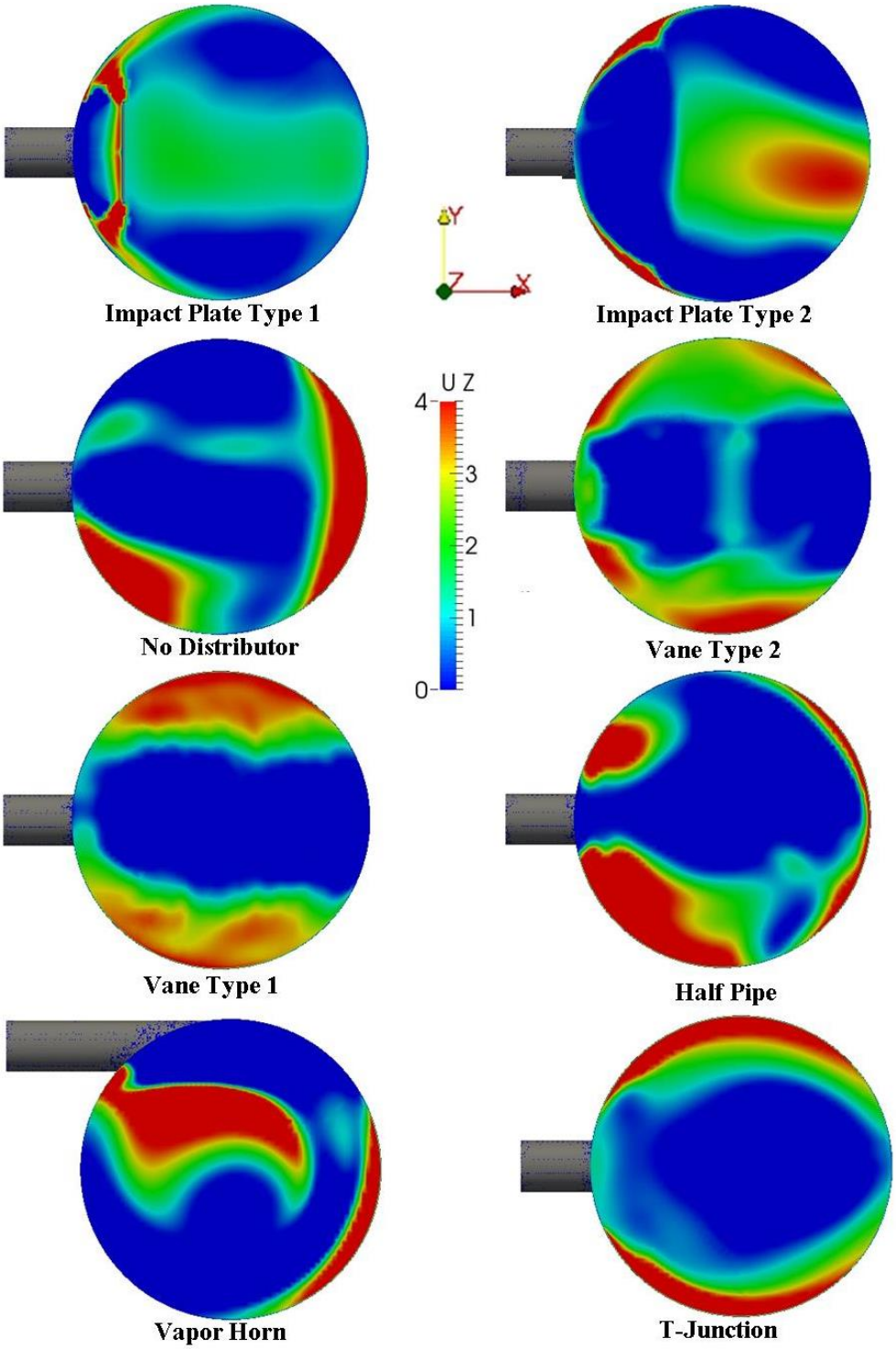

APPENDIX V, 1(1)

Vertical velocity profiles on a vertical plane in the distributor study
(High design values, outlet pipe hidden for clarity)

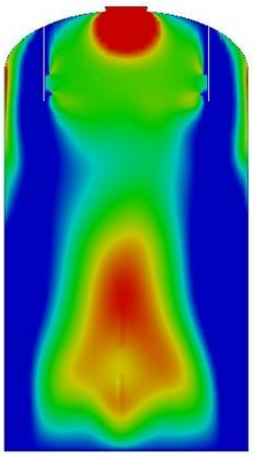

Impact Plate Type 1

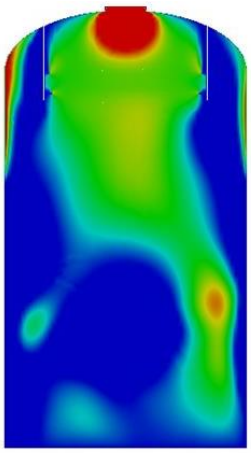

Impact Plate Type 2

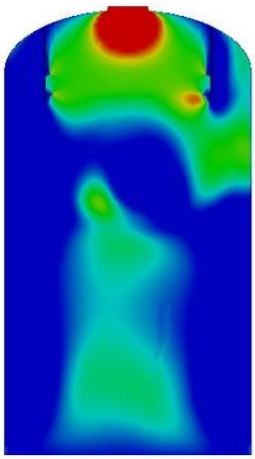

No Distributor

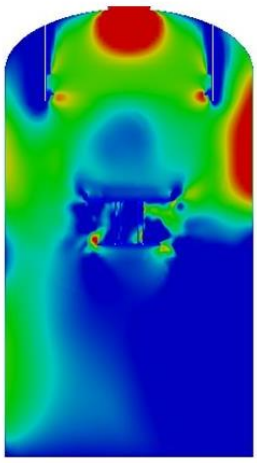

Vane Type 2

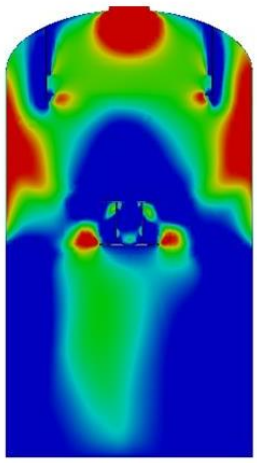

Vane Type 1

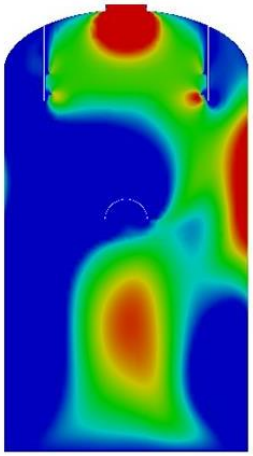

Half Pipe

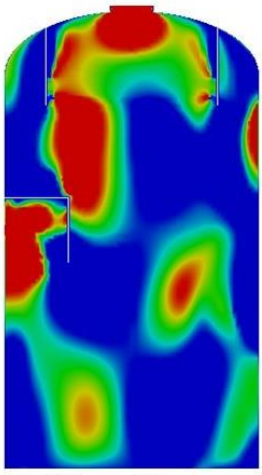

Vapor Horn

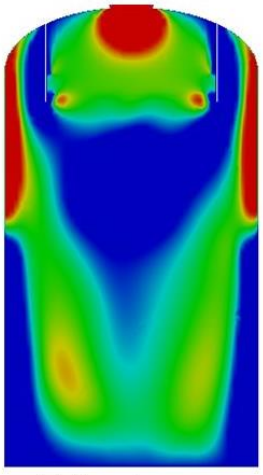

T-Junction

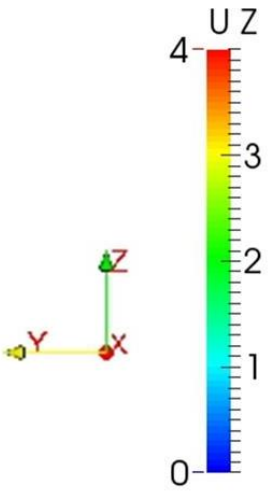

APPENDIX VI, 1(1)

Vertical velocity profiles 5 cm below the demister in the distributor study (Low design values)

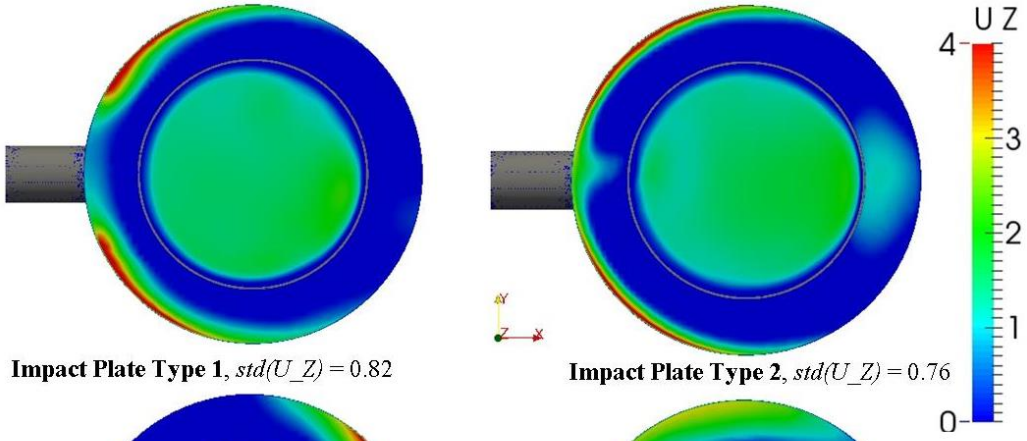

Impact Plate Type 1, *std(U_Z)* = 0.82

Impact Plate Type 2, *std(U_Z)* = 0.76

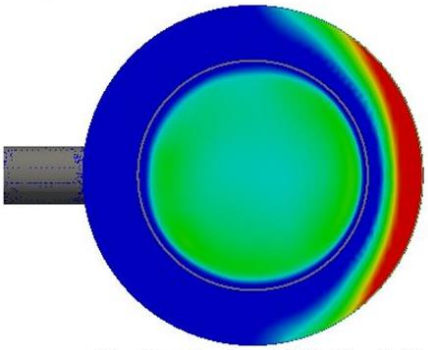

No Distributor, *std(U_Z)* = 0.95

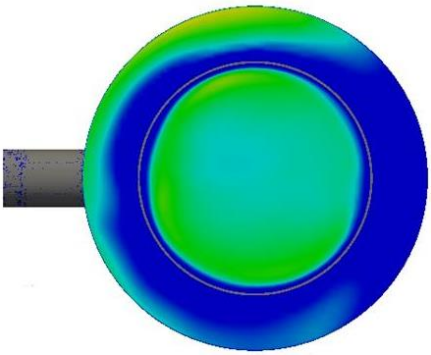

Vane Type 2, *std(U_Z)* = 1.05

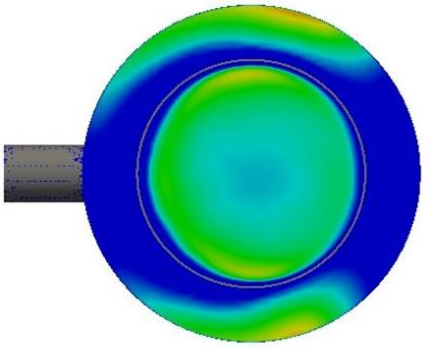

Vane Type 1, *std(U_Z)* = 1.13

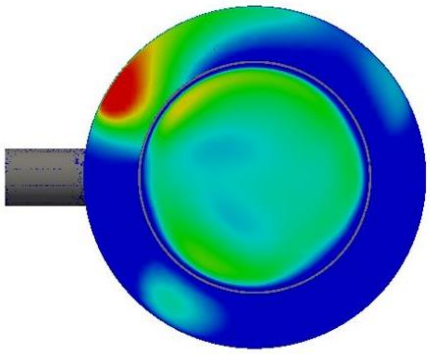

Half Pipe, *std(U_Z)* = 1.09

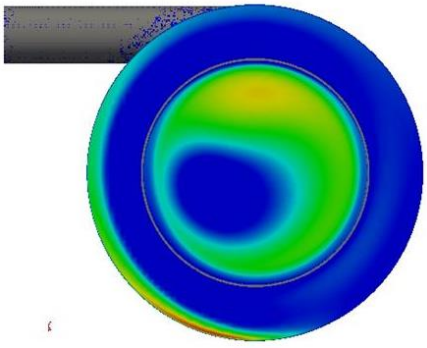

Vapor Horn, *std(U_Z)* = 0.96

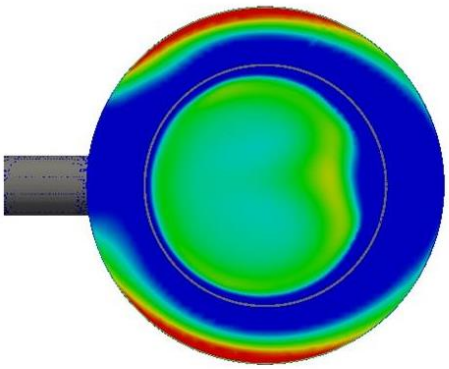

T-Junction, *std(U_Z)* = 1.24

APPENDIX VII, 1(1)

Relative pressure profiles in Pascals on the bottom of the separator vessel in each case of the *Distributor study* (High design values)

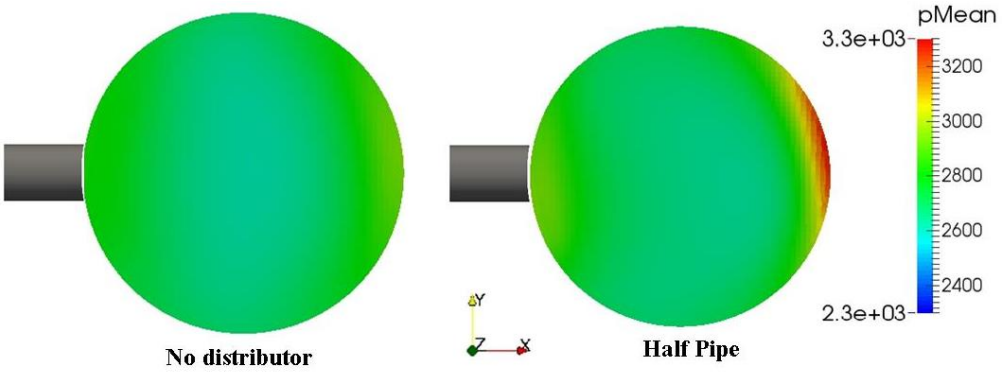

No distributor

Half Pipe

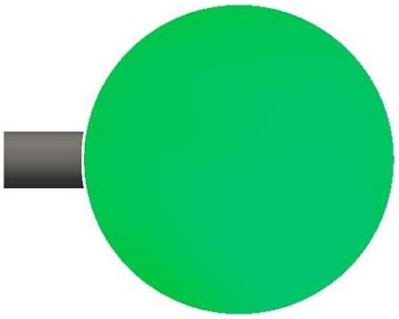

Vane Type 1

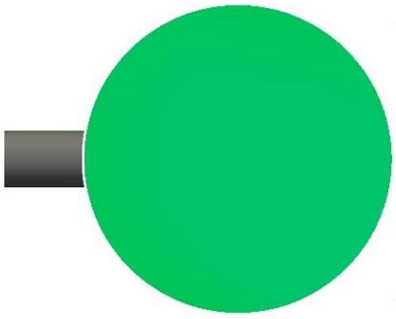

Vane Type 2

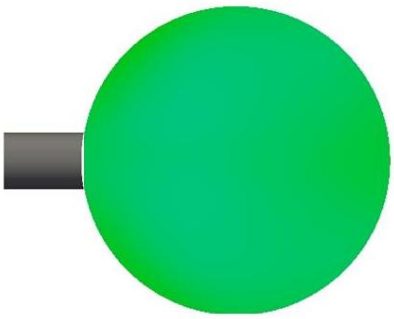

Impact Plate Type 1

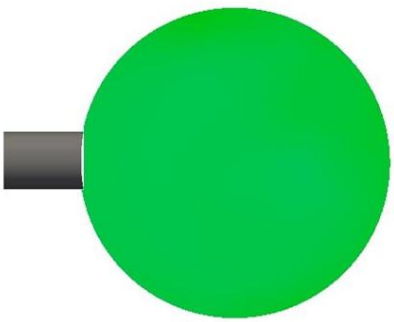

T-Junction

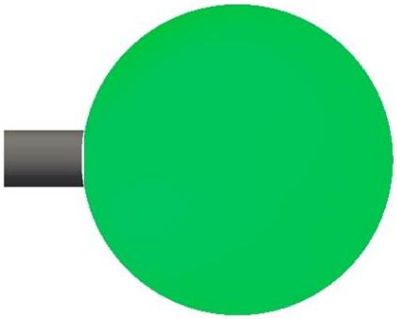

Impact Plate Type 2

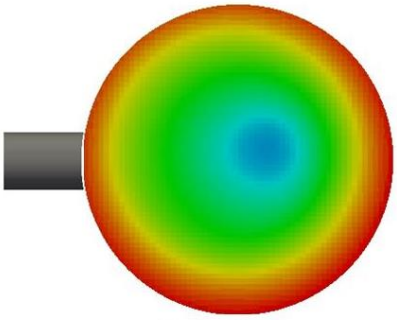

Vapor Horn